Master thesis : Design and development of non-contact electrodes electrooculogram acquisition system for sleep measurements

Auteur : Pham Phu, Thê
Promoteur(s) : Redouté, Jean-Michel
Faculté : Faculté des Sciences appliquées
Diplôme : Master en ingénieur civil biomédical, à finalité spécialisée
Année académique : 2025-2026
URI/URL : http://hdl.handle.net/2268.2/25186

UNIVERSITE DE LIEGE
FACULTE DES SCIENCES APPLIQUEES

Master thesis : Design and development of non-contact electrodes electrooculogram acquisition system for sleep measurements

PHAM PHU Thê

Thesis presented to obtain the degree of :
Master of Science in Biomedical Engineering

Thesis supervisor :
Redouté Jean-Michel
Daily supervisor :
Toussaint Laura

Academic year: **2025 - 2026**

Acknowledgments

I would like to express my sincere gratitude to my supervisor, Prof. Jean-Michel Redouté, for giving me the master thesis opportunity that suited my interests and based on my capacities. I am grateful for the thrust and support placed in me. His teachings provided the theoretical foundation of this work and greatly contributed in its realization.

My sincere thanks go to Laura Toussaint the PHD student following my work in detail for her technical support and helpful advice during all steps of my master thesis development. Her insights and availability were greatly appreciated and helped in many issues I faced.

I would also like to thanks all the members of the Microsys laboratory, who made me feel comfortable in this working environment, provided access to equipment, technical resources and multiple advices whenever needed.

A special thanks is addressed to Angel Calderon and Olivia Monfort for their contribution in my work providing great advices in respectively the PCB design and headband design.

Finally, I would like to express my deepest gratitude to my parents and family for their unconditional support, patience and encouragement throughout my studies. They were always there for me and gave me an environment to work in the best condition.

Summary

Physiological signal monitoring plays an important role in the assessment of sleep quality and the diagnosis of sleep disorders such as sleep apnea. During sleep, eye movements provide valuable information about sleep stages, especially during rapid eye movement (REM) sleep. The electrooculogram (EOG) is commonly used in sleep studies to detect eye movements and to support sleep-stage classification. However, conventional EOG acquisition systems rely on wet or dry contact electrodes placed near the eyes which can be uncomfortable, restrictive and poorly tolerated during overnight or long-term measurements. These limitations motivate the development of alternative acquisition techniques that improve comfort and ease of use while maintaining sufficient signal quality.

This work presents the design, development and experimental validation of a non-contact electrooculogram (EOG) acquisition system. It is intended for easy-to-use, comfortable by reducing skin irritation and wearable physiological monitoring, making them more suitable for overnight and repeated measurements. Non-contact electrodes measure biopotential signals through a thin insulating layer, such as fabric. However, they also introduce very high electrode–skin impedance and increased sensitivity to environmental noise, especially power-line interference.

The system was first modeled and analyzed using LTSpice simulations to understand the impact of modified skin–electrode interface of non-contact electrode. A dedicated PCB was designed and implemented, integrating an analog front-end with impedance buffers in the non-contact electrodes and amplification stages, filtering and grounding strategies in the main board. The design is made versatile to allow for the use of wet, dry or non-contact electrodes, adjustable gains and filters to study their impact on signal quality. After troubleshooting, a repeatable measurement protocol was defined with timed eye-movement phases to ensure consistent comparison between experimental runs.

Experimental recordings were performed using fully non-contact recording electrodes and a grounded reference electrode. The output signal was acquired with an oscilloscope and post processed by a Python code. This code is dedicated to plot the output but can also apply digital 50 Hz notch filtering, compute the signal-to-noise ratio (SNR), apply the Fast Fourier Transform (FFT) over the signal. The results show that the system is able to detect typical eye activities such as left and right movements, blinking and random eye movements.

Despite these encouraging results, the measurements remain strongly affected by power-line interference and by experimental factors such as reference electrode coupling, skin moisture, electrode pressure, and environmental conditions. Overall, this work demonstrates the feasibility of non-contact EOG acquisition as a proof of concept for sleep monitoring applications.

Contents

List of Figures

List of Tables

Introduction

Today, personalized medicine and wearable devices are increasingly being used to collect information about human health. Personal monitoring systems allow patients to record physiological signals and better understand factors that may affect their health condition. These data also support medical diagnosis, as clinicians rely on a combination of methods such as anamnesis, physical examination, physiological signal monitoring, medical imaging, and blood analysis to identify diseases and select appropriate treatments.

Currently, patients are monitored either in hospitals or at home using electrodes, cables and dedicated measuring devices. Most biomedical signal monitoring techniques are based on wet electrodes (Ag/AgCl with conductive gel). These electrodes require direct skin contact, which can cause discomfort or complications during long-term use. The conductive gel may dry after a few hours, leading to signal degradation. In addition, such equipment often requires a medical prescription and trained personnel for installation and data analysis, increasing the overall cost of the procedure. A common example is the Holter monitor used for cardiac measurements, which uses disposable wet electrodes to record the electrocardiogram (ECG) and provides valuable information about heart activity in a home environment.

Improving patient comfort and ease of use is therefore a key aspect in the design of modern monitoring devices, especially for frequent or long-term home use. In addition, wearable systems must be reliable, safe, and stable over time. These challenges apply to all physiological signals recorded. As a result, alternative technologies have emerged to replace traditional wet electrodes. One example is photoplethysmography, which relies on light reflection or absorption and is widely used in pulse oximeters. Another promising alternative is the use of non-contact electrodes, which rely on capacitive coupling instead of direct skin contact. This is the technology investigated in this work through the design of both electrodes and analog conditioning circuits. Non-contact electrodes have already been proposed for monitoring signals such as the electrocardiogram (ECG) and electroencephalogram (EEG), both of which provide critical information for medical diagnosis.

One particularly promising application of non-contact electrodes is neonatal monitoring. In newborns, especially premature babies, the skin is extremely sensitive, and adhesive wet electrodes can cause irritation or injury. Non-contact electrodes could allow the monitoring of physiological signals such as heart rate or breathing in a safer and more comfortable way, while reducing stress for both baby and medical staff. Several non-contact technologies exist, as reviewed by Krbec et al. (2024) [1], but this work focuses specifically on the development of capacitive electrodes capable of measuring signals through fabric.

The objective of this master's thesis is to monitor physiological signals using non-contact electrodes. Instead of wet or dry electrodes, the aim is to design a system capable of measuring physiological signals without direct contact with the skin, through capacitive measurement. This approach enables integration of the system into clothing or textiles, making daily monitoring easier and more comfortable. Non-contact electrodes and their front-end electronics have been studied by Chi et al. (2009) and Wang et al. (2022) [2,3], particularly for cardiac and brain signals. Their results showed that capacitive measurements can remain relatively accurate even in motion or with variable electrode-skin distance, especially for ECG monitoring.

Non-contact technology has been studied for more than 15 years, limited to specific physiological signals already mentioned. However, this approach can potentially be extended to other signals, new medical applications and diagnosis methods. Table 1 summarizes the main differences between wet, dry, and non-contact electrodes. It highlights that non-contact electrodes exhibit much higher impedance than other electrode types. As a result, placing an ultra-high-input-impedance buffer close to the electrode compensates for the high fabric resistance and small coupling capacitance [4]. It is realized by preventing signal attenuation and reducing noise pickup before transmission but also increase the complexity of the implementation. Additional challenges with signal quality and noise sensitivity makes the design of a non-contact acquisition system even more difficult.

Table 1: Comparison between electrode types (simplified)

Property	**Wet Electrodes**	**Dry Electrodes**	**Non-Contact Electrodes**
Impedance	Low (hundreds kΩ)	Medium (MΩ range)	Very High (hundreds MΩ)
Noise/Artifact Sensiti.	Low	Medium	High
Signal Quality	Excellent	Good to Moderate	Low to Moderate
Signal to Noise Ratio	24.9dB	3 to 24dB	1.8 to 3.7dB
Biocompatibility	Moderate	High	Very High
Skin Preparation	Required	Not required	Not required
Comfort	Medium	High	Very High
Maximal duration	Short (minutes–hours)	Medium (hours–days)	Long (days-week)
Usability	Clinical	Wearable	Clothes integrated
Typical Application	ECG/EEG/EOG	Home monitoring	Long term/sleep tracking

If sufficiently precise and reliable, non-contact electrodes could significantly change the way physiological signals are measured. They would enable less intrusive, more bio-compatible, more comfortable and longer-duration monitoring, with electronics integrated directly into clothing. These benefits have some tradeoffs since there are increased complexity, power consumption and cost that required to compensate for lower signal quality and higher artifact sensitivity. In term of applications, such system are designed for longer term and non-irritating measurements with the integration of electronics and electrodes into clothes as it can measure through a fabric layer.

Many sleep disorders can be diagnosed by monitoring a combination of multiple physiological signals. The clinical reference method for sleep assessment is polysomnography (sleep study), which is performed in hospitals or sleep laboratories. This examination provides information for diagnosing disorders such as obstructive sleep apnea, insomnia, breathing disorders and movement disorders. A special focus is put into obstructive sleep apnea which is estimated to affect up to one billion people worldwide. During polysomnography, signals such as brain activity, eye movements, heart activity, muscle tone, oxygen saturation and breathing effort are recorded overnight.

However, polysomnography is often inconvenient for patients since it requires to take the medical appointment a long time in advance. During the night involves numerous sensors directly attached to the body and may disturb natural sleep patterns. Patients frequently need time to adapt to the hospital environment, a phenomenon known as the “first-night effect” and won’t sleep as they would in at their home. In addition, the procedure is costly due to the involvement of specialized equipment, trained technicians and medical analysis. These limitations contribute to underdiagnosis and undertreatment of sleep disorders due to limitation in hospital beds, economic reasons or non representative poor quality sleep of the patient.

To adapt part of sleep assessment to home use, this work proposes a solution based on non-contact electrodes the associated signal processing unit and the holding head gear. The wearable system de-

veloped in this thesis focuses on the acquisition of eye movements using the electrooculogram (EOG). Based on the result obtained for simple eye movements, an extension of this work could be applied to the sleep monitoring. Although this approach does not provide the full range of information obtained from polysomnography, it could deliver valuable insights into sleep quality and sleep stages.

Because a large proportion of the population is affected by undiagnosed obstructive sleep apnea (OSA) [5], this work focuses on a signal that can help detect this disorder and relatively simple to monitor. The electrooculogram was chosen because it provides useful information for sleep staging while requiring fewer electrodes than electroencephalography (EEG). Previous studies from Virkkala et al (2015) [6, 7] have shown that EOG alone can be used to identify different sleep stages over a night.Eye movements monitored by EOG provide data about wake and sleep stages without many of the constraints of full polysomnography. By identifying these stages, we could determine if the patient experienced sleep apneas, since apneas often cause brief arousals or micro-awakenings during the night thus influencing the sleep stages.

Sleep duration and quality strongly influence daily behavior, cognitive performance, mood and long-term health. Poor sleep is associated with increased risk of cardiovascular, metabolic and neurodegenerative diseases. Collecting more information about an individual's sleep can be beneficial, especially in cases of sleep disturbance. Improving sleep assessment and monitoring can therefore have a significant impact on overall health and quality of life.

This work represents a first step toward simplified detection of eye movements using a wearable device based on non-contact electrodes. It focuses on the complete design, simulation, and implementation of a custom analog signal processing system and its associated front-end non-contact electrodes. The proposed system is specifically designed to overcome the very high input impedance and increased noise sensitivity associated with non-contact electrooculogram (EOG) measurements through fabric.

The work includes the modeling of the electrode–skin capacitive interface, the design of high-input-impedance buffering stages and the implementation of analog filtering and amplification circuits adapted to low-amplitude biopotential signals. Special attention is given to noise reduction and power-line interference rejection, which are critical challenges in non-contact EOG acquisition.

The acquired signals are filtered and amplified to obtain stable and measurable outputs suitable for further processing. The thesis presents experimental results obtained from simulations, breadboard prototypes and a final printed circuit board implementation. Design choices are justified based on theoretical considerations and experimental observations. Finally, the limitations of the current system are discussed, and perspectives for future improvements and extensions of the proposed wearable non-contact EOG system are presented.

Objective

The main objective of this master thesis is to design, implement and experimentally validate a non-contact electrooculogram (EOG) acquisition system that improves user comfort while maintaining the ability to detect eye movements reliably. This work aims to explore whether non-contact electrodes can be used for EOG monitoring in applications such as sleep analysis where long-term wearability is essential.

More specifically, the objectives of this work are:

- **To acquire the essential background knowledge required to understand the clinical needs** in the sleep diagnostics sector, with a particular focus on identifying the limitations of existing monitoring solutions. This includes understanding how sleep disorders such as **obstructive sleep apnea affect patients**, how they are currently diagnosed, and which technical and practical limitations of current systems.
- **To understand the differences in the electrode type and their working principle**, comparing classical wet electrode to dry or non-contact alternatives with the electrical modeling of the skin–electrode interface and characteristics.
- **To understand the physiological principles of the electrooculogram (EOG)** and its relevance for sleep-related applications, particularly for the identification of eye movements and sleep stages such as REM sleep.
- **To identify and analyze existing related studies** in order to understand the current state of the art in electrooculogram acquisition systems and in non-contact and wearable technologies. This objective aims to compare different design approaches, electrode types and signal processing strategies that could inspire our design.
- **To design and simulate the analog front-end electrode and main board for non-contact EOG acquisition**, including impedance buffering, amplification, filtering, and grounding strategies. Using LTSpice and breadboard prototype to evaluate circuit behavior before final implementation.
- **To design and fabricate a dedicated PCB** integrating the complete analog signal conditioning chain, with additional adjustable gains, filters, grounding configurations, power supply unit and shielding. The realization of a functional hardware is a key step for this project.
- **To develop a repeatable experimental measurement protocol and positioning**, based on controlled eye-movement sequences, ensuring consistent and comparable EOG recordings across multiple runs and configurations. Non-contact electrodes position and attachment methods is investigated.
- **To experimentally evaluate the performance of the non-contact EOG system**, by analyzing recorded signals, identifying typical eye-movement patterns and assessing the impact of noise sources such as power-line interference and environmental conditions. Implement the associated Python code for visualizing the recorded signal and apply additional function

Chapter 1

State of the art and background knowledge

Inspired by recent advances in signal acquisition technologies, this master's thesis focuses on development of the electronics required to measure the electrooculogram (EOG) using non-contact electrodes. This work fits within the growing trend of personal health devices that continuously inform users about their physiological state. EOG signals have a wide range applications, ranging from medical diagnosis to human–computer interaction and assistive communication systems based on eye movement control [8, 9].

As introduced previously, the main objective of this thesis is to develop a measurement system for the EOG signal to help detect sleep-related conditions, which remain underdiagnosed. This work represents a first step toward non-contact electrode monitoring of multiple physiological signals and primarily focuses on the design, implementation and experimental validation of the electronic system for simple eye movement. The clinical sleep application and advanced data processing of the acquired signals are beyond the scope of this thesis and would require further investigation.

This chapter provides the background information necessary to understand the design choices of the proposed system. It first introduces the existing clinical standards in sleep monitoring to highlight where our approach may bring new advantages. It then presents the main sleep disorder targeted in this work and compares different types of electrodes that can be used for physiological signal acquisition. The chapter also introduces the basic principles of the electrooculogram and reviews relevant literature related to non-contact electrooculogram measurements, before focusing on system design in the following chapter.

The electrooculogram reflects eye movements through voltage variation measured over time and is one of the physiological signals recorded during a sleep study, also known as polysomnography (PSG). Polysomnography is the clinical gold standard for diagnosing sleep disorders [8, 10]. In more specific cases, home sleep apnea tests (HSATs) are used to diagnose obstructive sleep apnea (OSA) using portable devices at home. Both PSG and HSAT procedures are reviewed to establish a clinically accepted reference to adapt our proposed device, identify their limitations and position the contribution of this work.

This chapter also reviews the main aspects of obstructive sleep apnea, including its symptoms, physiological mechanisms and contributing risk factors. There is an importance of a finding an accessible way to diagnose it as undiagnosed and untreated OSA increase risks of multiple health complications. Epidemiological data, associated risks and common treatment approaches are presented to emphasize the clinical relevance of this sleep condition [5, 11–13].

Compared to conventional physiological signal monitoring methods, the electrodes used in this work are non-contact. The following sections describe the differences in operating principles and characteristics between wet, dry, and non-contact electrode configurations. Particular attention is given to the skin–electrode interface and its associated electrical models, which are essential for understanding the signal acquisition challenges. A comparative analysis of electrodes characteristics is also discussed in this

section [4, 14–17].

Before attempting to measure the electrooculogram (EOG) using non-contact electrodes, it is necessary to understand its physiological origin and typical signal characteristics. The EOG originates from the potential difference between the cornea and the retina, which changes with eye orientation [18]. This section reviews the basic principles of EOG generation and common electrode configurations. EOG signals typically have smaller amplitudes and have an overall lower frequency content than those of the electrocardiogram (ECG). Sleep related eye movements are also discussed in this section.

Together, these sections provide the background knowledge required to understand the existing clinical approaches and identify current needs in this field. A particular focus is placed on obstructive sleep apnea, as non-contact electrodes could contribute to its diagnosis through long-term EOG monitoring. Several related studies are reviewed in the final section of this chapter. These studies either focus on non-contact electrodes acquisition system for ECG and EEG measurements or on EOG acquisition using different type of electrodes. The design choices made in these works are discussed in relation to specific challenges such as noise, impedance and motion artifacts. In addition, a study on sleep stage classification based on EOG signals is reviewed, highlighting the relationship between eye movements, sleep quality and sleep staging.

1.1 Clinical methods for sleep assessment

This section presents the clinical procedures used to diagnose sleep-related disorders. The goal is to understand how current methods work, identify their limitations, and see how the proposed application could support diagnosis without replacing the existing ones. We focus on polysomnography and home sleep apnea testing to understand which physiological signals are measured and how they are used. Obstructive sleep apnea (OSA) is the main disease diagnosed through sleep studies, which is why it will be detailed in this section.

1.1.1 Polysomnography

Also called sleep studies, polysomnography (PSG) is described by J. Rundo et al. (2019) [8, 10] as the gold standard for diagnosing sleep-related disorders. According to Rundo: "Polysomnography refers to a systematic process used to collect physiological parameters during sleep." The study records multiple physiological signals simultaneously overnight in a hospital setting, under the supervision of a sleep technician.

It enables the detection of sleep disorders, mainly sleep-related breathing disorders such as obstructive sleep apnea (OSA). However, it is also used to diagnose other conditions, such as hypoventilation, periodic limb movement disorder, narcolepsy, night seizures, and chronic insomnia.

In Belgium, according to 2023 data from INAMI [19], around 85,000 polysomnography services are performed each year, with an average annual cost of approximately 285.46 € per patient. The total annual expenditure is about 26,135,640 €, highlighting the importance of developing simpler and more accessible diagnostic tools to reduce hospital load and cost. The rate of this practice has increased by about 3% per year since 2013, showing a growing awareness and diagnosis of sleep-related conditions like OSA. Most sleep studies (71.68%) are requested by pneumatology departments, confirming the focus on breathing sleep disorders.

The standard sleep study (Type I) includes multiple physiological signals described below. Figure 1.1 [20] provides an overview of all signal that can be measured and their corresponding sensor placement during a sleep study:

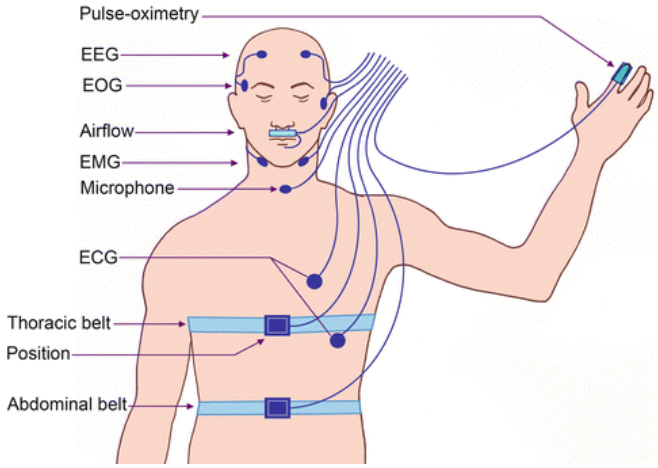

Figure 1.1: Polysomnography electrode and measurement device setup

- **Electroencephalogram (EEG)** — measures the electrical activity of the brain from different areas (frontal, central, occipital). The sleep stage can be determined from the EEG information combined with complementary electrooculogram and chin electromyogram signals. There are different states of consciousness, reflected in the EEG signal patterns. These ranges from the wakefulness (alpha wave, high frequency and small amplitude) to deep sleep state (delta wave, low frequency and high amplitude), with intermediate states in between. During a full night, the human sleep progresses from the wakefulness to cycles composed of stage 1-3 sleep and a rapid eye movement (REM/ also called paradoxical) sleep. These cycles last approximately 60-100 minutes and a complete night should be composed of 4-7 cycles. Thanks to the combination of multiple physiological signals, abnormal sleep patterns can be detected.

- **Electrooculogram (EOG)** - measures the potential difference between the retina and cornea [18]. It is used in sleep staging together with the EEG, mainly to identify sleep stage transition. Eye movements are essential for detecting rapid eye movement (REM) sleep within each sleep cycle. These measurements are independent of the ambient light conditions and detect eye orientation changes in multiple directions relative to the electrodes. It is therefore an important signal to record during the PSG to determine waking versus sleeping stage and identify REM sleeping phase. This signal is presented more in detail in the next section, as it is the main focus of this master thesis.

- **Chin electromyogram (EMG)** — records muscle activity to differentiate REM sleep from other stages. The distinction is based on the reduction of chin muscle tone during REM sleep. Two electrodes are placed below the mandible for this purpose. The combination of the 3 previous signals is currently used to determine the sleep stages of the patient during the polysomnography as shown in Fig 1.2.

- **Electrocardiogram (ECG)** — monitors heart rate and rhythm to detect abnormalities such as heart failure, faster rate (tachycardia), slower rate (bradychardia) or non constant rate (arrhythmia). Cardiac dysfunction may lead to poor blood oxygenation and contribute to sleep troubles. The ECG uses 3 electrodes, placed on both arms with a reference on the right leg.

- **Respiratory signals** — airflow and respiratory effort are recorded using airflow sensors. Oronasal thermal airflow sensors detect the temperature changes between inspired and expired air while nasal pressure transducer detects pressure variation. Belts or sensors around the chest or abdomen measure the respiratory effort from the deformation detected by piezoelectric elements. These recorded signals are used to identify respiratory events such as apneas.

- **Oxygen saturation (SpO_2)** — measured using a pulse oximeter on the finger, based on light transmission and reflection through the finger. This measurement allows to get the blood oxygen saturation based on the radiation intensity properties. It is mainly used to assess hypopneas and determine the need for night oxygen supply.
- **Limb electromyogram (leg EMG)** — measures leg movement on anterior tibialis muscles to diagnose sleep movement disorders such as restless leg syndrome.
- **Body position and video** — record the patient's position to correlate apneas with sleep posture (supine or prone).

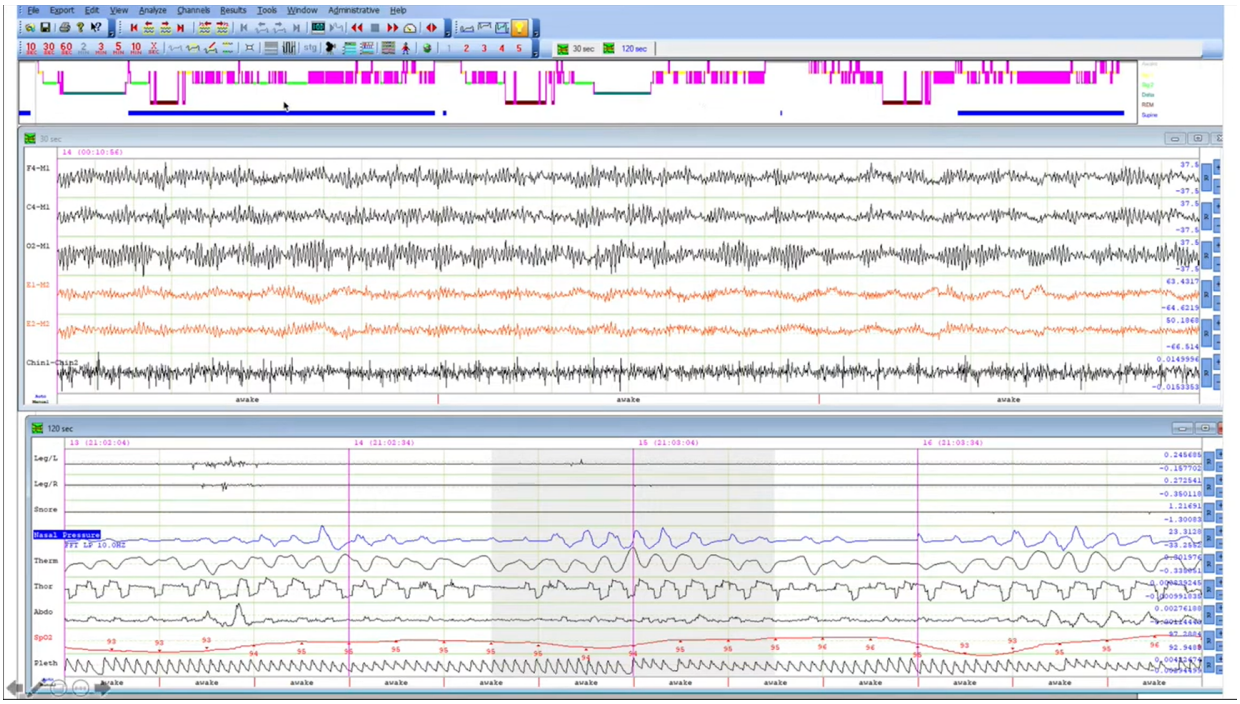

Figure 1.2: Software view of polysomnography with all physiological signal recorded in parallel

Figure 1.2 [21] shows the combination of all physiological signals recorded during polysomnography and how they are monitored. The data collected overnight are analyzed to determine sleep stages and to identify abnormal events. The upper part shows the hypnogram, which represents the transitions between wakefulness and the sleep stages (S1–S3 and REM). These sleep stages are clinically identified using EEG, EOG, and chin EMG signals . In the second part,, a single epoch is shown, corresponding to a 30 seconds recording window composed of these 3 signals to determine the patient's current sleep stage. The measurement last the whole night and are subdivided into consecutive 30 second epochs. The lower part displays slower physiological signals, such as respiratory and limb movement, which are analyzed over longer time windows (typically 120 seconds). The combination of all these signals provides relevant diagnostic information for sleep disorders.

Despite being the gold standard, PSG remains an expensive and complex procedure requiring hospital infrastructure and trained personnel. It is also affected by the "first-night effect," where the patient's sleep quality is reduced due to the unfamiliar environment (hospital or sleep laboratories) and due to the discomfort caused by multiple electrodes attached to the body. This factor must be considered when diagnosing any sleep related disorders. Moreover, hospital capacity limits the number of tests, even though the global prevalence of OSA is estimated at 936 million adults worldwide [5].

1.1.2 Home sleep apnea test

An alternative to overnight sleep studies in hospitals or sleep laboratories is the Home Sleep Apnea Test (HSAT) described by Kapoor et al. (2015) [22]. These tests are more convenient for patients because they can be done at home using a portable recording device during the night. HSAT mainly targets the detection of moderate to severe obstructive sleep apnea (OSA) in adults. The device is more compact than full polysomnography and includes fewer sensors. Overall, it is easier and more comfortable for the patient to wear. The goal of HSAT is to support early detection of OSA and the initiation of appropriate treatment.

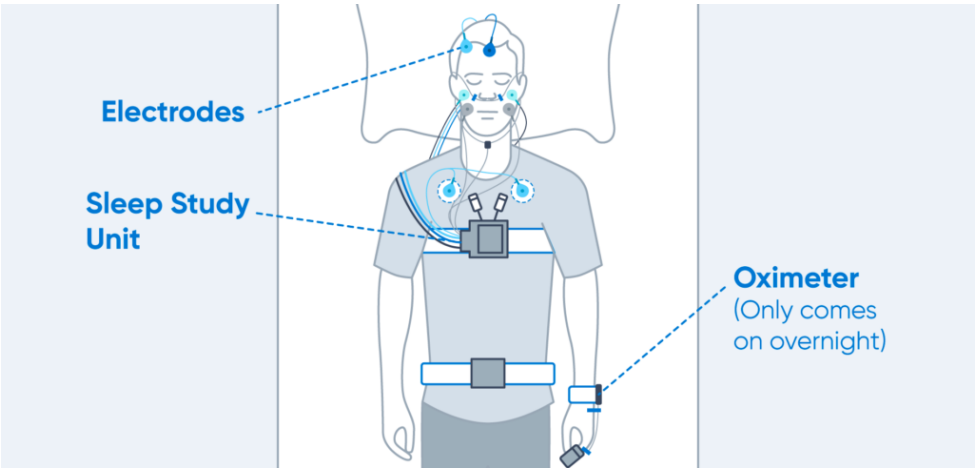

Figure 1.3: Home sleep apnea test configuration schematic

There are different types of HSAT depending on the number of recorded signal. Figure 1.3 [23] illustrates a typical HSAT setup, showing that the device uses electrodes, a main sleep recording unit placed on the chest, respiratory belts and pulse oximeters. The most common ones measure respiratory airflow, respiratory effort through belt, oxygen saturation with an oximeter and heart rate using ECG electrode. Some devices can also include additional measurements, such as body position or EEG signals, as shown in the illustration with a forehead electrode. By combining these data, the system provides a less precise overview of the patient's sleep condition compared to a full polysomnography (PSG). However, HSAT often underestimates the severity of sleep apnea. The recorded data is either analyzed by a technician after the night or processed using an algorithm, which can reduce the precision. HSAT also lacks many key physiological signal required for accurate sleep staging, which are not yet realizable at home due to the use of wet electrodes and complex acquisition systems.

In a PSG, the electroencephalogram (EEG) is the key tool for identifying sleep stages and provides important information when combined with eye and chin movement signal. HSAT can only estimate sleep stages indirectly using physiological signals such as heart rate variability, breathing patterns and blood oxygen saturation. While HSAT is clinically validated for diagnosing sleep apneas, it is not intended for accurate sleep stage classification. In addition, HSAT is not suitable for patients with serious comorbidities or those who require supplemental oxygen, as these conditions can interfere with the test accuracy.

We highlight that HSAT devices do not record the electrooculogram (EOG), although it could provide valuable information for sleep staging. Our approach using a non-contact EOG system integrated into a headband directly addresses this limitation. It aims to provide sleep staging-related information offered by EOG without the discomfort associated with conventional wet electrodes, positioning it as a potentially more user-friendly solution for long-term home monitoring than existing HSAT devices.

In classical EOG measurements, the standard wet electrodes are placed around the eyes and might

cause discomfort, skin irritation or gel dry out over a long recordings. Even with these comfort issues, wet electrodes are clinically used for a single overnight measurement since it is widely available and accepted. However, for long term or repeated measurements wet electrode may not be an ideal solution, and alternative such as non-contact electrode are currently investigated as alternatives for physiological signal measurement. These electrodes types are presented in the next section and compared with their wet and dry counterparts.

These two clinically accepted methods to diagnose sleep apnea have some limitation. Both require specific setups: either a technician to correctly place the sensors electrodes. The patient has to sleep in an unknown controlled hospital environment or HSAT devices must be used, which lack some key physiological signals (such as EEG, EOG, EMG) and limiting diagnostic accuracy. These procedures can be uncomfortable for patients, relatively invasive and typically provide data over only a short period of time, typically a single night.

Other less common techniques can also be used to study sleep disorders. These include magnetic resonance imaging (MRI) and other brain imaging methods, which provide detailed insights into brain activity and structure. However, due to their high cost and complexity, they are mainly reserved for research purposes or for complex or uncertain cases after initial diagnosis.

In a home environment, patients may also be asked to wear a wrist activity monitor (actigraphy) [24] for several days or weeks. This device records body movements and their timing to distinguish between sleep and wake periods. Irregular movement patterns can indicate potential sleep disturbances.

Additionally, some EEG devices designed for home use already exist and use wet electrodes connected to a small recording unit. These systems allow partial brain activity in a home environment without being too cumbersome.

In this thesis, we propose using non-contact electrodes to record physiological signals in a more comfortable and user-friendly way. This design could enable patients to monitor their sleep more regularly in daily life, providing valuable information on how sleep evolves over time or in response to treatments and lifestyle changes. By focusing on eye movement measurement through non-contact electrodes, this work aims to develop a simpler and less invasive method for sleep staging and apnea detection. Single-channel EOG based sleep staging is a research topic in development. Virkkala *et al.* (2015) and Rahman *et al.* (2018) [6, 7] showed that EOG alone can detect different sleep stages over a night using trained neural network on recorded data. Ultimately, this approach supports the growing field of personalized medicine and the development of wearable health technologies by providing patients accessible tools to better understand sleep and overall health.

1.2 Obstructive sleep apnea

Obstructive sleep apnea (OSA) is the most common sleep-related breathing disorder. It is estimated to affect up to 936 million people worldwide aged between 30-69 years [5] when considering OSA with mild to severe form. Even though it is this widespread, a major challenges is the significant underdiagnosis: approximately 85% of individual with OSA have never been diagnosed [11]. Many affected individuals are unaware of their health condition, which could lead to serious consequence. Combined with limited hospital capacity and the high cost of the polysomnography, this situation highlight the need for the development of alternative diagnostic approaches to inform the patient of their sleep quality.

The primary symptoms of obstructive sleep apnea commonly include loud snoring, episodes of gasping or choking during sleep, morning headaches, excessive daytime fatigue, memory and concentration trouble, decreased libido, irritability, mood disturbances and restless sleep. These symptoms result from repeated interruptions in breathing (apneas) or partial obstructions (hypopneas) which can cause micro-arousals and disrupt normal sleep.

During sleep, muscles in the upper airway relax, particularly in the nasopharyngeal region. In patient with OSA, those muscles may no longer maintain airway open, leading to obstruction or restricted the airflow. According to the American Academy of Sleep Medicine, an episode of airway obstruction to be qualified as a hypopnea is defined as at least a 30% reduction in airflow lasting at least 10 seconds, accompanied by either a 3% oxygen desaturation or an arousal from sleep [25].

When such events occur 5 or more times per hour, the patient may be diagnosed with obstructive sleep apneas. These repeated airway collapses lead to reduced or stopped breathing, which lowers blood oxygen levels (hypoxemia) and triggers a physiological stress response. Over time, these repeated mechanisms contribute to severe long-term health consequences. 3 severity level of OSA measured based on the apnea-hypopnea index (hourly frequency of apnea during sleep) going from mild (5-15 episodes per hour), moderate (15-30 episodes per hour) and severe (more than 30 episodes per hours).

Multiple factors contributes to the development of sleep apneas [11]:

- Genetics factors as the OSA prevalence is variable depending on the ethnicity from different countries in the world, due to the skull and airways anatomical differences.
- Physical characteristics where people with obesity, facial malformations or enlarged/thickened oronasal tissues upper airway related tissues are more likely to develop OSA. Obesity is the most frequently studied risk factor for OSA.
- Medical/particular conditions such as pregnancy, diabetes, hypothyroidism or chronic nasal congestion...
- Lifestyle factors including consumption of alcohol, tobacco use and certain drugs that can increase of airway obstruction.

Each apnea episode during the night leads to increased heart rate and blood pressure, often followed by an arousal from sleep due to the apnea episode. As a result, the sleep cycle is disrupted, with reduced time is spent rapid eye movement (REM) sleep and overall decreased sleep quality. If left untreated, sleep apnea can lead to a wide range of long term health complications. It includes hypertension, cardiovascular disease, stroke risk, metabolic dysfunction (like insulin resistance, type 2 diabetes...), cognitive/mood disorders, weakened immune system and increased mortality risk [12, 13]. Untreated OSA also increase the risk of traffic and workplace accidents. Many lives and costs could be spared if more potential patient are diagnosed and treated.

Knauert *et Al.* (2015) [12] have compiled data about the medical consequences of untreated obstructive sleep apnea syndrome. Due to repeated airflow obstruction, increases in heart rate, blood pressure and frequent arousals from sleep, many adverse effects occur more frequently in patients with OSA. The Figure 1.4 from [12] illustrates the increased risk ratios according to various diseases.

The OSAS increase the risk compared to non-OSAS patients and different ratios are considered. An odd of an event correspond to the $\frac{\text{Number of events}}{\text{Number of non-events}}$, then Odds Ratio for OSA related disease compares the odds of disease occurrence in OSA patients to those in non-OSA patients, it is given by:

$$\frac{\text{Odd of disease in OSA patient}}{\text{Odd of disease in non-OSA patient}}$$

An alternative is to measure the risk of an event which corresponds to the $\frac{\text{Number of events}}{\textbf{Total number of events and non-events}}$, then get the Relative Risk that compares disease probabilities between groups:

$$\frac{\text{Risk of disease in OSA patient}}{\text{Risk of disease in non-OSA patient}}$$

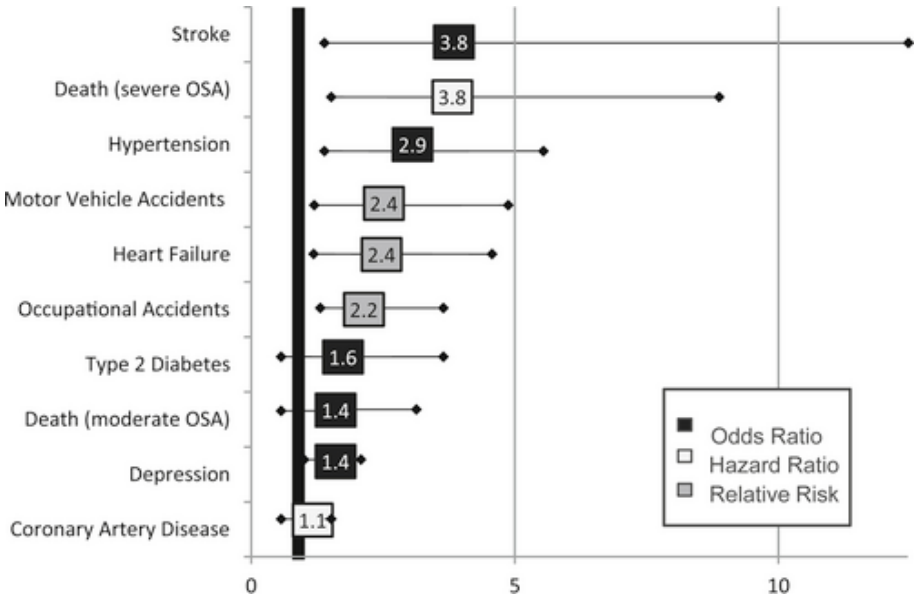

Figure 1.4: Increased risks in obstructive sleep apnea syndrome

The last being hazard ratio where the hazard rate (group event at any point of time) gives the Hazard Ratio that compares the event rate of events over time between two groups, here :

$$\frac{\text{Disease rate in OSA patient}}{\text{Disease rate in non-OSA patient}}$$

Based on the metrics on the Figure 1.4, obstructive sleep apnea significantly increase the chance in contracting a disease and higher risks are related to the severity of the undergone OSA. Since sleep apneas affect heart rate, blood pressure, blood oxygen levels and sleep continuity, many of the associated health complications involve the cardiovascular and circulatory systems as well.

When properly diagnosed, OSA is treatable. Lifestyle changes are recommended of obese patient as a weight loss would effectively reduce the frequency of apnea. The reduction in alcohol and tobacco use would reduce OSA frequency as well as lateral sleeping position. In extreme cases, gastrointestinal or upper airways surgeries are considered for obese patient.

The first-line treatment is continuous positive airway pressure (CPAP), which delivers continuous flow of pressurized air via a mask to maintain the airway open during sleep [11,13]. Alternatives treatments less frequent treatments include oral device on the mandible, surgical interventions or behavioral changes in sleeping. These treatments not only reduce apnea frequency but also improve quality of life by decreasing daytime sleepiness and improving alertness and mood

In summary, OSA is a serious and widespread disorder with serious health implications, yet it remains largely underdiagnosed. Its principal mechanism involves repeated airway obstruction during sleep, leading to physiological stress and many adverse effects. Effective treatments exist, but requires the patient to be diagnosed first. Developing a less intrusive and more user-friendly monitoring methods, such as non-contact electrode systems, could enable earlier detection of OSA and more widely access to diagnosis.

1.3 Comparison of electrode types

Physiological signals such as the electrocardiogram (ECG), electroencephalogram (EEG), and electrooculogram (EOG) are widely used to study and monitor human physiological functions and identify related diseases. Usually, these signals are recorded using disposable wet Ag/AgCl electrodes, which remain the

clinical standard because they provide high-quality signals, consistent and stable electrode-skin contact. The general principle behind electrodes is that they are the interface between biopotential signal, where the current is carried by ions in the body and electrical signals in the post-electrode circuit carried by electrons [26,27]. Different types of electrode exist, each corresponding to a different electrical equivalent circuit based on the electrode material, skin-electrode interface and body placement as the interactions between ions and electrons differ. The EOG signal, which is the main signal studied of this report, is also commonly acquired using wet electrode in different configurations, presented in the next section.

However, although wet electrodes offer good performance, they have some limitations related to comfort, hygiene, and signal stability during long-term recordings. The presence of the conductive gel reduces the electrode-skin impedance and improves signal quality [16]. However, The use of gel and the direct skin contact may cause discomfort, skin irritation, allergic reactions and signal degradation as the gel dries out.

These issues have motivated research into dry and non-contact electrodes, which aim to improve patient comfort and enable wearable and long-term duration monitoring [15–17]. New electrode types interact differently with the body, either through direct skin contact without gel for dry electrodes or without direct contact of the electrode with the skin surface by introducing a fabric or non conductive layer intermediate for the non-contact electrodes. These devices can be easier to use and more comfortable to the user at the cost of a lower signal precision. The main challenge is the increased noise affecting the signal, which must be filtered and amplified to obtain satisfactory results.

Each electrode type can be modeled with a different electrical equivalent circuit based on the properties of the electrode and the signal transmission principle. The equivalent circuit of the skin-electrode interface considers body resistance on one side, typically at the surface with the stratum corneum, different tissues in the body are modeled using a parallel resistor and capacitor. On the other side, the electrode receive the signal through a direct contact or capacitively with non-contact electrodes. These different topologies are compared to see the advantages of each in electrode-skin interface impedance, signal quality, skin reaction and user comfort.

This section compares three main electrode categories - wet, dry, and non-contact - focusing on their working principles, electrical characteristics, signal performance, skin-electrode interface. We also describe their equivalent electrical models and compare their advantages and disadvantages in typical biomedical applications.

1.3.1 Wet Electrodes

The particularity of wet electrodes is that they use a conductive electrolyte gel to ensure low-resistance contact between the electrode and the skin. The electrode surface is typically made of silver/silver chloride (Ag/AgCl) and are considered non-polarizable, in interaction with the skin, it behaves like a resistor in parallel with a capacitor.

Current flows between the electrode to the electrolyte (gel) based on the frequency of electrochemical reduction and oxidation reactions at the surface.The electrode interface does not allow any electronic or ionic charge transfer across the boundary. Instead, charges accumulates on both sides, creating a concentration gradient that fluctuates based on the measured physiological signal potential [26,27]. Here,the conductive gel acts as an ionic bridge between the metal electrode and the skin, significantly reducing impedance and stabilizing the electrode potential [15].

Advantages

- Low electrode-skin impedance and excellent signal quality.
- Stable and repeatable performance in controlled conditions.
- Well-characterized and widely validated in clinical practice.

- Commercially available cheap and disposable.
- Adherence to the skin with gel preventing motion artifacts.

Disadvantages

- Requires skin cleaning and gel application.
- The gel dries over time, increasing impedance, modifying the results and limiting the measurement duration.
- Possible skin irritation and allergic reaction.
- Not suitable for long-term or daily-life use [16].

1.3.2 Dry Electrodes

Dry electrodes are similar to wet electrode but operate without conductive gel, relying on direct physical contact with the skin. They are typically made from conductive metals, carbon composites, conductive polymers or flexible conductive surfaces to interface with the skin.

The conduction principle remains similar, with ionic charge accumulation near the electrode surface fluctuating with biopotential measured. However, the absence of electrolyte gel of dry contact electrodes result in a higher skin-electrode impedance, leading increase in thermal and motion artifacts. To compensate, front-end amplifiers must have very high input impedance. This kind of electrode are studied as a solution to avoid gel-related issues and reduce/avoid the skin preparation, making them more comfortable and suitable for home or wearable application [16]. Another challenge is maintaining stable contact with the skin, adding a adhesive material to stick the electrode would reintroduced the same disadvantages of wet electrodes while applied pressure on the electrode influences the amplitude of the signal.

In term of signal quality and comfort for the patient, dry electrodes lie between wet and non-contact electrode. They generally provide lower signal to noise ratio than wet electrodes but improve comfort, as it does not require skin preparation or adhesive material. While remaining more precise, less noisy and less comfortable than non-contact electrodes.

Advantages

- No gel or preparation needed.
- Reusable and suitable for long-term or wearable systems.
- Improved comfort and biocompatibility than wet electrodes.
- Can be integrated into portable devices.

Disadvantages

- Higher impedance and lower signal quality.
- More susceptible to motion artifacts.
- Performance depends on skin condition, pressure and movement.
- Require special high input impedance amplifiers (additional cost).

1.3.3 Non-Contact Electrodes

Unlike other electrode type, non-contact electrodes detect biopotentials without direct contact with the skin. They rely on capacitive coupling between the body and the electrode through a dielectric layer, such as clothing, air, or an insulating material.

The body and the electrode acts as the two plates of a capacitor and the body potential variations induce currents displacement across this capacitance. These electrodes are then buffered and amplified using ultra high input impedance amplifier (typically above 10 GΩ). The coupling capacitance depends on the dielectric constant, electrodes area and distance between the electrode and the skin [15, 17]. An estimation of the coupling capacitance considering the electrode dimension, dielectric impact and thickness can be made using

$$C = \frac{\epsilon_r \epsilon_0 A}{d}$$

Where **C** is the capacitance in F, ϵ_r is the relative permittivity of the dielectric and highly depend on the dielectric used, ϵ_0 is the vacuum permittivity ($8.854 * 10^{-12}$ F/m), **A** is the non-contact electrode capacitive plate area in m^2 and **d** is the gap between the plate and the body which correspond to the thickness of the dielectric in meters.

Many capacitive electrodes design and dielectrics have been reviewed by Umar *et Al.* (2021) [17]. This study examine multiple metal conductor used as the plate (Aluminum, gold, PCB, silver, copper) and multiple type of dielectric (metal compound, fabric-based or polymer-based). Each requires conditioning circuit and has advantages or constraints due to the dielectric or electrode material.

In our case, the capacitance of a printed circuit board-based non-contact electrode using cotton as dielectric is estimated based on the dimension of the designed electrode, the thickness and composition of the fabric layer. The printed circuit board for the electrode is designed to be approximately the size of a 2 euros coin, the radius of the measuring metal plate is 1.25cm resulting in an area of $A = 2\pi r^2 \approx 7.854cm^2 = 7.854 * 10^{-4}m^2$. The thickness of the dielectric fabric is $d = 0.52mm = 5.2 * 10^{-4}m$. The relative permittivity of cotton is not a fixed value, changes can occur due to the moisture content of the cotton. Dry cotton has a relative permittivity between 1.3-1.6 and between 4 and 10 for wet cotton as a dielectric [28]. Altogether, we can determine the capacitance for dry and wet case respectively :

For Dry Cotton ($\epsilon_r \approx 1.6$):

$$C_{\text{dry}} = \frac{1.6 \times 8.854 \times 10^{-12} \times 7.854 \times 10^{-4}}{5.2 \times 10^{-4}} \approx 21.3 \text{ pF}$$

For Wet Cotton ($\epsilon_r \approx 10$):

$$C_{\text{wet}} = \frac{10 \times 8.854 \times 10^{-12} \times 7.854 \times 10^{-4}}{5.2 \times 10^{-4}} \approx 133.6 \text{ pF}$$

Non-contact electrodes are particularly interesting in wearable health systems, sleep monitoring, long-term application, neonatal monitoring where comfort, hygiene and ease of use are essential.

Advantages

- No skin contact - highest comfort, more compatible with biological tissues.
- No preparation or gel required.
- Safe and convenient for continuous monitoring.
- Easily integrated into clothes or portable devices.

Disadvantages

- Signal recorded more affected by noise.
- Very high impedance (pF-level capacitance).
- Much more sensitive to motion artifacts and to 50Hz powerline interference.
- Require special amplifiers and careful signal conditioning (complexity and additional cost).

1.3.4 Electrical Equivalent Model of Electrodes and Skin

The electrical equivalent circuit of each electrode type can be represented by a combination of resistive and capacitive components that model the skin–electrode interface, as illustrated in Figure 1.5, adapted from Liu *et al.* (2023) [16]. The three configurations (wet, dry, and non-contact) show how electrodes are used in practice, including a physical representation of the electrode, its approximate size, and its contact mechanism.

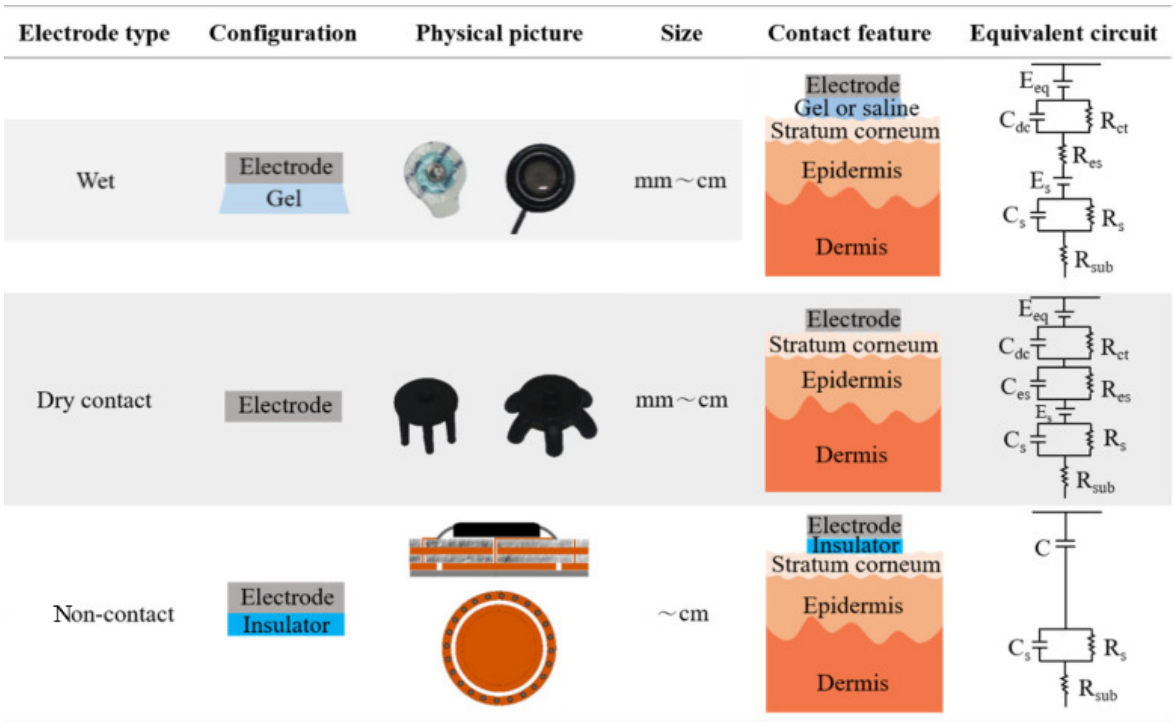

Figure 1.5: Electrode configuration, electrode skin region and equivalent circuit for wet, dry and non-contact electrodes

On the right side of the figure, the corresponding equivalent electrical circuits describe how the biopotential signal propagates from the body to the electronic front-end through the electrode, the gel or dielectric layer and the different layers of the skin. Each configuration highlights how resistive and capacitive elements are introduced or modified depending on the electrode type. In general, the interface is modeled by a parallel resistance and capacitance representing the electrode–skin interface, it is placed in series with the electrical properties of the skin layers described below [15]. Additional components are included or removed depending on whether the electrode uses conductive gel, direct contact, or capacitive coupling through an insulating layer.

The skin itself plays a major role in the impedance of biopotential measurements and is explicitly represented in the equivalent circuit for wet and dry electrodes. It is commonly modeled as a multilayer

structure composed of the stratum corneum, epidermis, and dermis. The stratum corneum, which is the outer layer, has a high resistance and capacitive behavior due to its low water content and acts as the main barrier to current flow. The deeper layers, namely the epidermis and dermis, are more conductive and contribute lower resistive components to the model. The relative contribution of each layer depends on the electrode type, contact quality and presence of gel or dielectric material. Since the non-contact electrode often uses a non conductive fabric dielectric, this element introduce a huge resistor in parallel with a small capacitor in series to the electrode capacitance in the model. The fabric dielectric makes the skin layer impedance negligible.

For wet electrodes, the conductive gel significantly reduces skin impedance and enables high-fidelity biopotential measurements. In the equivalent circuit, the gel is represented by a resistance (R_{es}) in series with the parallel combination of resistance (R_s) and capacitance (C_s) that model the skin impedance. The gel resistance is usually low, under 1 kΩ, while the skin impedance is typically between 10 kΩ and 100 kΩ with capacitance values around 10–50 nF [15, 16]. The low overall impedance allows wet electrodes to provide high-quality signals with minimal motion artifacts.

In the case of dry electrodes, there is no conductive gel, and the metal surface is in direct contact with the stratum corneum. This layer has higher resistance and similar capacitance, which increases the total impedance. In the equivalent model, the absence of the gel removes R_{es} and R_s becomes larger, between 30kΩ and 1MΩ, while C_s remain around 10–50 nF. However, dry electrodes usually need high-input impedance amplifiers to achieve similar signal quality as wet electrodes.

For non-contact electrodes, there is no direct contact between the electrode and the skin instead, a dielectric material such as fabric, plastic or air separates them. This structure forms a coupling capacitance (C) between the skin and the electrode, which replaces the direct resistive path found in wet or dry electrodes. The capacitance value of C depends on the dielectric constant of the material, the distance between the electrode and skin as described earlier.

The dielectric is not shown in the Figure1.5 non-contact model, if added an insulating dielectric layer would be the main source of impedance represented by a parallel capacitor and resistor in series to the shown model. The equivalent circuit includes this coupling capacitor in series with the skin impedance C_s and R_s (negligible when using a fabric dielectric).

To associate a order of magnitude for the input impedance of non-contact electrode using fabric dielectric, the skin impedance would lie around 100kΩ-1MΩ // 10-50nF, non conductive *fabric* dielectric around 200MΩ//20pF and the air gap would give between 1pF-1nF. As a result, non-contact electrodes have very high impedance compared to the other type of electrode and are more sensitive to motion and noise but they offer the advantage of comfort and hygiene. The challenge is to keep clear enough signal while removing as much noise as possible analogically.

1.3.5 Comparison and Discussion

These models highlight the trade-off between signal quality and user comfort that exists across different electrode types. According to what we saw, improving electrical contact at the skin–electrode interface reduces impedance and noise but often requires direct contact, skin preparation or liquid gel that may reduce comfort and usability during long-term recordings. On the other hand, electrodes designed to maximize comfort and minimize skin interaction typically introduce higher impedance and increased sensitivity to noise. Different electrodes are associated to variations in the equivalent electrical circuit, depending on their contact mechanism and interface properties.

After describing the principles and electrical models of wet, dry, and non-contact electrodes, it is important to compare their characteristics and performance. The following section presents a summary of their main features such as impedance, signal quality, biocompatibility, comfort, and usability. These parameters are based on recent experimental studies and reviews that evaluated the performance of different electrode technologies for bioelectrical signal acquisition [15–17].

Table 1.1: Comparison between electrode types

Property	**Wet Electrodes**	**Dry Electrodes**	**Non-Contact Electrodes**
Impedance	Low (2.8 kΩ-200 kΩ)	Medium (10 kΩ–2 MΩ)	Very High (>100 MΩ)
Signal Quality[1]	Excellent	Good to Moderate	Low to Moderate
Signal to Noise Ratio	24.9dB	3 to 24dB	1.8 to 3.7dB
Correlation	Reference[1]	60% to 98%	78% to 92%
Coherence	Reference[1]	34% to 90%	60% to 80%
Biocompatibility	Moderate	High	Very High[2]
Skin Preparation	Required	Not required	Not required
Comfort	Medium	High	Very High
Artifact Sensitivity[3]	Low	Medium	High
Maximal duration	Short (minutes–hours)	Medium (hours–days)	Long (days-week)
Usability	Clinical	Wearable	Clothes integrated
Typical Application	ECG/EEG/EOG	Home monitoring	Long term/sleep tracking

Table 1.1 summarizes the comparison between the three types of electrodes. Wet electrodes remain the reference standard for clinical applications because they provide the highest signal-to-noise ratio (SNR) and stable impedance. Dry electrodes offer a good balance between performance and usability, making them suitable for wearable devices. Non-contact electrodes prioritize comfort and hygiene but require complex amplification circuits and still suffer from motion-related noise [15–17].

[1]Signal quality section results were obtained mainly for weak EEG signals from Liu et Al [16]. The main factor to evaluate signal quality is the signal-to-noise ratio (SNR) used to compare the strength of signal of interest over the background noise. Correlation and coherence are 2 other factors that are also used to compare the similarity degree of dry and non-contact electrode to standard wet electrodes. These are respectively measured in time domain and frequency domain. Eventually, many studies and data were reviewed by Liu et Al. leading to a wide range of result for dry electrodes.

[2]Biocompatibility refers to compatibility of a external device to our physiological system without adverse reaction. The measurement system should not provoke any immune response or damage the subject. Some standardized methods are required depending on the application and the length of the measurement. Notably, some test requires in vitro cytotoxicity test and skin irritation test with the electrode presence. Results are different depending on the electrode type used for the experimentation but, overall, dry and non-contact electrodes were preferred as no gel was applied. Note that non-contact electrode does not have high biocompatibility due to the different dielectric are available, some material might be harmful due to chemical reaction with sweat. Very high biocompatibility is associated with a cotton dielectric.

[3]Artifacts in the final signal can appear due to the relative motion between the body and the electrode but not only. Signal changes could be the result of transversal or lateral motion, physiological signal which is not targeted, equipment interference and also environmental. Reduce or eliminate such artifacts requires computational techniques in combination of what is realize in this report.

Each electrode type has a specific range of applications depending on the trade-off between signal quality, comfort, and practical usability:

- **Wet electrodes**: ideal for precise, short-term measurements, clinically accepted and available.
- **Dry electrodes**: suitable for portable and medium duration monitoring with intermediate signal to noise ratio.
- **Non-contact electrodes**: Still in development for long term unobtrusive and seem-less monitoring, though still limited by high impedance and noise.

1.4 Fundamentals of the electrooculogram (EOG)

1.4.1 Definition and principle

The Electrooculogram (EOG) is a method used to record the electrical potential difference between the cornea and the retina [18, 29, 30]. This signal is measured using a pair of surface electrodes placed on the skin around the eyes, usually in the periorbital region. What the EOG records is the voltage difference between the front of the eye (positive cornea) and the back of the eye (negative retina). This electrical potential inside the eye is stable and does not depend on light condition. Because of this, the EOG can be measured even when the person is in complete darkness or has their eyes closed.

The electric potential across this dipole is called the corneoretinal potential and its amplitude usually lies between 0.4 and 1.0 mV while its useful frequency content lies between 0.1 and 12Hz. This standing potential originates from ionic gradients generated by the metabolic activity of the retinal pigment endothelium and the outer retina. Because this dipole is stable and always present, it serves as the source of the EOG signal. Eye movement cause a rotation in the dipole accordingly, which changes the potential detected by electrodes placed on the skin. It is important to note that the measured signal can be contaminated by other physiological signal such as the electromyogram, electrocardiogram or electroencephalogram which may occur in the same frequency range. External noise, interference and motion artifacts are also significant challenges in the measurement of the eye movement.

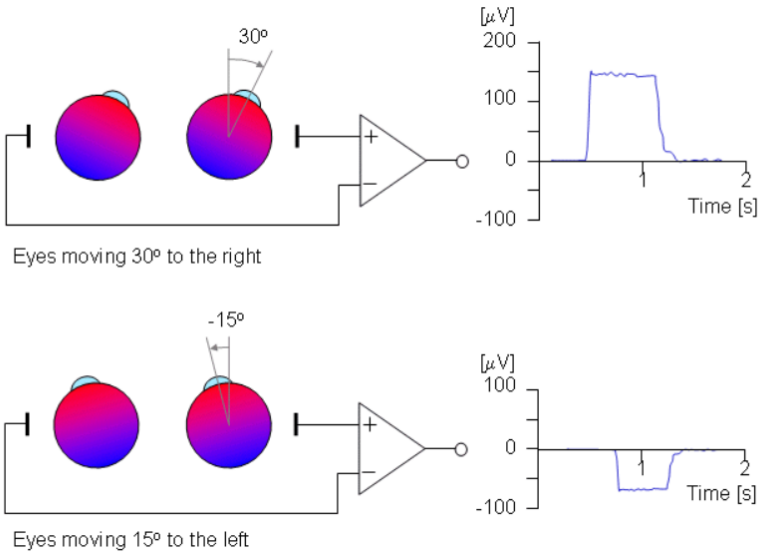

Figure 1.6: Electrooculogram potential measurement according to the eye movement

An example is shown in figure 1.6 [18], electrodes placed on each side of the eyes for horizontal EOG can sense how the positive pole (the cornea) moves closer to one side while the negative pole (the retina) moves toward the other. The EOG amplifier measures the difference between these two electrodes before and after the eye movement, which can occur in less than 500ms [29]. It produces a voltage signal that

corresponds to the rotation of the dipole between the initial and final eyes positions. In this case, moving the gaze toward the right electrode leads to an increase in measured potential while looking in the other direction decreases it. The signal amplitude is approximately proportional to the angle of eye rotation.

Because of this mechanism, the voltage variation recorded by the EOG provides direct information about both the direction and the amplitude of eye movement. The polarity of the signal indicates the movement direction. On average, the EOG signal changes by about 5 to 20 μvolts per degree of eye rotation. This relationship between angle and voltage is approximately linear for small angles, but becomes less accurate for larger eye movements.

Advantages

- Comfortable measurement using dry and non-contact electrodes EOG
- Can be embedded in wearable devices
- Simple device and cost effective
- Clinically established in polysomnography

Disadvantages

- Requires frequent calibration due to variability corneoretinal potential
- Susceptible to muscle artifact and baseline drift
- Interference from other physiological signals

1.4.2 Electrode placement and application

The previous setup uses two electrodes to determine the potential difference between the left and right sides of the eyes with an additional reference electrode often placed on the forehead. This configuration allow detection of horizontal eye movement but nothing in the vertical direction. For REM sleep detection, this is generally sufficient as it records increased horizontal eye movement activity from the random rapid eye movement. The timing and intensity of these movements are recorded and can provide relevant information about the user sleep stages.

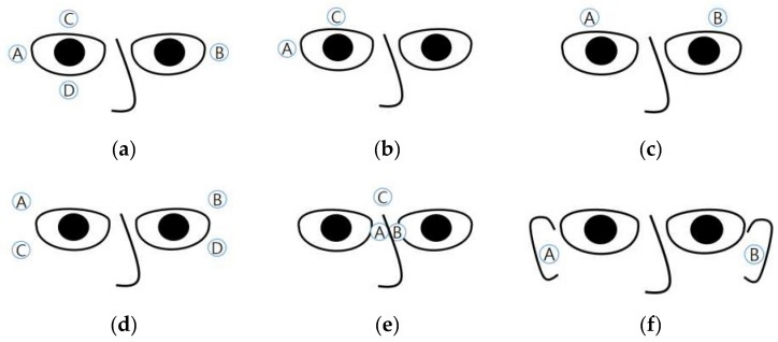

Figure 1.7: 6 electrode setups to measure the electrooculogram

However, other electrode placements exist for more precise eye movement measurements or improved wearability. Won-Du Chang (2019) [30] presented 6 different electrode configurations reported in the

literature to measure the EOG shown in Figure 1.7. Clinical EOG measurements for eye diseases diagnosis, polysomnography or human-machine interfaces through eye movements are typically measured using the 1.7a configuration. This allows to measure simultaneously horizontal and vertical direction using the difference of potential between electrode pairs A-B and C-D. With both signals, the continuous tracking of eye position can be used for diagnosis or human-machine interface.

Configuration 1.7b is a simpler alternative using only 2 electrodes. It is less precise and less stable than the full configuration but still achieve approximately 80% accuracy over 8 directions. Configuration 1.7c uses a headband with embedded electrodes positioned above or next to the eyes and detect mainly horizontal eye movement. This configuration is used in this work to increase comfort and usability for the final user. Configuration 1.7d uses 4 electrodes placed at the outer eye corners and detects multiple eye movements direction with an accuracy of approximately 87.1%. Configuration 1.7e embeds electrodes inside nose-pads of wearing glasses, allowing convenient measurement of both horizontal and vertical EOG. Finally, last configuration 1.7f records in-ear horizontal EOG signal, with lower precision compared to external electrode placements.

1.4.3 Eye movement during sleep

The EOG is an essential component of polysomnography (PSG), the clinical gold standard for sleep assessment, as it is used in conjunction with EEG and chin EMG to determine the transitions between wakefulness and the sleep stages [8].

Sleep is a complex and dynamic biological process essential for energy regulation, physiological recovery and brain maintenance. The sleep architecture consists of repeated cycles alternating between Non-Rapid Eye Movement (NREM) sleep and Rapid Eye Movement (REM) sleep [31, 32].

A typical sleep cycle begins with NREM Stage 1 (N1), a light sleep phase characterized by muscle tone relaxation and slowing brain wave activity. This progresses into Stage 2 (N2), a more stable light sleep stage associated with decreased heart rate and body temperature, representing approximately 45% to 55% of total sleep duration. The body then enters Stage 3 (N3), or deep slow-wave sleep, which is critical for physical recovery, immune system strengthening and tissue repair. Finally, the cycle ends with REM sleep, a stage characterized by vivid dreaming, rapid eye movements and brain activity similar to wakefulness. REM sleep plays a key role in memory consolidation and emotional processing while the body's voluntary muscles are inhibited.

The characteristics of eye movements detected by the EOG are used to determine these stages [18]:

- **NREM Sleep (Stages N1-N3):** During the transition into sleep (N1 and N2), eye movements are typically slow, appearing as slow rolling movements. In Slow Wave Sleep (N3/SWS), the deepest stage of NREM, physiological eye movements are minimal or completely absent.
- **REM Sleep:** This stage is physiologically characterized by a reduction in muscle tone (detected by EMG signal) and bursts of rapid eye movements, which stage's name is from. The EOG signal during REM shows high-frequency, high-amplitude deflections corresponding to the rapid changes in the eye position.

Monitoring these transitions is critical for diagnosing disorders such as obstructive sleep apnea (OSA). Respiratory events often cause brief arousals or micro-awakenings that fragment the normal sleep cycle, reducing the time spent in the restorative N3 and REM stages [11]. By tracking these sleep stages using EOG, the severity of sleep fragmentation due to respiratory disturbances can be indirectly assessed.

This chapter with the 5 first sections has described the EOG signal, electrode configurations and the difference of non-contact electrode based on its principle compared to clinical wet electrode for sleep

quality assessment. The electrodes used in the EOG constitute the front-end of the signal acquisition system. In addition to the non-contact electrode design, this work places particular emphasis on signal conditioning. The electrooculogram signals are affected by 50Hz power-line interference, physiological noise, motion artifact and have very low amplitude. The signal processing design is essential to filter out unwanted noise/interference and amplify the frequency content of interest to extract the usable EOG measured. These aspects are further developed in the next chapter, which focuses on the electrical design and prototyping of the proposed system.

1.5 Related studies on physiological signal acquisition system

All the information seen until now provides the necessary background on the clinical context, the targeted health condition, non-contact technologies and the signal we aim to measure. To complete the state of the art, this section reviews studies focusing on non-contact biopotential measurement, electrooculogram (EOG) monitoring systems and EOG-based sleep classification. These papers include the design of the front-end electrodes and the analog signal-processing chain required to measure physiological signals. By combining these implementations with our own bioelectronics knowledge [26], including wet-electrode ECG prototyping, we developed our own design for a non-contact EOG monitoring system.

1.5.1 Studies on non-contact biopotential measurements

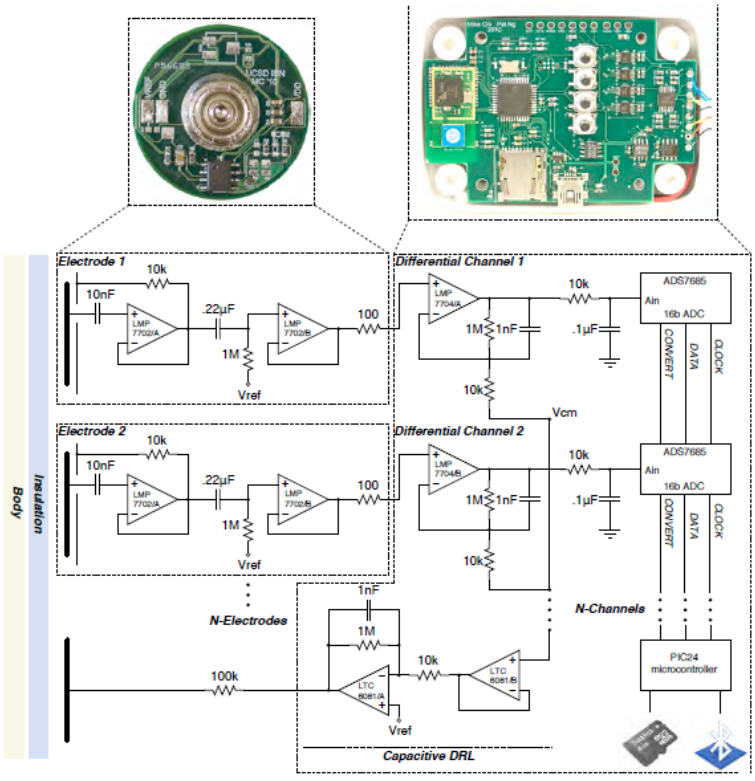

Figure 1.8: Schematics and PCB of Chi et al (2010) for wireless non-contact ECG/EEG system

One of the earliest complete work on non-contact electrodes was published by Chi *et al.* in 2010: "Wireless Non-contact Cardiac and Neural Monitoring" [14]. Their system uses a network of capacitive electrodes with a driven-right-leg (DRL) circuit to suppress common-mode interference, particularly 50/60 Hz power-line interference. The paper presents the advantages and limitations of non-contact electrodes together with the complete electrical schematic, PCB implementation and justification of design choice.

The electrodes rely on a LMP7702 operational amplifier combined with passive components to set the input impedance and filtering. Their design served as a reference for our own non-contact electrodes implementation, although the signal-processing board was adapted for EOG acquisition.

Figure 1.8 [14] shows the complete circuit schematics of the monitoring system composed of 2 main parts. The first part consists of multiple non-contact electrodes containing the sensing plate, shielding, buffering stage and a high pass filter. The second part is a separate signal processing base unit where amplification, digitization, active grounding and digital processing are implemented. Signal amplification is performed using a differential LMP7704 channel, digitization is controlled by a PIC24 microcontroller with an ADS7685 ADC and a capacitive driven right leg circuit provides active grounding. Data are transmitted wirelessly using a Bluetooth module. Experiments on ECG and EEG measured through clothing showed performance comparable to wet electrodes over short recordings (10 seconds). Stable operation was demonstrated for recordings lasting up to 10 hours. This work confirmed that non-contact electrodes can provide comfortable and reliable physiological measurements.

More recently, in 2022, Wang et al. published the paper "Flexible Non-contact Electrodes for Wearable Biosensors System on Electrocardiogram Monitoring in Motion" [3]. In this work, they developed a wearable ECG system using two flexible capacitive non-contact electrodes and a flexible driven-right-leg (DRL) electrode to reduce common-mode noise. The electrodes are built on a flexible printed-circuit structure with a central sensing plate, a shielding ring to reduce noise and signal stability during motion. The signal acquisition circuit is not detailed in this study as shown in Figure 1.9 [3]. The flexible electrodes are made of thin, round, 2-layer flexible PCBs without embedded electronics unlike the Chi et al implementation. The main board contains the power supply system, anti-aliasing filters, driven right leg active grounding circuit and an ADS1299 evaluation board for high-resolution signal acquisition and analog to digital signal conversion. The CC3200 module controls data acquisition and transmits the signal to a computer for real time display.

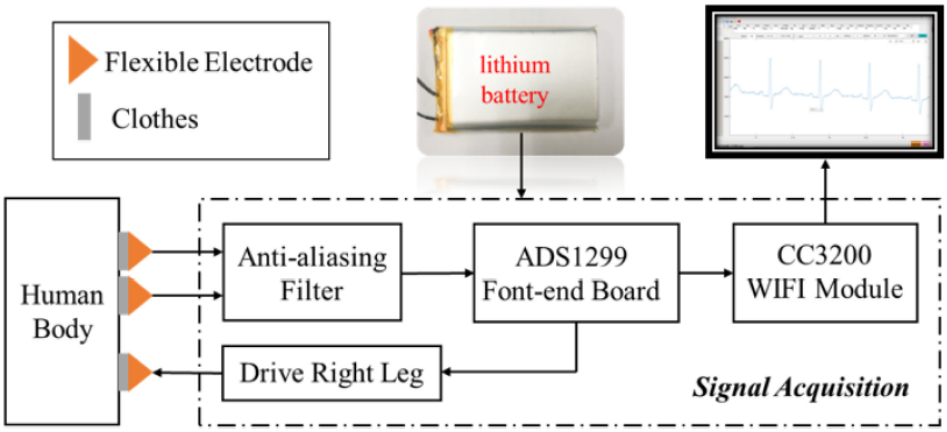

Figure 1.9: Design block diagram of Wang et al. (2022) flexible non-contact electrodes monitoring

The authors studied how several factors affect ECG measurement quality, including electrode size, insulation thickness and motion conditions. They tested three different electrode sizes and different insulation layers. They showed that thinner insulation and medium-sized electrodes provided the best compromise between signal quality and robustness. Motion tests were performed at walking speeds from 2 to 7 km/h, demonstrating that the clear ECG could still be detected with increased motion artifacts. Their non-contact electrodes achieved high correlation coefficient with standard wet electrodes in both "at rest"(99.7%) and "in motion"(97.53%) tests, with only a moderate drop in signal quality at higher speeds. Overall, Wang et al. demonstrated that flexible non-contact electrodes can provide reliable ECG monitoring during movement while offering better comfort and suitability for long-term wearable use.

1.5.2 Studies on electrooculogram acquisition and processing

Wearable devices using non-conventional dry or non-contact electrodes to measure the electrooculogram (EOG) are a less commonly researched subject in the litterature. Recently, S. Debbarma and S. Bhadra have published 2 studies on this topic. The first on the design of a dry contact EOG monitoring system published in 2021 "A Lightweight Flexible Wireless Electrooculogram Monitoring System With Printed Gold Electrodes" [33]. The second study on a non-contact version of the first study published one year later with improved robustness to noise, motion artifacts and multiple electrode pattern titled "A Flexible Wearable Electrooculogram System With Motion Artifacts Sensing and Reduction" [34].

In the first study, Debbarma and Bhadra designed a single-channel EOG acquisition system using printed dry gold electrodes on a thin, lightweight and flexible board. The electrodes, analog electronics (amplifier, filter, battery, wireless module) and power supply are all embedded on the same flexible board. It forms a single system headband simple to wear and suitable for long term measurement. The circuit design is described in detail, as shown in Figure 1.10 [33]. The system uses a rechargeable lithium-ion coin-cell providing up to 7 hours 40 minutes of operation. The gold electrode are directly patterned on the flexible PCB for the full acquisition system in one device. The headband is placed on the forehead with the electrodes over both eye, with a reference electrode positioned at the center of the forehead. The analog front end circuit is includes of high pass filters (fc = 1.6Hz) placed before and after the instrumentation amplifier, an 2nd order active Butterworth low pass filter (fc = 47Hz) and amplification stages using an INA818 (as instrumental amplifier) and a LMC6484 (as second stage amplifier set at high gain). Active shielding and driven right leg circuit are implemented to reduce capacitive coupling and common-mode noise. The micro-controller and Bluetooth module digitize and transmit signal to a receiving computer wirelessly.

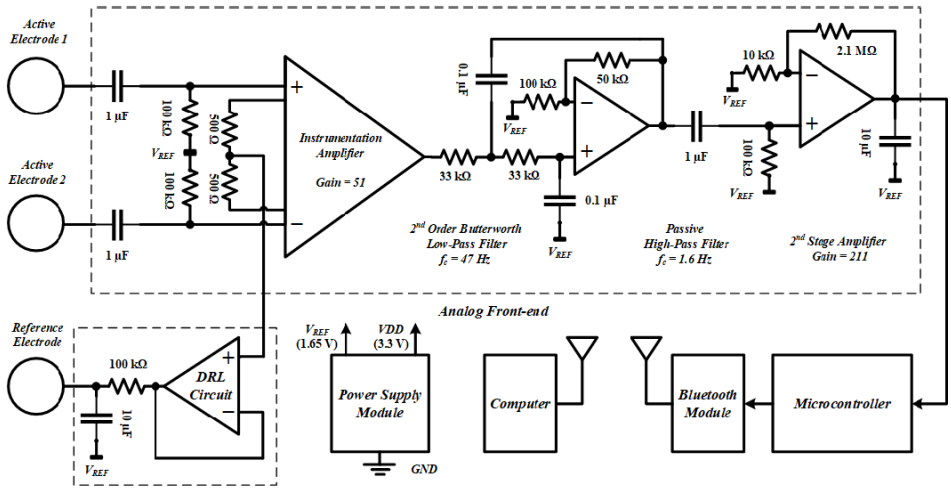

Figure 1.10: Complete circuit of the dry gold electrode on flexible board for electrooculogram monitoring by Debbarma et al (2021)

Experimental results demonstrated reliable detection of standard eye movements such as blinks, wink, horizontal and vertical rotations. The amplitude and waveform of the EOG signals were comparable to those obtained with clinical wet electrodes. Different electrode placements were evaluated and an additional feature-extraction algorithm was implemented to classify all eye pattern. The system achieved accuracy between 70 and 82.5% over a limited dataset. The authors also illustrated some potential use in REM activity detection and sleep monitoring where baseline EOG of Non-REM phase is followed by a high-frequency, high-amplitude signals during rapid eye movements.

In their second paper, the authors further developed the design toward a fully non-contact capacitive EOG system on flexible lightweight substrate. This version targets not only comfort and wearability but also improved robustness to motion artifacts. Such artifacts arise due to vibration, relative movement of the subject and air gap between the electrode plate and the skin. To reduce these effects, the non-contact electrodes are arranged in 2 pairs around the eyes, with optimized geometry and placement. In the case of non-contact electrode, skin-electrode impedance model modified due to the presence of dielectric and air gap capacitance, which depend on the electrode size, geometry, distance and the dielectric material. Sweat and motion further influence this impedance.

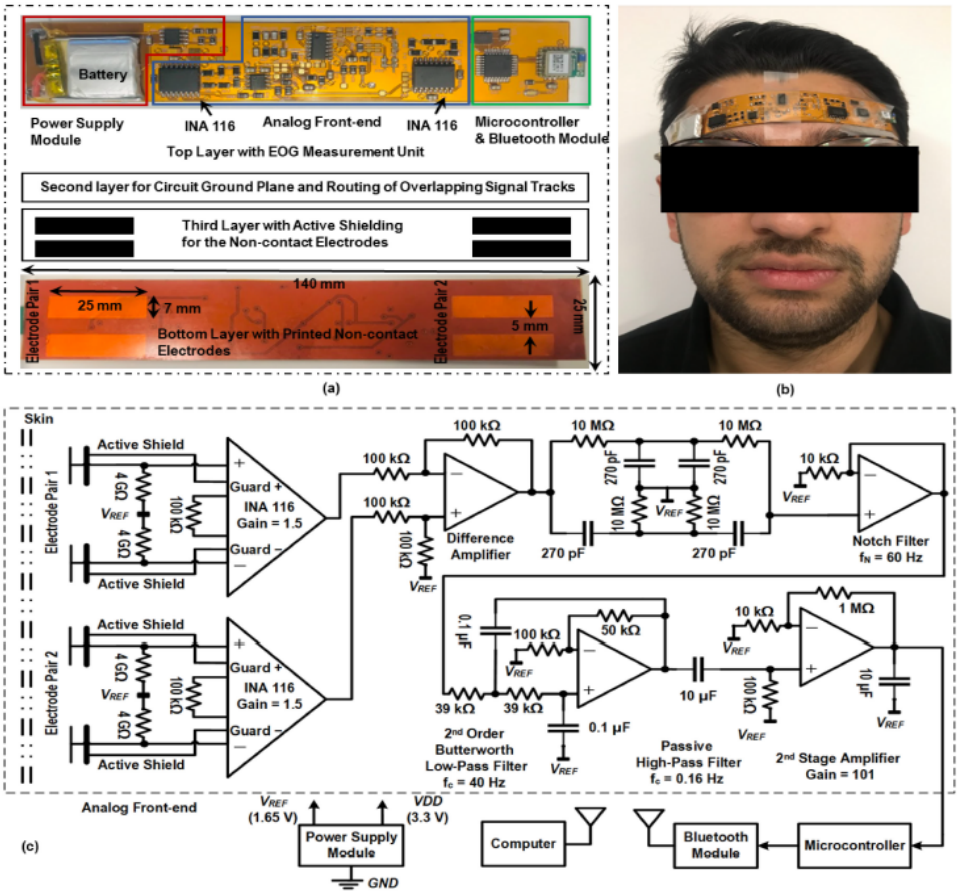

Figure 1.11: a) 4 layer flexible printed circuit board design, b) experimental setup associated with the FPCB, c) Circuit diagram for contact electrodes for EOG acquisition system on flexible PCB

The electronics circuit remains close to the previous design, as shown in Figure1.11 [34]. The flexible headband pcb design is shown and described on top of the circuit, it is designed to be worn on the forehead as can be seen in the b part. The updated system uses two pairs of non-contact electrodes with active shielding, two low-gain instrumental amplifiers (INA116), a difference amplifier and an additional notch filter for 50/60Hz interference. Unlike the earlier design, no driven right leg circuit is used. The same 2nd order low pass filter, high pass filter, second stage amplifier, microcontroller and Bluetooth module are retained.

By using 4 electrodes, the system can differentiate blinks, horizontal and vertical movements, while reducing motion artifacts. The measurement were realized under different conditions and the device could still detect key EOG features such as blinks and lateral movements under motion (small head or body movements). Motion however did introduce noise and decrease signal quality, 5 different electrodes con-

figurations (among circular, rectangular and interdigitated) are used to detect and suppress these artifacts. The authors showed that horizontally parallel circular/rectangular pair of electrodes significantly improved the reliability of the recorded signals.

Beyond sleep-related detection of eyes movements, EOG has been widely studied as a human-computer interface that can have great impacts for people with disabilities. Deng *et Al.* (2009) proposed a paper on "EOG-based Human–Computer Interface system development" [9] to acquire, amplify, filter and convert the eye movement to a digital signal. Their study reviews multiple eye tracking techniques using infrared video, infrared oculography, magnetic coil, optical eye tracking system and electrooculogram using clinical wet electrodes. The proposed hardware includes an instrumental amplifier (INA128), an adder to balance the signal, 2nd order active high pass filter (fc = 0.05Hz), second order active low pass filters (fc = 19-23 Hz) and a SPCE061A microprocessor. The results of the designed system is then analyzed digitally. The system achieved eye-movement classification with additional code and logic above 90%.

Electrooculogram sleep phase classification

A final relevant set of studies establishes link between EOG measurements and clinically meaningful sleep information. The system should be accurate and precise to measure physiological signals, it must be associated with diagnostic value targeted. Virkkala *et Al.*(2007) [6] describes "Automatic sleep stage classification using two-channel electro-oculography", demonstrating that EOG alone can be used for sleep staging with a 72-73% accuracy. This result shows that EOG signals segmented into 30-seconds epochs can provide useful sleep-stage information to the patient. By identifying time of micro-arousal, sleep-cycle disruptions and eye-movement patterns associated with apnea event, the electrooculogram could contribute in the diagnosis of sleep apneas or sleep cycle.

The study proposes an automatic method to classify sleep stage (separating wakefulness, rapid eye movement sleep REM, stage 1 sleep, stage 2 sleep and slow wave sleep SWS) based on 263 subjects polysomnography data. Half of the data were used for training purposes of the model and the remaining for validation. EOG signals were recorded near the left and right outer eye canthi and referenced to a mastoid electrode using a digital 16-channel Embla A10. Signal processing used 2 seconds analysis windows, frequency filtering by discrete Fourier transform and inverse discrete Fourier transform between 0.5-6Hz. Cross-correlation and peak-to-peak amplitude differences are used to determine associated sleep stages. Based on the preprocessed data, the sleep stage classification model is trained with 4 binary decision-tree to determine each sleep stages. Different thresholds are set to separate the features based on the determined cross-correlation and peak-to-peak amplitude. By applying the decision tree model the 5 stages of sleep/wake (wake, stage 1 sleep, stage 2 sleep, REM sleep, slow wave sleep) are determined. Their results show that reasonably good sleep-stage information can be obtained using only EOG signals instead of full data from polysomnography. The final model achieved an overall epoch-by-epoch agreement of approximately 72% with clinical sleep scoring, demonstrating that meaningful sleep-stage information can be obtained from EOG signals alone..

Chapter 2

Experimental section

The base of the implementation of our work started from the development of an analog wet-electrode ECG measurement device on a breadboard. This project, associated with the theoretical information given in Prof. Redouté Bioelectronics course [26], provided the essential knowledge for physiological signal monitoring. The different design choices for the amplifiers, filters and driven right leg are based on this theory and on complementary scientific papers such as the circuit found in articles from the previous section [2,9,14,33,34]. The particularity of our work compared to the initial ECG monitoring lies in 3 main aspects : (1) non-contact electrode measurements, which require electronics for impedance conditioning integrated into the design of the electrode [35–37], (2) specific tuning of the filters for electrooculogram frequency range and (3) the need to limit noise effects, especially 50Hz power-line interference, in the output signal.

The first section is dedicated to the description of each element used in our implementation. Elements from the main signal processing board and the front-end non-contact electrodes are overviewed together with the source of interference. In our work, we use multiple filters, instrumentation amplifier, buffers, second stage non-inverting amplifier and a driven right leg circuit all of which require tuning of the associated resistance and capacitance values. An adaptation to the lower amplitude signal (0.4-1 mV) and lower bandwidth (0.1-10 Hz) of the electrooculogram is necessary to obtain a clean and measurable output.

The signal recorded by non-contact electrodes is significantly noisier and more susceptible to interference than signals from wet or dry electrodes. This is due to the fundamental difference in how they couple to the body (capacitive coupling instead of a mainly resistive path). The high impedance makes the system very sensitive to common-mode (CM) noise, especially from the 50 Hz power grid. The power-line interference effects are discussed to see their impact on the resulting signal. Non-contact electrodes are also more susceptible to motion artifacts, because any relative movement between the electrode and the skin significantly modifies the electrical properties of the interface.

When every basic element has been described and tuned for non-contact electrooculogram acquisition, the electrical circuit must now be simulated and tested on a breadboard prototype to verify that the concept works. LTSpice is the software used in this work to simulate the circuit using transient and AC analysis over successive versions of our acquisition system. Using these analysis allow us to predict the effect of each component in the system, including whether it will amplify the signal of interest while reducing 50Hz and other sources of noise with filters.

Software analysis gives important insights about the system and signal behavior but hardware testing remains necessary to confirm that the non-contact electrodes can work in practice. We reproduced the simulated circuit on a breadboard while testing with different type signal transmission (with wet, dry and non-contact electrode). This prototype gave us important insights that were taken into account in the

PCB design. We identified several key aspect, such as the useful tuning range for the filter cutoff frequencies, the need for a notch filter and the role of a grounded reference electrode. These are further discussed in the corresponding subsection.

Based on the results from the previous analyses and test, we designed our own printed circuit board version to measure eye movement in a non-contact matter. The last section focuses on the specificities the design of the PCB version of the electrode and the main board. The main differences with previous version is associated with the use of variable resistance used to adapt the cutoff frequency/bandwidth of the filters, to change the gain of amplifiers in different stages and the power supply management. This section describes the different subpart in the physical PCB implementation.

Altogether this chapter give the principal steps of evolution of our project design. This leads to the final design tested in the following chapter. It is used together with the cotton headband designed to comfortably maintain the electrode on the forehead.

2.1 Front end and analog physiological signal monitoring

The design of our non-contact electrode acquisition system is based on already existing examples and theory. Figure 2.1 modified from [35] gives an overview of the main elements required for this type of system. This section focuses on the theoretical basis associated with the elements used in the software simulation, breadboard prototype and final PCB implementation. As shown in the block diagram, we divide our implementation in 2 main stages :

The front-end electronics, used to detect the capacitive physiological signal with buffers/preamplifiers for the impedance matching and high pass filtering; and the main analog signal conditioning board, dealing with amplification (including additional preamplification), filtering and active grounding through a dedicated driven right leg circuit. The filtered and amplified output signal is then sent to the measuring unit, in our case the oscilloscope, which displays the signal evolution over time. Using the measured data, we have written a python code to analyze and extract essential features. This last part could be realized using a micro-controller with an ADC and a wireless communication system (Bluetooth or WIFI) to transfer the data to a receiving unit, as found in the related studies. This section is mainly based on the work realized by I.Sadighiani (2019) in her master thesis in the University of Liège called "Design and implementation of a contactless ECG acquisition system" [38] modified and adapted for the electrooculogram acquisition.

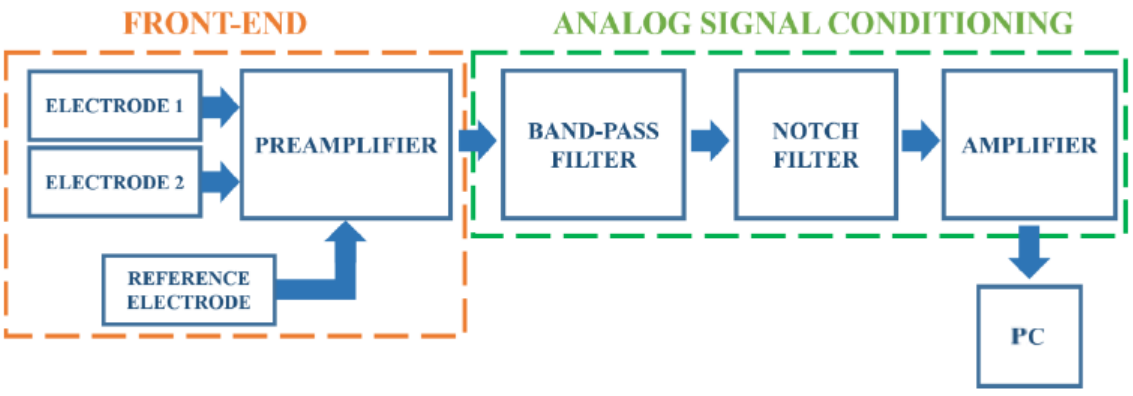

Figure 2.1: Overview block diagram of main elements required on the main board and on the non-contact electrodes

2.1.1 Front-end non-contact electrode

The front-end non-contact electrode based on the Chi et al. (2010) implementation of Chi et al (2010) [14]. Figure 2.2 represents the circuit used in our application, although some modifications in the high pass filter characteristics may be considered. Other existing implementations for the non-contact electrodes are proposed by Portelli et al. and Parente et al. [35, 36].

These electrodes are implemented on a printed circuit board and require additional design consideration described in the section 2.3. They couple capacitively to the body through the bottom copper-fill sensing layer on the PCB, measuring the electrical potential variation arising from the corneo-retinal potential. The recorded eye movements signal is affected by broadband noise from other physiological sources, thermal noise and electromagnetic interference. These effects must be addressed in the analog processing chain.

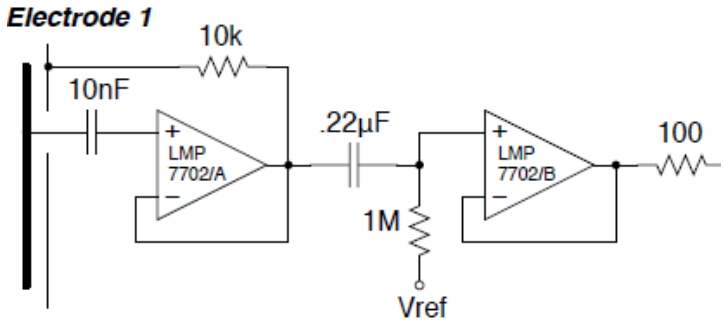

Figure 2.2: Non-contact electrodes schematics

As shown in Figure 2.2, this electrode includes both active and passive components. Each electrode, we use 2 capacitors, 3 resistors and 2 operational amplifiers acting as buffers. It uses a LMP7702 [39], an inexpensive, high precision, low noise CMOS operational amplifier suitable for ultra-high impedance applications. This op-amp is used as a buffer directly on top of the electrode. It handles the high impedance of the skin-electrode interface and converts it to a low-impedance output that can be processed by the rest of the system.

Impedance buffers

We have determined in a previous section that the coupling capacitance of the non-contact electrode is quite small, about 21pF. The capacitive impedance is given by $Z_c = \frac{1}{2\pi f_c}$ and is inversely proportional to both frequency and to the capacitance. Since the EOG signal lies at low frequencies and the capacitance is small, the resulting impedance is very high. In addition, the dielectric layer used with non-contact electrodes further increase the effective impedance. A fabric layer such as cotton can be represented by a parallel $200M\Omega$ resistance and a $20pF$ capacitance [17]. Together, these elements raise the non-contact electrodes impedance up to hundreds of mega-ohms, which is several order of magnitudes above the wet electrodes (where the gel helps to reduce impedance) used in clinical applications.

Given that the electrode-skin interface impedance can be in the hundreds of mega-ohms range, the front-end amplifier must have an input impedance that is several orders of magnitude higher to avoid loading the electrode. A high input impedance is essential to prevent signal attenuation, loading of the recording electrode and affect the characteristics of the electrodes causing waveform distortion.

Signal attenuation occurs when a voltage divider is formed between the electrode impedance and the amplifier input impedance. The voltage at amplifier input is given by :

$$V_{in} = V_s \frac{Z_{in}}{Z_s + Z_{in}}$$

where V_{in} is the amplifier input voltage, V_s is the physiological surface voltage, Z_{in} is the amplifier input impedance and Z_s is the electrode skin interface impedance. If the amplifier input impedance Z_{in} is too low, this signal is attenuated. Therefore, the ratio $\frac{Z_{in}}{Z_s}$ should be large enough for V_{in} to avoid signal attenuation and remains close to V_s.

When the amplifier input impedance is too low, the resulting current through the interface

$$I = \frac{V_s}{Z_s + Z_{in}}$$

becomes non-negligible and flows through the electrode–skin interface. this can modify the interface behavior and introduce distortions in the measured signal.

For these reasons, the amplifier is used as a unity gain buffer. The signal should not be amplified nor attenuated and almost no current from the electrode should be drawn from the electrode so that the measurement is not disturbed. By doing this, the amplifier preserves the original biopotential and transfers it to the rest of the circuit with much a lower op-amp output impedance, before any filtering or amplification performed on the main signal-processing board. LMP7702 is well-suited for this task because its extremely high input impedance, very low input bias current and lower output impedance. It allows the electrode voltage to pass the amplifier too the main board without significant loading, preventing attenuation and distortion even when the source impedance is extremely high, as in capacitive EOG sensing.

To further stabilize the input stage, Chi's design includes a $10k\Omega$ resistor and a 10 nF capacitor. The $10k\Omega$ resistor electrically isolates the amplifier output from the active shield/guard, preventing the shield capacitance from feeding back into the input and causing instability or oscillations. The 10 nF capacitor acts as an input protection and filtering element: it limits fast voltage changes, reduces high-frequency interference and protects the input from sudden charge injection caused by motion or electrostatic effects. Together, these components improve the stability and robustness of the ultra-high-impedance front-end without affecting the low-frequency EOG signal. [14]. In addition, they contribute to patient safety in case of a amplifier default to prevent the supply 5V DC signal to provoke a macro-shock. These occurs when electric current flows through biological tissues, this could be possible through the electrode sensing area or the guard. On top to the very high impedance from the fabric impedance (>100MΩ), the resistor and the capacitor discussed here also serve to limit macro-shocks. The shield/guard part is further discussed in the PCB design section to provide an complete view of the electrode design.

Because capacitive electrodes do not naturally provide a DC path for biasing network for the amplifier, their output includes a floating and undefined DC offset. This offset must be removed early in the chain to avoid saturating later amplifier stages. For this reason, a passive high-pass filter (HPF) is inserted after the unity-gain buffer. With a cutoff frequency around 0.7 Hz, this filter removes slow variations, electrode drift and centers the signal around a defined reference voltage. Filter characteristics are discussed together with the other filter designs in section 2.1.3.

Following the high pass filter, a second amplifier buffers the signal further reduce the impedance, isolate the high-impedance stage from the rest of the system and maintain signal integrity over long interconnection. This reduction in impedance comes with a tradeoff in power consumption because it requires an additional active component. Cables and PCB traces add a capacitive load at the amplifier output that can cause instability. The 100 Ω series resistor isolates this capacitance, limits fast current and keeps the amplifier stable so the signal can be transmitted without distortion. Overall, the impedance adaptation stage guarantees that the biopotential is transferred with minimal distortion.

2.1.2 Noise sources

Physiological signal monitoring devices are subject to several fundamental noise and interference mechanisms. Since the amplitude of the EOG lies between a few tens of microvolts and several millivolts, many

noise sources can easily exceed the magnitude of the useful signal [26, 27, 40]. Disturbances may originate from the man-made electromagnetic activity in the environment, often refered to as ("electrosmog"), including 230 V power-lines, radio transmitters, mobile phones and railway systems. According to Webster, these external fields couple into biopotential front-ends through capacitive coupling, inductive coupling and common-mode injection.

A second important noise mechanism is thermal noise, caused by random movement of charge carriers inside conductors. All resistors and semiconductor devices in the circuit contribute thermal noise, which set a lower limit on the smallest detectable signal in systems. Thermal noise has a white power spectral density, meaning that its uniformly distributed over the frequency spectrum. In non-contact electrodes, the high impedance associated with skin-electrode impedance and dielectric layer can reach hundreds of MΩ, which significantly increases thermal noise at the amplifier input. Thermal noise is represented by the root mean square (RMS) voltage $V_{n,rms} = \sqrt{4KTR\Delta f}$ where K is Boltzmann's constant, T is the absolute temperature in K, R is the resistance value and Δf is the bandwidth. From this expression, it is clearly visible from the formula that both the impedance of the electrode and the system bandwidth strongly influence the thermal noise component.

Motion artifacts form another major noise category. They result from mechanical changes at the electrode–skin or electrode-fabric interface, which cause fluctuations in the coupling capacitance and can generate static electricity. For non-contact electrodes, even small movements of the fabric or variation in the air gap can significantly modify the capacitive coupling, producing large low-frequency artifacts. In addition, noise originating from other physiological signals, as the ECG or EMG, can interference with the EOG signal because of overlapping frequency ranges.

These disturbances strongly affect the measured input signal, especially when using high-impedance non-contact electrodes, making the system particularly sensitive to noise. This reduces signal accuracy and makes interpretation more difficult, as noise can complicate the useful signal interpretation or be confused with physiological activity. It is essential to address these effects using multiple complementary strategies in the acquisition system design. Filtering, shielding, preamplification and active grounding are among the techniques used in our implementation to reduce noise impact.

Power-line interference

In most biopotential systems, 50/60 Hz power-line interference is the dominant source of disturbance and this effect is even more pronounced for high-impedance electrodes. The electric power distribution network generates both electric and magnetic fields that couple into the measurement system. As a result, a 50 Hz unwanted component appears in the recorded signal, reducing the signal-to-noise ratio. Non-contact electrode setups, due to their very high input impedance, are especially affected by power-line interference, as shown later in this chapter through experimental measurements.

Figure 2.3, adapted from J. G. Webster's Medical Instrumentation (2009) [27], identifies three main coupling mechanisms between the power-line and biopotential measurements. The original calculations were performed for wet contact electrodes. In the following discussion, these formulas are adapted to non-contact electrodes, for which the skin–electrode impedance is several orders of magnitude higher.

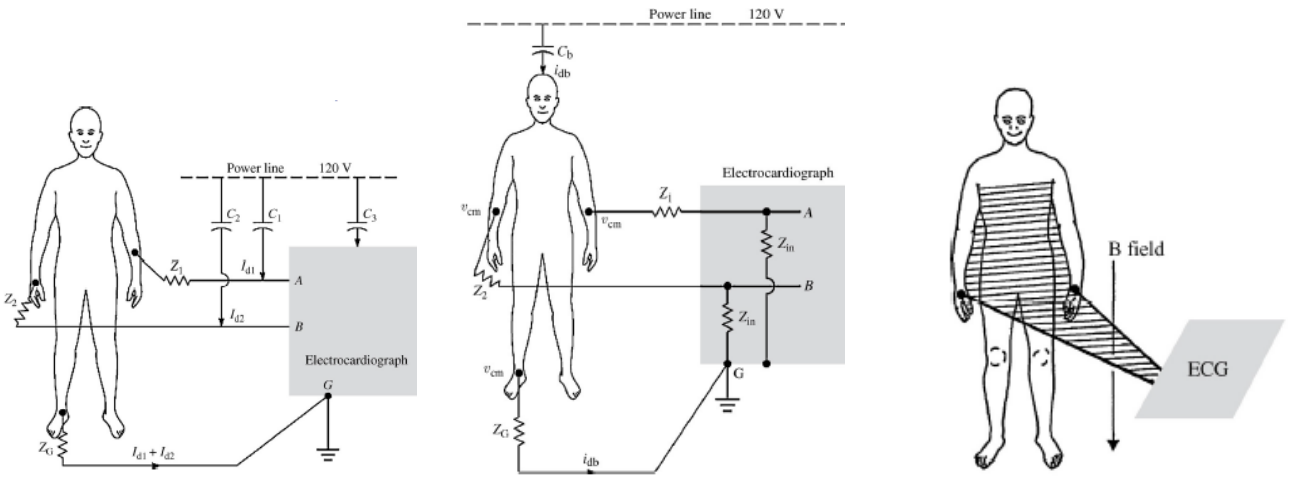

(a) Case 1 electric coupling with leads and device

(b) Case 2 electric coupling with body

(c) Case 3 magnetic field coupling

Figure 2.3: Power-line coupling schematics

In the first case, the power-line capacitively couples with the acquisition system, including the electrodes and connecting wires. Because the amplifier input impedance is much larger than the skin–electrode impedance with the buffering stage at the electrode, displacement currents flow through capacitances C_1 and C_2, through the body, toward earth potential. Based on this model, Webster derived the differential voltage generated by power-line interference between electrodes v_A and v_B as

$$v_A - v_B = i_{d1}Z_1 - i_{d2}Z_2$$

In their numerical example, $i_{d1} = i_{d2} = 6$ nA and the skin-impedance mismatch between electrodes was approximately 20 $k\Omega$. In our application, the skin–electrode impedance mismatch can reach values as high as 200 $M\Omega$. Because of the much higher impedance, the coupling current is expected to be lower and we assume a value of approximately 5 pA. Applying Webster's formula gives $v_A - v_B = (5pA).(200M\Omega) = 1mV$ which is significantly higher than the value obtained with wet electrodes (120 μV). This interference amplitude is of the same order of magnitude as the EOG signal of interest (0.4–1 mV), making it non-negligible. It must be considered in the system design and appropriate strategies must be implemented to reduce its impact on the output signal.

The second case involves capacitive coupling between the power-line and the body, represented by capacitance C_b. In this configuration, a displacement current i_{db} flows from the power-line through the body to earth without passing through the electrode leads. In Webster's example, values of $i_{db} = 0.2$ μA and ground impedance $Z_G = 50$ $k\Omega$ were used, leading to a common-mode voltage on the body of $v_{cm} = i_{db}Z_G = 10mV$. For non-contact electrodes, especially when using a capacitive reference or ground electrode, both i_{db} and all impedance values differ from those in Webster's model. This can result in larger common-mode voltages, although additional measurements are required to quantify this effect precisely.

In both cases, the conversion of common-mode voltage into a differential interference voltage depends on the finite input impedance Z_{in} of the amplifier. Assuming a known mismatch between electrode impedances and $Z_1, Z_2 \ll Z_{in}$, the differential interference voltage can be approximated as

$$v_A - v_B = v_{cm}\frac{Z_2 - Z_1}{Z_{in}}$$

For wet-electrode ECG measurements, using $v_{cm} = 10mV$, $Z_2 - Z_1 = 20k\Omega$ and $Z_{in} = 5M\Omega$ results in a noticeable but manageable interference in the differential voltage. In non-contact EOG systems, all

these values in the equation are increased, making the interference more severe. Depending on the ratio between v_{cm}, $Z_1 - Z_2$ and Z_{in}, the interference can have more or less impact in our circuit. Experimental measurements presented in the next chapter confirmed that non-contact electrodes have strong 50Hz components (with its harmonics) mainly due to electric-field coupling with power-line.

Common-mode noise arises from these coupling mechanisms between the power-line and either the body or the measurement device. To reduce its impact, biopotential amplifiers are designed with a high common-mode rejection ratio (CMRR), often exceeding 80 dB, meaning that differential signals are amplified 10,000 times more than common-mode signals [26]. However, as shown in the previous equations, mismatches in skin–electrode impedance can convert common-mode signals into differential interference, limiting the effectiveness of CMRR alone.

Figure 2.3(c) illustrates magnetic-field coupling and how the acquisition is influenced. A loop formed by the patient, the cables and the acquisition system which can be penetrated by a magnetic fields, inducing unwanted voltages. Reducing the loop area is important to limit magnetic coupling, this can be achieved by twisting the wires and using magnetic shielding. Additionally, nearby electronic devices such as phones or televisions can generate electromagnetic interference.

All the mechanisms described above contribute to an increase in interference amplitude. However, several strategies can be applied to reduce noise and improve the signal-to-noise ratio. For example, thermal noise can be reduced by minimizing resistance values where possible and by limiting the system bandwidth to the frequencies of interest using band-pass filtering.

To reduce power-line coupling, both passive and active shielding techniques can be applied to electrodes and cables. In our non-contact electrode implementation, the first buffer is also used to actively drive the guard layer, reducing capacitive coupling. Another effective approach is lowering the reference electrode impedance. During LTSpice simulations and experimental tests, we observed that using a non-contact electrode for signal acquisition combined with a dry or wet reference electrode significantly reduced the 50 Hz interference. This observation highlights the critical role of the reference electrode in overall signal quality. Studies such as Umar *et al.* (2021) [17] further investigate how electrode materials and dielectric properties influence impedance and noise performance.

Finally, additional noise attenuation is achieved through careful circuit and component selection. These aspects are discussed in the next section and include filtering (high-pass, low-pass, and notch filters), driven-right-leg circuits to actively suppress common-mode voltage, and the use of components with high CMRR and power-supply rejection ratio (PSRR), such as the LMP7702 and INA128 used in this work.

2.1.3 Main board design

After the front-end electrodes, the signal sent to the main board is already buffered. It keeps the same waveform as the biopotential signal but with a much lower output impedance.

Biopotential signals measured on the body surface have a very small amplitude (especially for EOG, ranging from a few tens of μV up to a few mV). As a consequence, the raw voltage collected at the electrodes is often too small to be directly measured at this stage. It can easily be hidden by DC offsets, noise, and 50 Hz interference. For this reason, a biopotential acquisition system includes an analog signal conditioning stage that amplifies the useful signal and limits unwanted components outside the frequency range of interest by using filters.

To realize this, we use an instrumentation amplifier, passive and active filters, a driven right leg circuit and a non-inverting amplifier. Our implementation for the main board design is based on another project from J.-M. Redouté's Bioelectronics lecture [26]. This previous project aimed to monitor the ECG with wet electrodes; several modifications are required to adapt it to non-contact electrode EOG monitoring.

Supplementary references are used to adapt our project, the work from I. Sadighiani (2019) [38] was particularly helpful, together with several scientific articles [14, 33, 35, 36].

These functions correspond to the classical chain of a non-contact biopotential amplifier as can be seen in Figure 1.5: (optional preamplification) + band-pass and notch filtering + reference electrode + second-stage amplification + output to the oscilloscope and computer. The design of these components is detailed in this section.

Biopotential amplifier

Biopotential amplifiers have specific requirements. The input impedance must be very high to avoid loading the electrodes and attenuating the recorded signal, as explained in the previous section. The output impedance should be low compared to the following stage so that the conditioned signal can be transmitted and measured without degradation. In addition, the amplifier must be able to detect very small voltage variations, which requires a high sensitivity and a stable, well-defined gain. Since physiological signals are very small, low input noise is essential to prevent the signal from being masked by noise. Good precision and linearity are also required so that the amplified signal accurately represents the original biopotential without distortion. Finally, a high common-mode rejection ratio (CMRR) and a good power supply rejection ratio (PSRR) are important to reduce interference from the environment and from the power supply, which is particularly critical in high-impedance, low-frequency applications such as non-contact EOG monitoring.

INA128 To meet these requirements, we connect the designed electrodes to an instrumentation amplifier. This component performs a differential measurement with a high common-mode rejection, while providing a first amplification step with low noise. This is ideal in physiological non-contact measurements, where common-mode interference can be orders of magnitude larger than the useful differential signal.

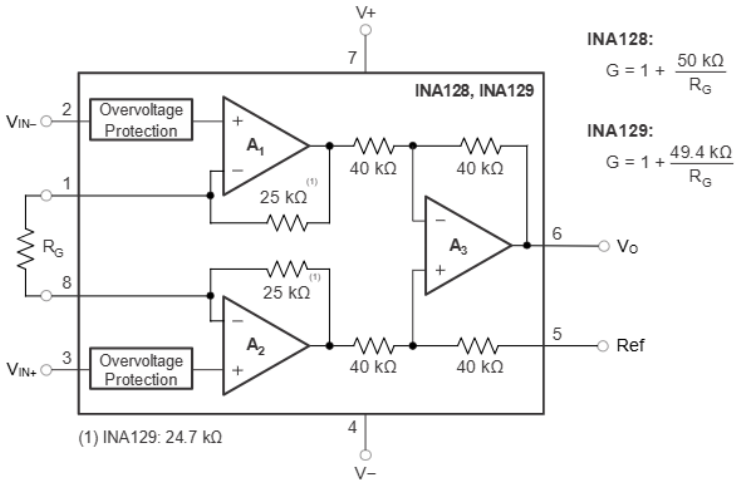

Figure 2.4: INA128 simplified schematics

In our design, we use the INA128 as instrumentation amplifier [41], shown in Figure 2.4. A first advantage is that it converts the differential input signal into a single output. This simplifies the design of the following filter stages and reduces errors caused by component mismatch. A second advantage is that it provides a well-defined gain for the low-level biopotential signal without adding significant noise. In addition, the instrumentation amplifier offers a high common-mode rejection ratio (CMRR) of approximately 120 dB, which attenuates common-mode noise such as power-line interference and improves the overall signal quality. The gain of the INA128 is set by an external resistor R_G and is given by the equation:

$$G = 1 + \frac{50k\Omega}{R_G}$$

Therefore, by selecting R_G (or using a variable resistor), the amplification can be adapted to different subjects and measurement conditions.

However, choosing the gain is a trade-off. If the gain is too large at the very beginning of the chain, noise and electrode DC offsets are amplified as well, which can reduce performance and even lead to saturation before the main filtering steps. For this reason, the instrumentation amplifier gain must be chosen carefully and combined with appropriate filtering and common-mode reduction techniques, such as a driven right leg circuit, in the rest of the signal conditioning board.

Second stage amplification After the instrumentation amplifier and the main filtering stages, a second amplification stage is implemented using a non-inverting amplifier configuration. This stage provides additional gain to obtain a usable output signal level for measurement and analysis. In theory, the gain of the instrumentation amplifier is intentionally kept limited in order to avoid excessive noise amplification and bandwidth reduction at the early stage of the acquisition chain. In practice, this assumption was not fully confirm by our experiments, as low gain instrumental amplifiers configuration performed worse than higher-gain counterparts. This behavior can be shown with LTSpice model where the low gain INA did not sufficiently amplify the EOG signal and most of the useful information was filtered out before the second stage amplification.

By placing this second gain stage after the filters, most 50Hz and out-of-band noise components are already attenuated, which reduces their impact when higher gain is applied. The gain of the non-inverting amplifier is defined by the resistor ratio $G = 1 + \frac{R_1}{R_2}$ which allows simple and flexible adjustment, notably by using a variable resistor as R_1. In our design, the LMP7702 [39] is used for this stage because of its high precision, low noise, high input impedance and good stability, making it well suited to provide additional amplification while preserving the quality of the filtered EOG signal.

Driven right leg and grounding

In biopotential measurements, a large part of the environmental electromagnetic interference couples capacitively to the human body and appears as a common-mode voltage at the electrode inputs. This common-mode voltage is often much larger than the useful differential signal and cannot be fully removed by analog filters alone, especially at 50 Hz (and its harmonics). The very high electrode–skin impedance makes the system highly sensitive to 50 Hz common-mode interference.

To reduce this disturbance, we evaluate two approaches : the active Driven Right Leg (DRL) feedback loop is commonly used in physiological signal acquisition systems [14, 26, 27]. An alternative approach proposed in several related studies a simpler capacitive reference electrode connected to circuit ground, without using the driven right leg circuit [35,37].DRL provides an active feedback and capacitive grounding is passive body reference to the circuit ground. Both approaches are implemented and evaluated in our design to determine which provides the best performance at the output, while preserving the EOG signal and reducing 50 Hz interference.

Driven Right Leg The principle of the DRL circuit is illustrated in the electrical model shown in Figure 2.5 [26]. The common-mode voltage v_{cm}, which is present at both input electrodes, is first sensed by the front-end amplifier. This common-mode component is then inverted, amplified, and fed back into the body through a reference electrode (traditionally placed on the right leg for the ECG, hence the name). This creates a negative feedback loop acting directly on the body potential. As a result, the common-mode voltage on the body is actively reduced to a low value, ideally close to zero.

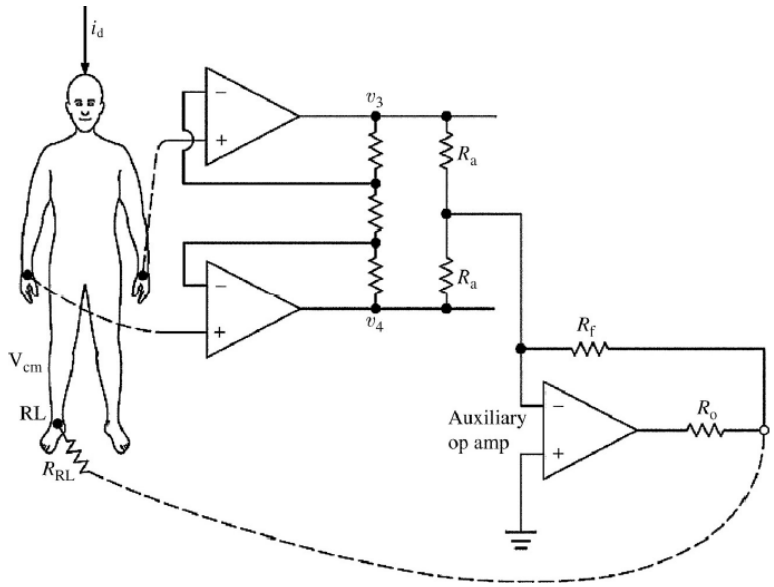

Figure 2.5: Driven right leg circuit with electrodes connected to the body

From the circuit model, the reduction of the common-mode voltage can be expressed as

$$v_{cm} = \frac{R_{RL} i_d}{1 + 2R_f/R_a}$$

This equation shows that the body common-mode voltage decreases as the loop gain increases. v_{cm} should be as small as possible and this is generally achieved by increasing the feedback resistor R_f or decreasing the input resistor R_a, which improves common-mode attenuation, R_{RL} is the right leg resistance introduced from the electrode lead and i_d is the interference current coupled from the mains. In practice, the DRL reduces the effective body potential relative to circuit ground by feedback, decreasing common-mode amplitude at the amplifier inputs.

This mechanism forces the interference current to flow toward the DRL amplifier output instead of flowing through the body-to-ground impedance. As a result, the common-mode interference seen at the instrumentation amplifier inputs is strongly reduced, improving the overall signal quality.

However, the solution shown in Figure 2.5, which consists in increasing R_f and decreasing R_a, is an idealized view and does not consider the rest of the circuit, the skin–reference electrode impedance and particularly the stability of such a circuit. Decreasing R_a is limited because the instrumentation amplifier may be required to deliver too high output current. Increasing R_f excessively can lead to stability issues, because the electrode impedance, buffer, and high-pass filter can introduce additional poles in the feedback loop. The DRL loop can become unstable because electrode impedance and input filters add phase shift (additional poles).

The design of our driven right leg is based on two main sources, the Chi et al. 2010 non-contact acquisition system design and the Bioelectronics lectures from Prof. Redouté which is based on Webster medical instrumentation (2009) [14,26,27]. First, Figure 2.5 considered that the driven right leg electrode connection to the body is represented by a resistor. In our case, we replace this resistor by the very high skin-electrode impedance Z_{el} associated with non-contact reference electrode, so v_{cm} becomes $\frac{Z_{eL} i_d}{1+2R_f/R_a}$. Thus, the skin electrode interface in non-contact electrode strongly influences the v_{cm}.

The proposed driven right leg circuit from Chi and Redouté are similar, they deal with stability and have a high inverting amplifier gain to feed back common-mode voltage and increase common-mode rejection ratio (CMRR). Based on these, Figure 2.6 illustrates our implementation of the driven right leg

circuit. We have considered the skin-electrode interface for non-contact measurements, with the fabric layer represented by the parallel high resistor and low capacitor. We designed the system to have a high common-mode rejection at low frequencies using the 1 $M\Omega$ path and kept it low at high frequencies to improve stability in our measurements using the 1nF capacitor and 10 $k\Omega$ resistor. The buffer in the driven right leg circuit isolates the instrumentation amplifier from the feedback loop, prevents loading of the input stage, and provides sufficient current drive and stability for effective common-mode voltage reduction. For EOG applications, the reference electrode is positioned in the middle of the forehead.

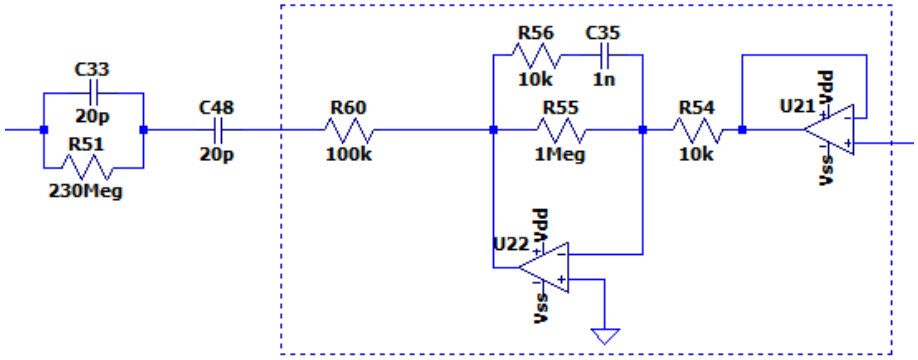

Figure 2.6: Driven right leg circuit design in our system

Capacitive reference electrode connected to the main board ground Through our experiments on the breadboard prototype and by studying several non-contact signal acquisition designs [35, 37], we obtained comparable or even better results while bypassing the driven right leg circuit. Instead of actively feeding back the common-mode signal, a reference electrode capacitively coupled to the body is connected to the circuit ground. A large resistor is placed at the electrode end to limit the current and ensure patient safety in case of fault conditions (microshock/macroshock prevention).

By grounding the body, the common-mode voltage induced by the power-line is reduced at its source. The body potential is forced to remain close to the circuit ground, which limits the amplitude of the common-mode signal appearing at the measurement electrodes. This grounding approach reduces power-line interference, especially because our system is battery powered and isolated from earth ground. In this configuration, the interference currents preferentially return to the circuit ground through the reference electrode instead of being converted into differential-mode noise at the amplifier inputs.

Although this method does not provide active common-mode suppression, it has several practical advantages in non-contact systems. The capacitive reference electrode is simpler to implement, avoids stability issues related to feedback loops and is less sensitive to motion-induced impedance variations. For high-impedance capacitive electrodes, this approach offers a good compromise between noise reduction, system stability, and design simplicity, while maintaining safe operation.

Filter design

Filtering is a key part of any physiological signal acquisition system. Biopotential signals such as EOG have a limited frequency bandwidth, while noise and interference can appear over a much wider frequency range. The purpose of filters is to limit the bandwidth to the frequencies of interest, reduce unwanted noise components, and improve the signal-to-noise ratio without altering the useful information carried by the signal. In practice, several types of filters are combined, each targeting a specific disturbance mechanism. Since the signal is heavily impacted by 50 Hz common-mode interference, filters operate together with

the driven right leg or grounding techniques to further reduce noise and interference. Therefore, tuning the filters is important to maximize the signal to noise ratio. 3 types of filter design are discussed in this section (high pass, low pass and notch filter) together with the associated circuit. Our main circuit board is designed with a passive second order low pass filter and an active twin-T notch filter. An additional high pass filter should be added to the main board design but was identified after the PCB manufacturing for this master thesis.

Passive low and high pass filters These types of filters in first order are respectively composed of a resistor and a grounded capacitor in series for low pass filter and the inverse configuration for high pass filter as shown in Figure 2.7. Their cutoff frequency is given by $f_c = \frac{1}{2\pi RC}$. In our implementation, we use a passive first order high pass filter on each electrode and a passive second order low pass on the main board. As previously said a complementary high pass is to consider in the main board. Passive filters are simple, stable, and do not introduce additional noise or power consumption.

Figure 2.7: Passive RC filters

High-pass filters are mainly used to remove DC offsets and very low-frequency drifts. These unwanted components comes from electrode offset voltages, slow variations at the skin–electrode interface, respiration and motion artifacts. In non-contact electrodes, the electrode–skin interface is capacitive and its impedance varies with motion and fabric thickness. It is important that the DC component is filtered before the first amplification stage to avoid saturation.

The high-pass cut-off frequency is chosen between 0.1 Hz and 1 Hz for EOG, so that DC offsets are attenuated, since they can saturate the INA, while preserving the 0.1-10Hz interesting EOG signal. There is tradeoff between the reduction of the DC offset and the integrity of the signal. A compromise must be found between stability, noise performance and cost.

Low-pass filters are used to remove high-frequency noise and limit the bandwidth to the physiological signal range. High-frequency disturbances include electromagnetic interference, high frequency noise and other physiological signal (like EMG). Since the useful content of EOG signals mainly lies below 10Hz, a low-pass filter helps obtain a cleaner and noise reduced signal.

In this work, a second-order passive low-pass filter is used. The cut-off frequency is selected high enough to preserve the relevant EOG components, while attenuating unwanted high-frequency noise. Using a second order filter gives a improved noise rejection without significantly increasing circuit complexity.

Twin-T notch filter Power-line interference at 50 Hz is the dominant source of noise in biopotential measurements, it is important to develop strategies to reduce it. Analog low-pass filters and grounding strategies are not sufficient to fully remove this interference, 50 Hz lies close to the useful frequency band of the EOG. For this reason, a dedicated notch filter is used to specifically reduce 50Hz. It is a band-stop filter focusing on a narrow range of frequencies, its cutoff/center frequency is also given by $f_c = \frac{1}{2\pi RC}$ and a quality factor Q is associated with the bandwidth of the notch filter. A higher Q is associated with a

narrower notch, rejecting a very specific frequency with less impact on surrounding frequencies. A lower Q corresponds to a wider notch bandwidth, more important attenuation of the cutoff frequency but affecting a broader range. Q was chosen as a compromise between 50 Hz attenuation and minimal distortion near the EOG band. Figure 2.8 present an active twin-t notch filter based on non-contact acquisition system and additional sources [34, 35, 42].

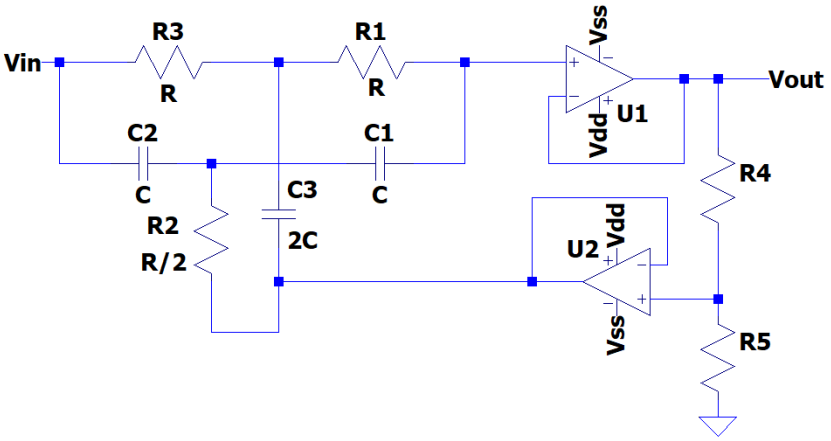

Figure 2.8: Active twin-t notch filter

The notch filter shown in Figure 2.8 is composed of 2 T-network RCR and CRC where R and C are chosen to have a cutoff frequency at 50 Hz. This filter is active and uses 2 amplifiers as buffers together with R4 and R5 to have a tunable quality factor Q. By tuning the ratio between R4 and R5, the quality factor, thus the bandwidth $\Delta\omega$/depth of the notch filter, can be modified following these formula :

$$Q = \frac{R4 + R5}{4 * R4}, \Delta\omega = \frac{\omega_n}{Q} = \frac{1}{RCQ}$$

The quality factor of active notch filter has a very wide range based on the resistors used in this right section where a passive notch filter have a quality factor limited to 1/4 only. Compared to a passive notch filter, an active Twin-T notch filter provides deeper and more stable attenuation at the notch frequency by compensating component mismatches through active feedback. With a higher Q factor, it preserves the signal amplitude outside the notch with a reduced bandwidth, mainly keeping useful biopotential signal. These characteristics make the active Twin-T notch filter interesting for non-contact biopotential signal acquisition, where 50 Hz rejection and signal integrity are critical.

This section has presented every component separately for the front-end electrode and the analog signal processing main board used in our non-contact electrooculogram acquisition system. Starting from the capacitive electrodes, the design deals with the very high electrode–skin impedance by using impedance buffers based on LMP7702. This ensures minimal electrode loading with less distortion and reduction of the interesting signal. Input protection, stabilization and safety aspects are handled through series resistors, capacitors and high-pass filtering to remove DC offset.

Power-line interference heavily are affecting the signal through electric coupling through the device, electrodes, body and through magnetic field coupling. Noise reduction techniques are required to manage the noise, those are present in the analog signal processing.

The main board then processes the buffered signal using an instrumentation amplifier (INA128) to provide differential amplification and strong common-mode rejection. Common-mode noise reduction is realized through two alternative strategies: an active driven right leg circuit or a capacitive reference electrode connected to circuit ground, both aiming to reduce body-coupled interference. Passive second

order low-pass (and high-pass) filters limit the bandwidth to the EOG frequency range. An active Twin-T notch filter specifically targets the 50 Hz power-line interference. The second-stage non-inverting amplifier provides the final gain adjustment, delivering a usable output level with low noise and controlled impedance for measurement. Altogether, this section establishes the theoretical basis of each individual element of the system. In the next section, this complete acquisition chain is analyzed as a whole through LTSpice simulations and then validated experimentally using a breadboard prototype to demonstrate proof of concept according to performance, stability and noise behavior.

2.2 Simulation on LTSpice

Before implementing the complete acquisition system on hardware, the electrical behavior of the circuit must be verified through simulation. LTSpice software is used in this work to model the full analog signal conditioning chain and to evaluate its performance. This chapter presents the simulation setup, the assumptions made for modeling the electrodes and noise sources and the results obtained from AC and transient analyses. Based on the theoretical design choices presented in the previous section, the complete non-contact EOG acquisition system is analyzed.

2.2.1 First version for the simulation (Dry)

Again this part is realized based on the project of the bioelectronics course from Prof. Redouté [26], it consists in the wet electrodes ECG acquisition system. We adapt this circuit for non-contact electrode to measure the electrooculogram. The first version of this adaptation is presented in the Figure 2.9 where modifications are made in the input EOG signal, the skin-electrode impedance, the non-contact electrode and the analog signal processing chain.

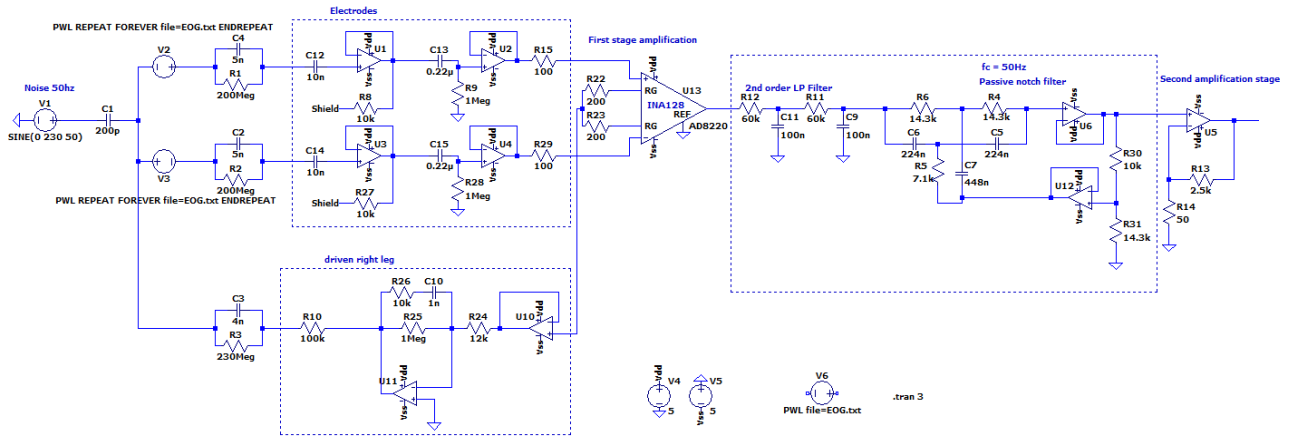

Figure 2.9: First version of the LTSpice simulation for "dry" contact electrode EOG acquisition system

First modification, the eye movement signal used in this LTSpice simulation is provided in the EOG.txt file, it corresponds to a single horizontal eye movement over 1 second extracted from the dataset from a study from Fang et al. (2018) [43]. This eye resulting voltage signal is set in our system using the V2 and V3 voltage generator. It is shown in Figure 2.10 (a), we observe a rapid eye movement lasting 1 second and with a amplitude of 1 mV.

Second, the source of noise as the common-mode power-line interference is modeled using respectively the 230V 50Hz sinus voltage generator capacitively coupled using a 20pF capacitor. It corresponds to the power-line coupling with the body that is sensed through the electrodes. This capacitor value depends

on the quality of the electric environment, poorly isolated electric environment have more coupling to the body. The skin electrode impedance is another potential source of noise due to the mismatch in the electrodes leading to the conversion of common-mode signal to differential mode, it is modeled using only a parallel $\approx 200M\Omega$ and a low capacitor $\approx 5nF$ mainly due to the dielectric layer. This was an adaptation of the model using wet electrodes where we increased the resistor value and decrease the capacitor to values that could be associated with fabric material as dielectric.

However, this first implementation missed a key capacitive component corresponding to the 20 pF coupling between the skin and the electrode, also the $\approx 5nF$ in the dielectric layer have a higher value than expected ($\approx 20pF$) for the capacitor that represents a fabric layer based on Chi et Al. (2010) values [15], these errors have been uncovered at a late stage of the master thesis. This made the LTSpice model work greater than the real case would, thus providing an unreliable model for representing non-contact application. Since the skin electrode impedance is increased, this model could approximately represent **dry contact electrodes** for EOG acquisition based on the section 1.3.

Since this was discovered late in our work, we are going to continue the explanation based on this version and rectify the results at the end with another, more physiologically true version. This latter version is analyzed at the end of this section and shows the output signal is more affected by 50 Hz interference due to the capacitance of the non-contact reference electrode.

Together with the signal of interest and added noise component, we can reconstruct the complete front-end and analog signal condition unit based on the individual component developed in the previous section. When everything is combined making the Figure 2.9 circuit, every step of the processing of the EOG signal with 50Hz common-mode interference can be analyzed and tuned to get an improved understanding of every single function.

The input signal signal received from the front-end electrodes corresponds to a very small differential EOG signal shown in Figure 2.10 (a), with a dominant 50 Hz common-mode interference impacting through capacitive coupling. These signal coming from the body interface with the recording and reference electrodes through the skin-electrode interface until it reaches the electrode design for impedance matching and high pass filter. As detailed before, buffers have very high input and low output impedance allowing for less distortion and attenuation. The high pass filter ($f_c = 0.7234Hz$) removes the DC component in the signal to avoid saturation in the first stage amplification.

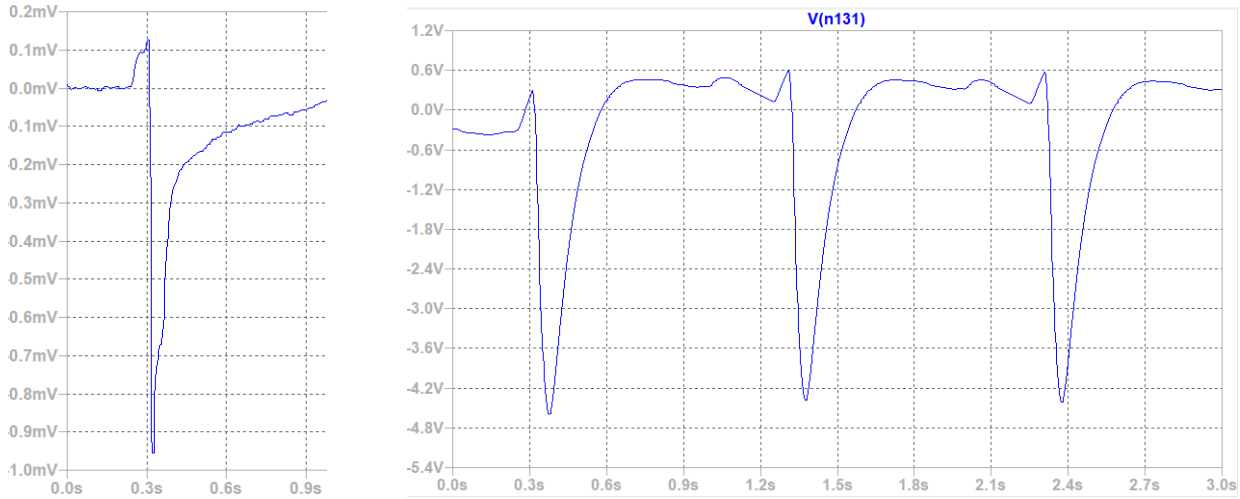

(a) Single movement input EOG signal

(b) V1 circuit EOG output over 3 seconds

Figure 2.10: Input and output of the eye movement voltage over time through the version 1 of the acquisition system

The signal provided to the main signal conditioning board is affected by 50 Hz noise, in this first version of the circuit, the instrumental amplifier with the driven right leg completely remove this 50 Hz component by with respectively the common-mode rejection ratio (CMRR) and DRL inversion, amplification and feedback. This complete removal of the 50 Hz in an early stage of the measurement represent an oversimplification compared to real non-contact electrode monitoring. It was verified through measurement on breadboard and PCB, the interference less signal in early stage corresponds more to wet or dry monitoring instead of non-contact.

Since the instrumentation amplifier (gain = 125) outputs a noise-less and low frequency electrooculogram in this version, the impact of the second order low pass filter ($f_c = 26.526Hz$) and notch filter ($f_c = 50Hz$, Q = 0.6125 (for R30 = $10k\Omega$) and Q = 3.875 for R30 = $1k\Omega$) is not obvious as it only smooths the interesting signal. The cutoff frequencies used in this model are chosen to remove as most noise/interference as possible while leaving the interesting signal unchanged. The last non-inverting amplifier (gain = 50) outputs Figure 2.10 (b), we can observe 3 repetitions of the same eye movement signal over 3 second. The initial 1 mV amplitude signal is amplified (global gain = 125*50 = 6250) and filtered resulting in an approximate 5 volts amplitude. This output corresponds to a noise free, smoothed signal that could be associated to an ideal wet electrode monitoring.

In summary, this first LTSpice model is mainly used to verify the correct operation of the analog acquisition chain. Even if this version does not fully represent a real non-contact electrode system, it allows the amplification, filtering, and general signal behavior to be observed. The strong rejection of the 50 Hz interference shows that this configuration behaves closer to a dry or wet electrode system than a non-contact one. Nevertheless, this model provides a useful reference and a starting point for further analysis. In the next subsection, an AC analysis of the complete circuit is presented to study the frequency response and validate the designed bandwidth.

2.2.2 AC analysis on the first version

After validating the time-domain behavior of the acquisition chain, a frequency-domain analysis is required to better understand the system performance. An AC analysis allows the verification of the designed bandwidth, the cutoff frequencies of each filtering stage and the attenuation of unwanted frequency components such as power-line interference. The figures presented in this section are obtained from the first version of the simulated circuit, some adaptations are realized to have a constant amplification over the interesting EOG bandwidth [0.1-10 Hz].

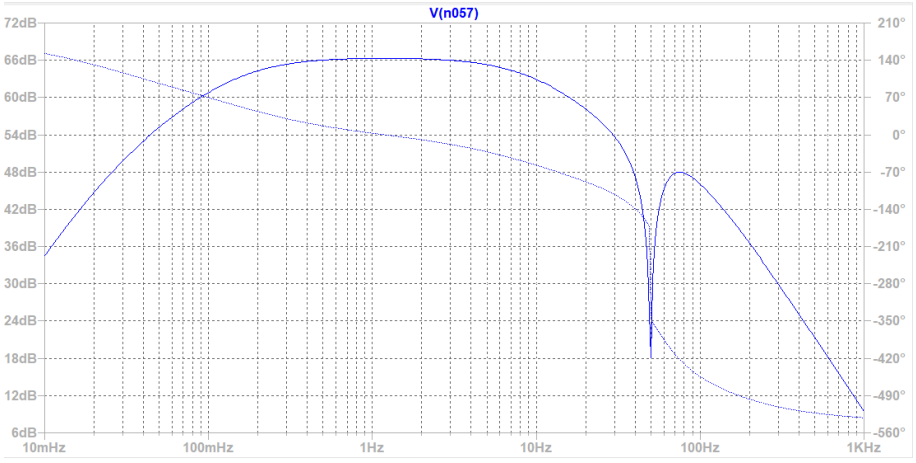

Figure 2.11: Bode plot at the output from the first version circuit adjusted

The final implementation of our project uses variable resistors, these allow to set different values for gain, for filter cutoff frequencies and bandwidth. Based on the first implementation shown in figure 2.9, we tuned the high pass filter to have a lower cut-off frequency and a narrower notch bandwidth to have Figure 2.11 bode plots at the circuit output. Theses slight adjustments allow to have the bandwidth of interest for the EOG to be amplified at the same magnitude ($\approx 66dB$).

It can be observed that low-frequency components (below 1 Hz) decrease with a slope slightly greater than 20 dB/decade. This behavior is mainly caused by the first-order high-pass filter and is reinforced by additional effects from the skin–electrode interface and other AC-coupled stages in the signal chain.

Within the EOG frequency band [0.1–10Hz], the signal is amplified uniformly by the two amplification stages with a total gain of approximately 66 dB. This flat gain region prevents signal distortion caused by different amplification levels at different frequencies. The filters are therefore tuned to have minimal impact on the signal of interest while still ensuring proper noise attenuation.

A trade-off exists between the reduction of the 50 Hz power-line interference and the preservation of the EOG signal. Lowering the low-pass filter cutoff frequency or reducing the notch filter quality factor (resulting in a wider notch bandwidth) improves the attenuation of the 50 Hz component. However, these choices also increase the risk of attenuating parts of the useful EOG signal.

In Figure 2.11, the cutoff frequency of the second low-pass filter is set to 26.526 Hz. As a result, a slope of approximately 40 dB/decade is observed at high frequencies. The notch filter quality factor is set to 3.875, which provides effective attenuation of the 50 Hz interference while leaving the EOG signal largely unaffected.

2.2.3 Completed version of the LTSpice model (non-contact)

Sections 2.2.1 and 2.2.2 present simulation results that show a clean output signal and well-controlled bode plots. However, these results are closer to the behavior of the acquisition system when using dry-direct skin contact electrodes. In order to correctly represent a true non-contact configuration, where the electrodes are separated from the skin by a cotton fabric layer, the skin–electrode interface model must be modified.

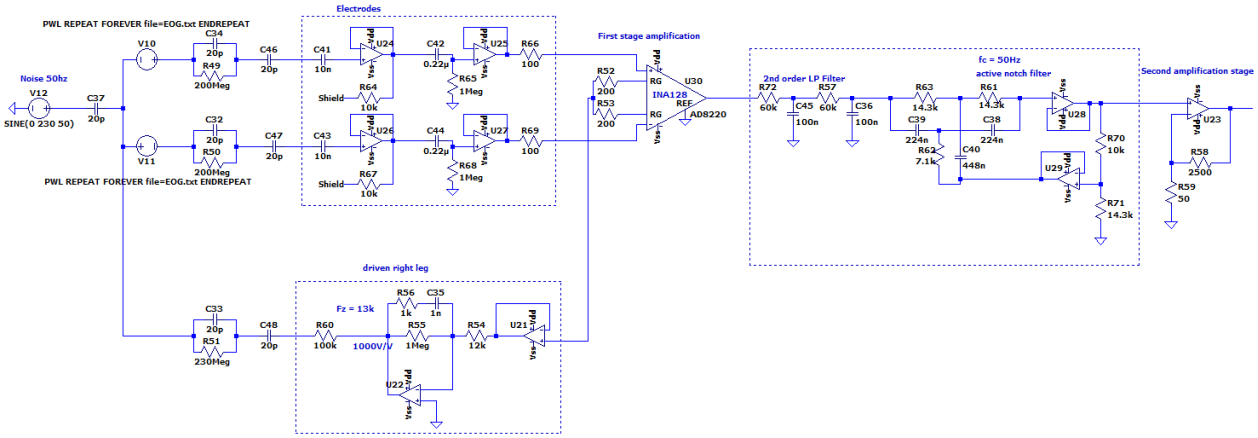

Figure 2.12: Completed version of the LTSpice simulation for non-contact acquisition system

In the completed LTSpice model, the non-contact interface is represented by a parallel combination of a 20pF capacitor and a 200MΩ resistor, modeling the insulating cotton layer. This impedance is

placed in series with an additional capacitive coupling of approximately 20pF, corresponding to the capacitance formed between the metallic electrode plate and the charged skin surface carrying the EOG signal. This updated interface is shown in the completed LTSpice model presented in Figure 2.12. An alternative version in the grounding process has been suggested before, the driven right leg is shorted by adding a connection to the ground between the DRL output and the skin electrode interface. Apart from this modification, the rest of the analog processing chain remains identical to the one introduced previously.

The introduction of these low-value capacitors strongly affects the behavior of the driven right leg (DRL) circuit. Due to the weak capacitive coupling between the body and the reference electrode, the DRL is no longer able to efficiently feed back the 50 Hz common-mode signal to the body. As a result, the common-mode rejection is significantly reduced and a large part of the power-line interference remains present at the output of the instrumentation amplifier. This behavior matches the experimental observations obtained from the breadboard and PCB prototypes.

Because a large portion of the measured signal is dominated by 50 Hz interference, the filtering stages play a critical role in improving the signal-to-noise ratio. Figure 2.13 (a) shows the transient output of the acquisition system, where a clear 50 Hz oscillation is visible with an amplitude of approximately 0.2V. The eye-movement-related downward peaks are still present but with a reduced amplitude of about 1V, compared to approximately 5V in the previous dry-contact-like version. In addition, the signal baseline is shifted to around -0.3V when no eye movement occurs. This offset may be caused by amplifier offsets and could be corrected by adding an additional high-pass filter stage between the instrumentation amplifier and the final output.

These results clearly show that small changes in the skin–electrode impedance model have a major impact on system behavior, transitioning the response from an almost interference-free signal to a noise-affected non-contact measurement.

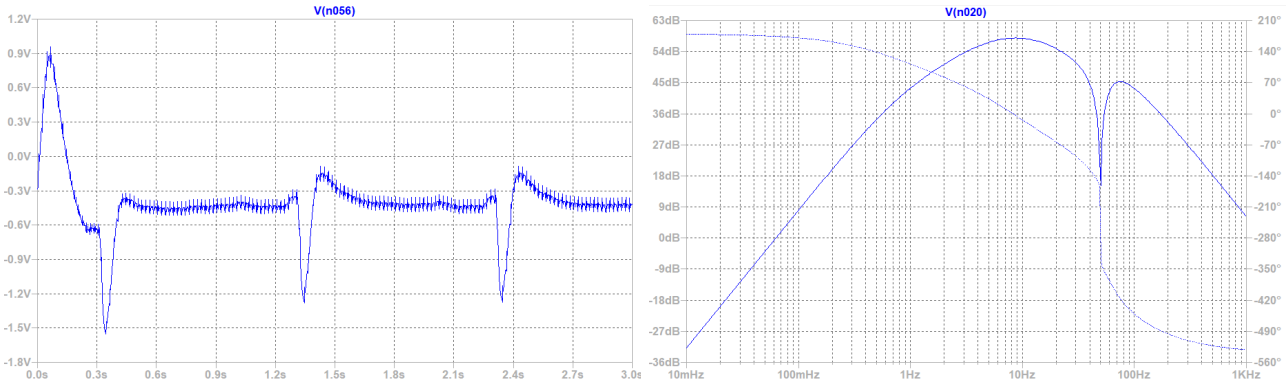

(a) Acquisition system output

(b) Bode plot

Figure 2.13: Transient and AC analysis of the completed version of LTSpice simulation

For the AC analysis, Figure 2.13 (b) presents the bode plot of the completed non-contact model. Compared to the previous version, low-frequency components are significantly more attenuated. A slope of approximately 40dB/decade is observed, indicating the presence of multiple low-frequency poles. Moreover, this attenuation starts at a higher cutoff frequency, around 3Hz, which partially overlaps with the EOG signal bandwidth and therefore affects part of the signal of interest.

At very low frequencies, the attenuation becomes much stronger. For example, a difference of approximately 60dB at 10mHz can be observed between the dry-contact-like model and the non-contact model. This highlights the difficulty of preserving low-frequency physiological information when using purely capacitive non-contact electrodes.

2.3 Prototyping on breadboard using multiple type of electrodes

Before designing the final PCB, the complete acquisition system was implemented and tested on a breadboard. This step is useful because it allows a fast and flexible evaluation of the circuit behavior using real components. The breadboard implementation makes possible to verify the signal amplification, filtering stages and general functionality of the system. It is possible to quickly adjust component values of resistors and capacitors. It also helps to identify practical issues that cannot be observed in simulation like unexpected noise, saturation or grounding problems.

We have tested multiple configurations of the circuit, notably by adding and removing different type of filter in the main part of the circuit, modifying their resistor value for gain and cutoff frequencies. The simulated circuit from the previous section is reproduced on hardware where everything hold on a single breadboard. This prototype have been tested with different kind of electrode to verify the working principle. The combination were multiple like with 3 wet electrodes, 2 recording dry or non-contact electrodes and a wet reference electrode.

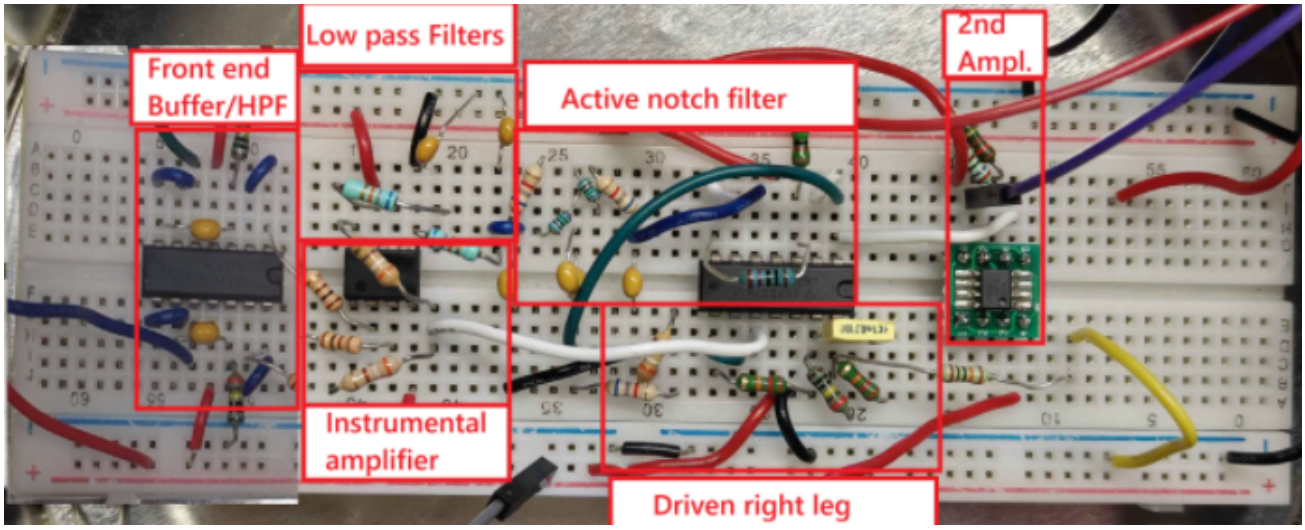

Figure 2.14: Breadboard implementation

The figure 2.14 represents our implementation on breadboard of the complete circuit, different parts are highlighted. Matching resistors and capacitors were used but it was not the case for all the active components in this prototype version. Instead of LMP7702, common LM2902 operational amplifier were used for the front-end buffer, active notch filter and driven right leg circuit. This operational amplifier is for all-purpose, have lower precision, higher offset and higher noise component. For the instrumentation amplifier and the second stage amplifier we used respectively the INA128 and LMP7702 as planned.

Everything has been setup by following the schematics but multiple issues were encountered during the testing. The breadboard implementation also has important limitations like long wires, parasitic capacitances, friction based connection and poor shielding. It makes the system more sensitive to interference, especially to 50 Hz power-line noise, the circuit is put inside a metal box to protect the circuit to power-line interference. Additionally, we had difficulties to reproduce the same result over different measurement sessions as in multiple occasion a cable would disconnect from the breadboard or some resistors be moved and not put back. An unexpected connection between 2 wire would short the circuit and the proximity of components can lead to unstable behavior and signal distortion. These limitations are critical for high-impedance non-contact electrode systems where small parasitic effects can strongly affect the measurements. For these reasons, the breadboard is mainly used as an intermediate valida-

tion step and a dedicated PCB implementation is required to obtain reliable and repeatable measurements.

This circuit has been tested in multiple cases with different types of electrode and different filter configurations. The electrodes used where either wet, dry or non-contact, where the dry and non-contact electrode are realized on PCB based on Chi et Al. 2010 design [14]and are shown in the section 2.4.2 figure 2.17. The electrode initially used with 3 wet electrodes (2 for recording and 1 as a reference electrode) to see if the circuit would work and see the impact of each block in the signal output with classical working electrode. This allowed us to adjust some gain and filter cutoff frequencies and make the overall circuit work as intended. After the non-contact electrode have been designed on PCB, we used these as recording electrodes in direct skin contact (dry) or non-contact through a cotton layer. During breadboard test, the reference electrode used is wet as it would feedback most common-mode signal and improve the output signal quality. By comparing different configurations in the front end part, we observed than the noise component in the output is increased when the skin-electrode impedance increase.

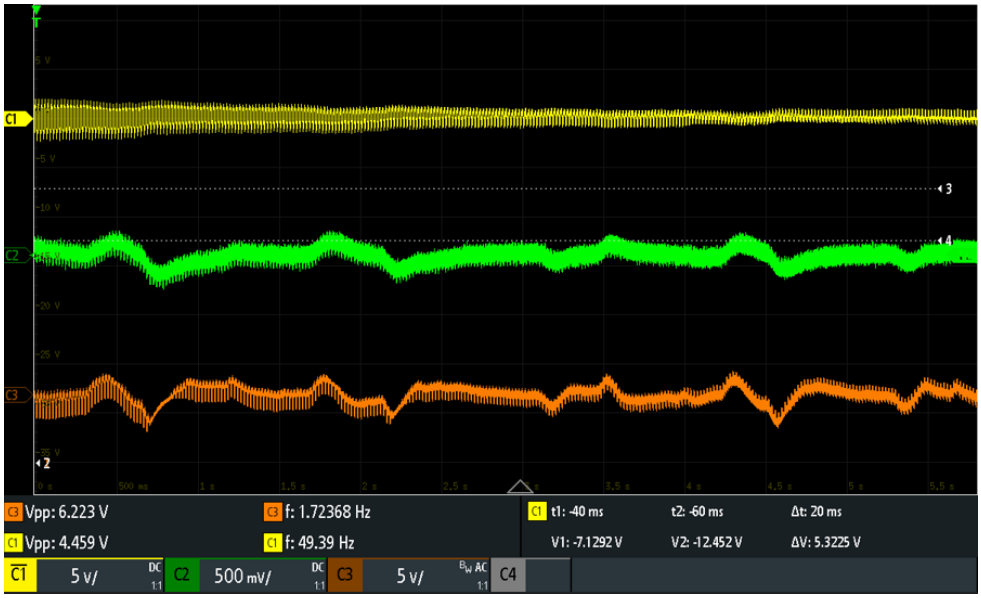

Figure 2.15: Breadboard intermediate measurements using non contact electrode

Figure 2.15 shows the intermediate and output signal measured on the breadboard device with non-contact recording electrode and wet reference electrode. The figure showed the oscilloscope display with the measurement in 3 different point of the circuit. In yellow, the signal is measured at the output of the instrumental amplifier showing that the filters are required as we can't distinguish any part of the EOG signal. In green, the signal is measured after both low pass and notch filter removing a part of the high frequency component, notably power line interference. The eye-related signal is visible with an amplitude around 300 mV (10x less than at the amplifier output) but they are is still affected non negligible 50 Hz component. In orange is the signal output on breadboad, it further reject power line interference thank to the second stage amplifier power supply rejection ratio and amplify the signal to a 6V amplitude

Multiple modifications can also be made in analog signal processing chain, multiple test are realized to see what filters are necessary and how they can be tuned. Filters such as notch, low pass, high pass are added or removed easy on breadboard, variations of the filters are also tested with testing active/passive or different order of filters. Based on the measurement, we were able to determine that an optimal solution is by using an active notch and a second order low pass filter. Working with this breadboard prototype gave us useful insights in how the circuit work and how each block affects the signal output. This is a key step to prove the concept before implementing the final version on printed circuit board. Some additional

challenges still have to be investigated such as the power supply of the circuit and the body attachment of the electrodes/acquisition system.

2.4 Printed circuit board design

After validating the acquisition system through simulation and breadboard testing, a dedicated printed circuit board (PCB) was designed to improve signal quality, stability, and reproducibility. A PCB is a physical support used to electrically connect electronic components. Conductive copper tracks are placed on an insulating substrate to replace long wires and manual connections and components such as resistors, capacitors and integrated circuits are soldered on. The PCB implementation reduces parasitic effects, improves grounding and allows a more compact and reliable realization of the non-contact EOG acquisition system. This chapter presents the main design choices made for the PCB implementation.

The section is divided into four main parts. First, the power supply design is discussed, focusing on the operational voltage of the active components and the chosen method/material to deal with dual voltage supply. Multiple alternatives exists but we chose a stable solution. Then, the electrode PCB design is presented focusing on layout and shielding/guard. Most of the electrode configuration has already been discussed in the front end design at the beginning of this chapter, this part focuses on how the hardware get implemented Subsequently, the design of the main board is described as well earlier in this chapter but the implementation on PCB is shown in this section. We used KiCad as a software used to design the project and the fabrication of the PCB is made in China by JLCPCB. The design has to be as compact as possible while having multiple degree of liberty in the filtering and the gain, this is made possible using variable resistors. Finally, the range of these rheostat are discussed to explain what choices in the design have been made in order to get the effective non-contact electrooculogram monitoring and what is the impact of each rheostat in the system.

2.4.1 Power supply

The way the power is supplied to the circuit is something that have been overlooked until now. The power supply of the acquisition system is a critical part of the design and directly affects performance, safety, noise level and portability. All active components used in this work require defined supply voltages to operate correctly, as specified in their datasheets especially the instrumentation amplifier INA128 and the operational amplifier LMP7702 [39, 41].

Up to this point when using the prototype, the system was powered using a laboratory DC voltage generator. Since this supply is powered by the mains, it introduced additional 50 Hz interference into the acquisition chain which negatively affected the measured signal. To reduce this source of noise and improve signal quality, we decided to move toward a battery-powered solution. Using batteries electrically isolates the system from the power-line, significantly reducing power-line coupling and making the acquisition system less sensitive to environmental interference. This choice also better fits the objective of developing a portable EOG monitoring device.

A key limitation of the INA128 comes from the range of input voltages it can measure correctly. According to the datasheet [41], the input common-mode signals must remain a 2 volts away from the positive and negative supply voltages. Since the signal recorded at the input of the INA128 lay in the mV range which is relatively near 0V, this means that the power supply must be stable and well balanced around this value. This is associated with the recommended dual power supply in the datasheet, the minimal range being $\pm 2.25V$ with the ground voltage located near the middle of the supply. If this condition is not respected, the instrumentation amplifier INA128 may saturate or behave incorrectly, the LMP7702 may also undergo the same kind of limitation but its has a greater power supply range where the signal must remain 0.3 volt away from the supply voltage. If the supply voltages drift or become unbalanced,

the amplifier may no longer work in its correct operating range, which can distort the measured signal.

Several power supply solutions were considered during the design phase to obtain the dual power supply. We initially aimed to use a common 9V battery to power the entire acquisition system. The voltage output of this battery must be adapted to generate a $\pm X$ V, where X is a chosen voltage to supply the circuit. This could be realized by making a relative ground in the middle the maximal voltage and 0 volt, by using new component such as a DC-DC converter or other methods discussed in this section.

One option is to use a new grounding reference, the positive and negative supply rails are defined base on this reference using discrete analog circuits based on operational amplifiers. This uses active components which increases power consumption and also raises the risk of introducing extra noise. Since the main objective of this project is to validate a non-contact EOG acquisition system rather than to develop a custom power supply, a pre-made and well-characterized solution was preferred. Using a proven power supply module reduces design complexity and ensures reliable operation, allowing the focus to remain on signal acquisition and processing.

To ensure a stable, symmetric, and well-controlled power supply, an isolated DC/DC converter was finally selected. In this work, the TEC 3 module from Traco is used, powered by a 9 V battery and providing regulated $+5\,\mathrm{V}$ and $-5\,\mathrm{V}$ outputs. This solution guarantees a known and stable operating voltage for the complete acquisition system and avoids power supply–related issues becoming a source of measurement errors. Given that the system measures signals in the microvolt range, using a proven and low-noise supply solution was preferred.

Figure 2.16 shows how we implement the TEC 3 module in our PCB to convert the 9V battery voltage to a [-5,+5] V and GND. A large electrolytic capacitor is placed at the input of the DC/DC converter to smooth the supply voltage and provide a local energy reservoir, reducing voltage drops caused by the battery. At the output of the converter, a low-ESR ceramic capacitor is used to filter high-frequency noise and stabilize the output voltage. This combination improves power supply stability and reduces noise propagation into the sensitive analog front-end.

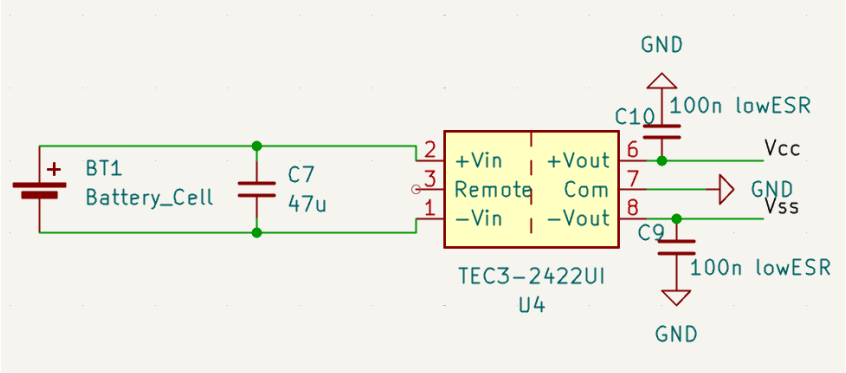

Figure 2.16: Power supply setup using the TEC 3 DC-DC converter

The main drawback of this approach is its power consumption, which limits battery lifetime and reduces long-term monitoring. Increasing the number of active components, including operational amplifiers and power conversion stages, increases energy consumption and may also introduce additional noise. This converter also took some place in the main PCB which increase its size by $\approx 30\%$.

Another option considered was the use of multiple batteries to generate a dual supply (for example 2 cells). These batteries should be put in series and the reference ground set to the voltage in between the 2 cells thus allowing for a positive and negative equal voltage. However, this solution presents a risk

of imbalance if one battery discharges faster than the others and this also doubles the size associated with the batteries. Over time, this could shift the ground reference away from the center of the supply, resulting in asymmetric voltages (e.g. +3 V and -2 V instead of ±3 V). For this reason, this solution was considered unreliable for project.

For these reasons, power optimization of our device is identified as an important direction for future work. Chi and Debbarma portable devices [14, 33] could respectively continuously monitor physiological signal for 10 and 7 hour where our implementation is bulkier and limited to a few hour using a 9V battery and the converter. Alternative solutions such as rechargeable lithium-ion batteries, more efficient DC/DC converters or lower-power analog components could significantly improve autonomy. While the isolated DC/DC converter is not optimal in terms of power efficiency, it provides a robust and low-noise solution for this prototype, ensuring reliable operation and allowing the focus to remain on the validation of the non-contact EOG acquisition concept.

2.4.2 Electrode design

The design and process about the electrodes have already been introduced in section 2.1.1 where Figure 2.2 shows the circuit that will put on top of the electrode. We have already discussed of the function of each component and we simulated both electrodes and main circuit in LTSpice. This section is dedicated to the design of the electrode on printed circuit board as shown in figure 2.17. The KiCad file and design is shown in appendix D, where the schematics is a reproduction of the circuit and the token shaped design is based on Chi et Al (2010) electrodes [2].

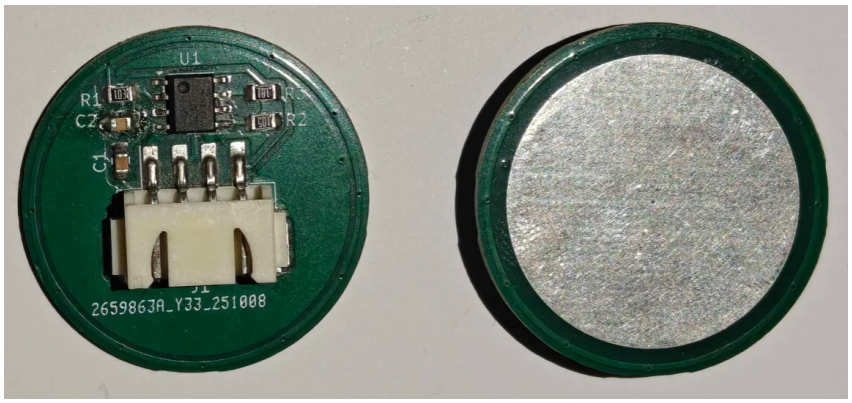

Figure 2.17: Top and bottom view of the non-contact electrode PCB

The printed circuit board for the electrode has 3 cm in diameter is made with 4 layers where the front-end circuit is soldered on top. The electrode is connected to the main board by using surface mount JST connectors on both side using 4 wires to supply power to the active component of the electrode (V+, V- and GND) and sending the front-end output to the main board. JST connectors are used because it is a simple, cheap and an already available connectors in the microsys laboratory. Alternatives using a smaller and shielded connectors + wires could be more investigated to improve potential noise effect. In our case, we considered it to be negligible compared to power-line interference through body coupling.

On the other side, the bottom layer is constituted by a round copper fill without coating on top. This copper plate is the sensing part of the electrode, it corresponds to one side of the capacitor that is realized by the coupling between the plate and the charged skin surface. This capacitor will sense any change in the charge on skin related to corneo-retinal potential linked to eye position. This signal will be sent to the top front-end electronics into the impedance buffers then to the main board. To complete the description of the electrode, the 2 remaining inner layer are used as a ground and a shield layer.

Guard and shield

External electromagnetic interference can strongly affect both the electrode interface and the signal path through capacitive coupling. Since non-contact electrodes and high-impedance circuits are particularly sensitive to electric fields, unwanted interference can easily be introduced into the measured signal, reducing signal quality and signal-to-noise ratio. To protect the measurement from these disturbances, guard and shield techniques are used. These techniques aim to reduce capacitive coupling, leakage currents and power-line interference.

The shield is a conductive barrier connected to a reference potential that protects the signal path from external electromagnetic interference, significantly reducing power-line noise in biopotential measurements. In addition to this, the bottom side of the electrode has an active guard all around the electrode to preventing noise and leakage currents.

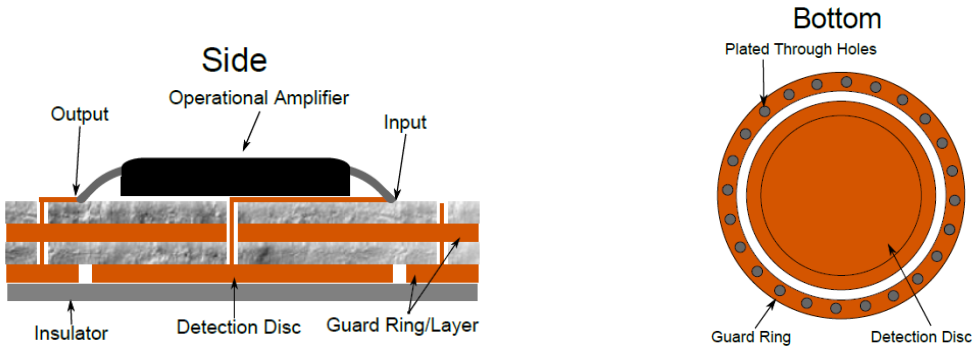

(a) Transversal view (b) Bottom view

Figure 2.18: Guard and shield of the non-contact electrodes configuration

The shield and guard are driven by the output of the first buffer so that they follow the electrode potential without loading it, minimizing voltage differences, leakage currents and capacitive coupling to preserve signal integrity in high-impedance non-contact measurements. The PCB shield and guard is designed on PCB following Portelli et Al (2017) [36] version where, in Figure 2.18, the inner layer connections are shown. From the different views in the figure, we can see that the signal input is sent in the operational amplifier and this output this connected to the inner layer shield and the surrounding guard. Through holes are used to connect different layer together, like with the operational amplifier output to the isolation layer and guard. The design is thought to physically separate the detected signal and the shield.

2.4.3 Main board design

Just like the electrodes, the general circuit design and all its subparts have been described earlier in section 2.1.3. The printed circuit board implements this circuit with multiple connectors, power supply unit and some adaptations to add flexibility in our design. The figure 2.19 shows the implementation of our circuit in PCB, we tried to design it to be as compact as possible (with available components) and manage to get a 5 x 4.2 cm PCB, the KiCad schematic and PCB design are given in the appendix D. Elements such as the JST connector, electrolytic capacitor and DC-DC converter are voluminous and may require to find alternative to improve the portability and to further reduce the size of the circuit.

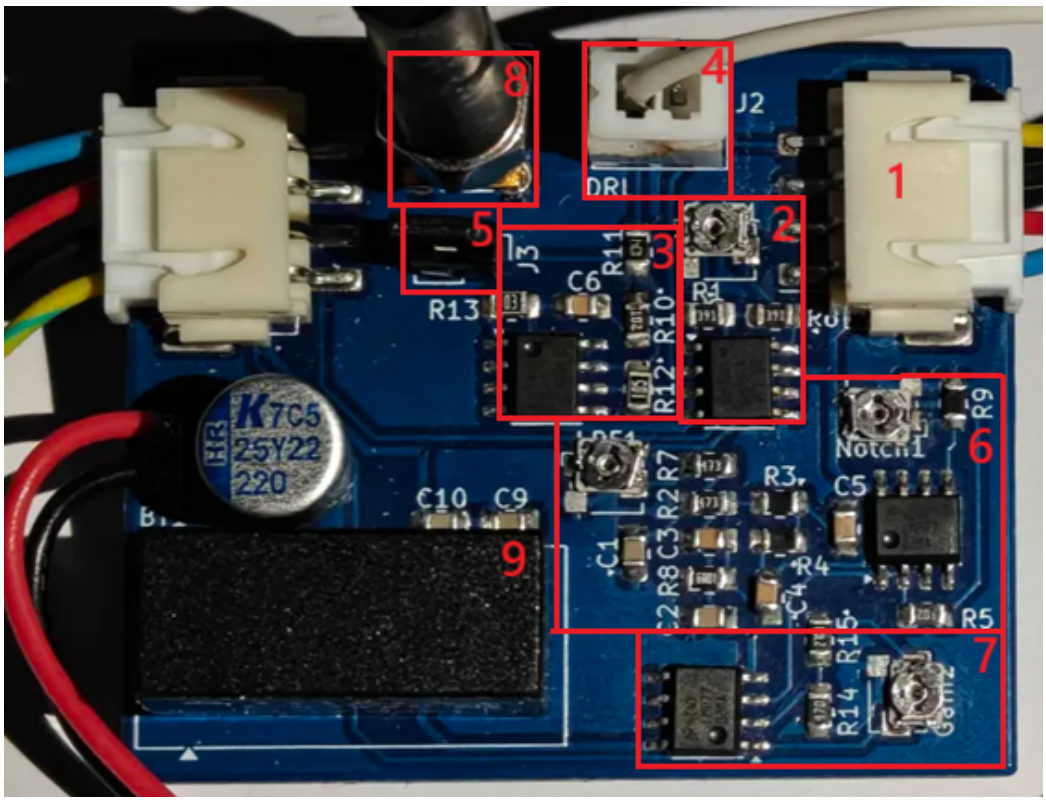

Figure 2.19: Top view of the main analog signal processing unit

Multiple areas with different functions can be seen in Figure 2.19:

1. Electrodes are connected through the surface mount JST connector on the top left and right of the PCB. Other pins of the connector are the power supply and ground for the active electrode.
2. The electrode output signal is sent to the instrumental amplifier present upper right part of the PCB for first stage amplification.
3. The common-mode signal is sent from the INA to the driven right leg circuit using operational amplifiers, multiple resistors and capacitors which are in the center of the circuit.
4. From the driven right leg, the common-mode signal is sent back to the body using the reference electrode connected to the PCB with the small JST connector in center top.
5. An additional small header + jumper is present in position J3, it serves to ground the reference electrode and short the driven right leg circuit. When the jumper is put on, the electrode is shorted and not when removed.
6. Instrumental amplifier output goes to the bottom left side where the second order low pass filter and active notch filter are realized using multiple resistors and capacitors. The notch filter operational amplifiers are present in the right most SOIC package.
7. The filtered signal is then amplified by the second stage operational amplifier in the bottom of the PCB.
8. The final signal is sent to the measuring unit or oscilloscope using a shielded cable that is connected to the PCB using a Molex connector on the top left of the figure.

9. Last element is the power supply block composed of the 9V battery clip connector, the DC-DC converter in the bottom left of the PCB and electrolytic/ceramic capacitors for stabilization of the power supply.

All together the printed circuit board amplify and filter the signal of interest before sending it to the oscilloscope, reject common-mode voltage and power all the active elements as presented in previous section. At the end of the analog chain, the output is sent through a shielded cable to the oscilloscope. To avoid introducing power-line interference, the measuring device should not be plugged to the grid. We use the LabNation Smartscope and its dedicated laptop software where both the Smartscope and laptop are powered by the pc battery. As the printed circuit board is powered using a 9V battery, the complete chain of circuit and oscilloscope are disconnected to the power-line, this aims to reduce interference in our output signal. Improvements can be made in portability and ease of use by using a micro-controller with a Bluetooth module to communicate the output information instead of the oscilloscope setup.

Measurement tuning on PCB Ranges by using rheostat

Some complementary adaptations of the system are made possible through the use of four variable resistors (rheostats) distributed across the PCB. In this work, inexpensive single-turn TC33X trimmers are used for the two amplification stages, the low-pass filter, and the active notch filter. Their resistance varies linearly between 0 and a defined maximum value and can be easily adjusted using a screwdriver, which makes tuning simple during testing and measurements.

The use of these variable resistors provides flexibility to adapt the system to different measurement conditions and to optimize the signal-to-noise ratio. By increasing or decreasing the gain, the useful EOG signal can be made more visible, while adjustments of the filter cutoff frequency and notch bandwidth allow better attenuation of noise sources such as high-frequency disturbances and 50 Hz interference. This tuning capability is particularly important in non-contact EOG acquisition, where signal amplitude and noise level strongly depend on electrode placement, motion, and environmental conditions.

Tests performed on the breadboard prototype showed that lowering the cutoff frequency of the low-pass filter or increasing the bandwidth of the notch filter generally lead to a reduction of noise in the output signal. However, this improvement comes with a trade-off: more aggressive filtering also attenuates parts of the useful EOG signal. As a result, each variable resistor on the PCB must be carefully adjusted to find a balance between noise reduction and signal preservation, ensuring that eye movement signals remain clearly detectable.

Function	Position	min value (R=0)	defined max value	Increasing R would
1st stage gain	(2)	gain (at 10%)≈313	gain ≈ 88.5	decrease gain
2nd stage gain	(7)	gain ≈ 5	gain ≈ 45	increase 2nd gain
Low pass filter f_c	(6)	fc = 32Hz	fc = 10.6	reduce more noise/signal
Notch quality factor	Right (6)	Q = 3.875	Q= 0.5795	reduce more noise/signal

Table 2.1: Rheostat effect on the device

Table 2.1 summarizes the effect of each rheostat on the system behavior. It illustrates the achievable range of gains, cutoff frequencies and notch quality factor. These adjustments allow the system to be tuned experimentally and highlight the flexibility of our analog conditioning acquisition system.

The gain of the instrumental amplifier is given by g = 1 + 50000/$R_{G,eq}$, where R_G is set to 800Ω with the parallel potentiometer (max resistance = 2000Ω) that can influence the $R_{G,eq}$ value and thus influencing the gain. *In the PCB design, the potentiometer used to adjust the gain of the instrumentation amplifier was incorrectly placed in parallel with the gain resistor R_G. When the potentiometer is

set to a low value, the effective resistance becomes very small, which results in an excessively high gain, theoretically near infinity. This can cause unwanted saturation and unstable behavior of the amplifier so the gain of the first stage must be set carefully. This issue was identified during testing and should be corrected in a future version of the PCB.

The gain in the second stage is given by g = 1 + $R_{A,eq}/R_B$, where R_A (between the negative input and the output of the amplifier) and R_B (between the negative output and the ground) are respectively set to 270Ω and 47Ω. To modify the gain, the variable resistor (max R = 2000Ω is put in series with R_A which effectively increase the $R_{A,eq}$ and the gain as well.

The low pass filter cutoff frequency is given by $1/2\pi RC$, where R is the combination of the initial resistor 50kΩ and the variable resistor (max R = 100kΩ) and C is the capacitor set to 100nF. Increasing the resistor value would decrease the cutoff frequency and impact more the signal and noise.

The notch filter quality factor is given by the ratio $Q = \frac{R4_{eq}+R5}{4*R4_{eq}}$ as defined earlier in section 2.1.3. With R4 initially being set to 1000Ω and R5 set to 14500Ω, the variable resistor (max R = 10kΩ) is in series with R4 to increase $R4_{eq}$ and also Q as a consequence. A higher Q is associated with a narrower notch bandwidth, rejecting a very specific frequency with less impact on surrounding frequencies. A lower Q corresponds to a wider notch bandwidth, more important attenuation of the cutoff frequency than previous case but affecting a broader range of voltage. Q is chosen as a compromise between 50 Hz attenuation and minimal distortion near the EOG band.

2.5 Head band design and final design

The fixation of the electrodes to the body is the last element to consider in order to complete the acquisition system design. The non-contact electrodes are able to measure biopotentials through a layer of cotton fabric, as they capacitively couple with the skin surface while the fabric acts as a simple dielectric layer. Because motion artifacts can easily saturate the signal in our system, maintaining the electrodes in a stable and fixed position relative to the skin is essential. In an ideal configuration, the PCB should integrates a microcontroller with a Bluetooth module for wireless data transmission, the fixation system should include all three electrodes, the main board, and a rechargeable battery within a single wearable structure.

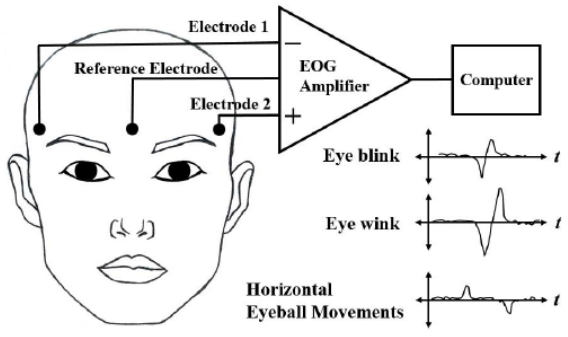

Figure 2.20: Electrode setup with forehead EOG monitoring

Such a wireless EOG acquisition device would be intended to monitor eye movements overnight and must be comfortable enough to be worn during everyday sleep. Initially, the use of a sleep mask integrating all components was considered. However, testing and informal feedback from potential users indicated that placing electronic elements directly over the eyes during sleep is uncomfortable and not well tolerated. An alternative solution is the use of a headband, where the electrodes, battery, and main board are

distributed around the forehead. This configuration is less intrusive, as no element is in direct contact with the eyes and is more suitable for long-term or overnight use.

An example of a headband-based EOG setup is shown in Figure 2.20, adapted from Debbarma *et al.* (2021) [33], where three electrodes are placed on the forehead and temples. This configuration allows the detection and differentiation of various eye movements such as blinks, winks, and horizontal eye rotations. In their implementation, the signal is directly sent to a differential amplifier and recorded using a computer.

Figure 2.21: Tailored head band on the alone and worn on a user

This inspired us for the design of our headband where the objective was to integrate the entire acquisition system into a single wearable item. A cotton headband was custom-made based on a reference design, with enough length to be comfortably worn around the head. It includes five pouches of different sizes to accommodate the electrodes, the main board and the battery. Figure 2.21 shows the tailored headband both alone and worn by a user. All components should be easily inserted into the pouches. For the measurements presented in this work, only the electrodes were placed inside the headband, as access to the main board was required to adjust rheostat values and evaluate different acquisition conditions.

In conclusion, this experimental chapter described the complete development process of the non-contact EOG acquisition system, from the front-end electrode design to the final wearable implementation. Each functional block was individually designed, simulated and validated through breadboard experiments before being integrated on a printed circuit board. The transition from breadboard to PCB, combined with the integration into a custom headband, allowed a more stable, compact and wearable system, better suited for non-contact measurements. Once fully assembled, the system can be used together with an oscilloscope and a computer to record, visualize and store EOG signals under different experimental conditions. This complete prototype constitutes the basis for the experimental measurements and performance evaluation presented in the next chapter, where signal quality, noise behavior, and practical usability are analyzed.

Figure 2.22: Complete non-contact EOG acquisition system

Chapter 3

Results and discussions

This chapter aims to present the methodology used to collect, process and analyze the experimental data obtained from the designed PCB. Once a working system is established, a measurement protocol is defined to ensure that each run follows the same procedure, allowing meaningful comparison between runs. Based on the recorded data, a Python code is used to plot the electrooculogram and extract key performance indicators, such as the signal-to-noise ratio. Further signal processing and analysis are performed by the code and analyzed in this work. Altogether, this process provides an evaluation of the performance associated with our non-contact EOG acquisition system. However complementary measurements are still required, notably to compare multiple hardware configurations and to investigate sleep-related REM detection. During the experimental phase, we observed that the results were strongly influenced by multiple parameters as the type and position of the reference electrode.

The following section focuses on the measurement protocol and the data-processing code used to record and analyze the electrooculogram in a repeatable manner. This framework enables direct comparison between different configurations, where only one parameter is modified at a time. By using the same recording duration, eye-movement phases and feature-extraction code, different cases can be compared based on the recording electrode type, reference electrode type, grounding strategy and variable-resistor settings for gain and filtering.

Due to time constraints after system validation, only a limited number of measurement runs could be performed. We chose to focus on a fully non-contact PCB configuration using a grounded reference electrode, with all variable resistors for gain and filtering set to their mid-range values. This configuration provides an intermediate and representative assessment of the PCB performance, although additional recording sessions would be required to further optimize the system parameters and improve EOG signal quality. Several eye-movement patterns can nevertheless be identified in the recorded data using the protocol defined in the previous section. Finally, frequency-domain analysis using the Fast Fourier Transform (FFT) and box plot of the signal-to-noise ratio across multiple runs are presented to evaluate system performance relative to noise.

Based on the experimental results and observations, the last section highlights the main factors that influence the quality of non-contact EOG measurements. The discussion focuses on the impact of power-line interference, reference electrode coupling, skin moisture, electrode pressure and environmental conditions on the measured signal. By comparing different experimental runs, this section shows how these parameters affect the signal-to-noise ratio, signal stability and the visibility of eye-movement-related features. Rather than proposing a fully optimized solution, the discussion identifies limitations of the current system and key directions for improvement These observations provide a clear link between the experimental results and the conclusions drawn in the following chapter, where future perspectives for non-contact EOG acquisition are discussed.

3.1 Measurement methods and procedure

After troubleshooting and confirming the working principle of the PCB version, only limited time remained for measurements. This strongly limits the scope of our results, since more data would be needed in future work to better understand the performance of the acquisition system.

This section proposes a measurement procedure with defined eye-movement timings to ensure that EOG signals recorded in different configurations correspond to the same movements in a repeatable way. By following the same protocol, electrode placement and eye-movement sequence, external artifacts and noise caused by the environment or parasitic movements are minimized. This procedure should be used for the runs performed in this master thesis and for future measurements to allow fair comparisons.

Note that, due to the use of variable resistors and the different electrode types available for recording and reference, many parameter combinations could be tested. A short subsection therefore describes the possible configurations and the one selected for this work. Since we were limited by time, part of the PCB design was based on empirical (non-recorded) tests and several components were chosen to keep the system versatile. Understanding how to tune the acquisition system remains important in order to find a more optimal and stable configuration with reduced inter- and intra-variability.

After recording the EOG using the procedure described below, the output from the main board is sent through a shielded cable to an oscilloscope (Labnation SmartScope) for visualization and recording. The SmartScope displays the voltage associated with eye movements and generates a CSV file containing voltage values over time. Our Python code uses this data to plot the signals shown in the next section, compute the signal-to-noise ratio, apply additional 50 Hz filtering and perform a Fast Fourier Transform (FFT) to analyze the frequency content of the measured signal.

Using this procedure and the analysis code, we obtained meaningful results for one “mid-range” configuration of parameters. This configuration was repeated 10 times to evaluate whether the measurement is stable over time and across runs. The results are presented and discussed in the next section.

3.1.1 Measurement protocol

Most measurements were performed on one 23-year-old male subject. Additional tests on more subjects are required to confirm reproducibility. The non-contact electrodes were placed inside the headband on the forehead of the subject and connected to the main board, which was positioned on a flat surface near the subject. The PCB and electrodes were powered by a 9 V battery and both the oscilloscope and computer were powered by the laptop battery. Isolating the subject, acquisition system and recording computer from power lines is essential to reduce the 50 Hz noise component that can mask the signal of interest. For this reason, instead of the Microsystem laboratories, recordings were performed in environments with reduced power-line influence (e.g., a cleanroom or a quiet room with lights switched off and as few plugged-in devices as possible).

To analyze the results obtained with our acquisition system, we recorded a series of 10 runs in order to observe variability between runs. These series are saved and compared across different setups. Each run lasts approximately 40 seconds and is divided into 8 phases of 5 seconds, during which specific eye movements are performed (usually two movements per phase). We estimated that this protocol provides a simple and fast representation of typical horizontal eye movements encountered during wakefulness or sleep and how they appear in the EOG.

The sequence of eye movements during one run is the following:

- 5 seconds of no movement
- 2 eyes movements to the left in 5 seconds

- 2 eyes movements to the right in 5 seconds
- 2 blinks in 5 seconds
- 2 closed-eyes movements to the left in 5 seconds
- 2 closed-eyes movements to the right in 5 seconds
- 5 seconds of random closed-eye movements
- 5 seconds of non movement

By standardizing a run and defining the timing of each eye movement, comparisons between runs and measurement series become more reliable. This approach ensures that observed differences in the recorded EOG signals are mainly caused by changes in the acquisition system configuration (electrode type, grounding method, gain, or filter settings), rather than by variations in the performed eye movements. In addition, this standardized timing facilitates the identification of signal segments associated with eye activity and rest period. This is particularly important for the computation of the signal-to-noise ratio based on our formula, as it allows a consistent separation between signal-dominated and noise-dominated time windows across all measurements, as described in the next section.

3.1.2 Possible recording configurations

Our non-contact acquisition system is specifically designed to allow multiple parameters to be adjusted giving versatility and improve performance depending on the measurement conditions. The main board includes variable resistors that allow modification of the filter characteristics and the gain values of the amplification stages, as explained in Section 2.4.3. In addition, JST connectors are used on the main board to connect the electrodes, which simplifies the replacement of electrode types. Permutation between the three electrode types (wet, dry, and non-contact) is possible for performance assessment and comparison. These electrode types can be applied either to the recording electrodes or to the reference electrode, and different electrode types may be combined between recording and reference electrodes.

The last configurable parameter is the grounding technique, which can be either the use of an active driven right leg circuit or a direct connection of the reference electrode to ground, as explained in Section 2.1.3. This selection is controlled by a jumper placed at position 5 in Figure 2.19; inserting the jumper shorts the DRL output to ground.

Overall, the four variable resistors can be adjusted continuously between 0 and their maximum value. To simplify the number of tested cases, we chose to use only three discrete positions: 0%, 50%, and 100% of the maximum resistance value. This already results in $3^4 = 81$ possible configurations in this simplified approach. For EOG signal monitoring, the two recording electrodes must always use the same electrode type (wet, dry, or non-contact) in order to avoid introducing differences related to unequal skin–electrode impedance. In addition, the reference electrode type has a strong influence on the output signal quality as seen in Section 3.3, the reference electrode should have a skin–electrode impedance that is lower or equal to the recording electrodes impedance.

As a consequence, a non-contact recording electrode can be combined with a wet or dry reference electrode, as this generally improves signal quality, even though it reduces comfort. The opposite configuration is not considered, since using a non-contact reference electrode with wet recording electrodes would only degrade performance without providing any practical advantage. Based on these constraints, six valid configurations are obtained from the electrode selection alone.

Depending on the grounding method (active driven right leg or direct grounding), two additional configurations can be obtained by changing the jumper position.

When all the possible cases are considered, up to $3^4 \times 6 \times 2 = 972$ different configurations could theoretically be tested to determine which setup provides the best signal-to-noise ratio, stability, or suitability for applications such as sleep monitoring.

Due to the very large number of possible configurations and the limited time available for this master thesis, we chose to focus on a single representative configuration. In this configuration, all variable resistors are set to their mid-range values, providing moderate gain and filtering. Fully non-contact electrodes are used for recording, as this is the main focus of the thesis. And the grounding technique used is the direct connection of the reference electrode to the main board ground. This configuration showed relatively stable and fully non-contact EOG measurements. However, depending on the level of 50 Hz power-line interference, the pressure applied by the headband and other parasitic effects, the recorded signal quality can vary from good to poor. These effects are discussed in the next section.

3.1.3 Python feature extracting code

With the selected recording configuration and the defined eye-movement protocol, the non-contact electrodes placed inside the headband record the EOG signal and send it to the main board for analog signal processing. The output of the main board is then sent to the Labnation oscilloscope for data acquisition. The Labnation software generates CSV files containing the recorded voltage values over time. These files are processed using Python functions, described in this section, to extract relevant features such as the signal-to-noise ratio and to plot the electrooculogram. All Python code used in this project is provided in Appendix D.

The CSV files generated by the oscilloscope follow a specific format. The first two rows contain metadata related to the measurement, including the sampling period of 0.00262144 s. The data is composed of up to approximately 14 000 samples for each run, where each sample corresponds to one voltage measurement taken at a given time. These samples are organized in four columns, each column representing the recorded voltage of one oscilloscope input channel during acquisition. The code should be able to extract all the data from the file.

The main Python script is stored together with the function files in a common directory, while a dedicated data subfolder contains the 10 recorded CSV files in a configuration. For each analysis run, the main script automatically browses the data folder and extracts the EOG measurements from all available CSV files. The extracted data are stored locally for processing and three optional functions can be applied. In the order presented in Appendix D, these functions correspond to: digital 50 Hz notch filtering, computation of the signal-to-noise ratio (SNR) and application of the Fast Fourier Transform (FFT). After these optional processing steps, the signal is plotted using the Matplotlib library. This process is repeated for all CSV files in the folder and the computed SNR values are stored in an array to generate a boxplot for further analysis.

The functions presented in the second part of Appendix D are implemented using existing Python libraries. Their principles, parameters and outputs are documented directly in the code. In summary:

- The notch filter is designed to remove power-line interference by targeting 50 Hz and its harmonics. The quality factor Q can be adjusted and the best results were obtained with a low Q, corresponding to a wider bandwidth and stronger attenuation of the 50 Hz component but affecting more frequencies as well.
- To compute the signal-to-noise ratio, two different methods were tested and compared. Defined as the ratio between the useful signal and the interference [26], the SNR is computed in decibels as the ratio between the root mean square (RMS) voltage of a **signal** segment and that of a **noise** segment:

$$V_{rms,signal} = \sqrt{\frac{1}{T_2 - T_1}\int_{T_1}^{T_2} v_{signal}(t)^2 dt} \text{ and } V_{rms,noise} = \sqrt{\frac{1}{T_2 - T_1}\int_{T_1}^{T_2} v_{noise}(t)^2 dt}$$

$$SNR = 20log(\frac{V_{rms,signal}}{V_{rms,noise}})$$

In the first method, the signal RMS is computed on the digitally filtered signal over the full measurement duration, while the noise RMS is computed on the unfiltered signal over the same duration.

In the second method, which showed more consistent and meaningful results, the signal RMS is computed on the original extracted signal during a time window with strong eye activity (5 seconds of closed random eye movements), while the noise RMS is computed during a time window with no eye movement.

Since the two methods rely on different signal segments used to compute the root mean square voltage, they produce different SNR values. Based on both the numerical results and visual inspection of the corresponding plots, the second method was retained for the analysis presented in this work as an output with a higher noise component would consistently give a lower SNR output.

- The Fast Fourier Transform function evaluates the contribution of each frequency component in the time-domain signal and provides the necessary information to plot the frequency spectrum of the measured EOG signal.
- Finally, the SNR values obtained from multiple runs recorded under the same conditions are set in an array, and an additional function generates a boxplot representation to visualize the variability and stability of the system performance over multiple runs.

3.2 Signal output analysis

This section presents the output signals obtained from the non-contact EOG acquisition system developed in this work. The motivations for such a device and the associated literature review were introduced in Chapter 1. Chapter 2 then described the implementation of the hardware used to acquire and process the EOG signal in the analog domain in order to extract the signal of interest. Combined with the measurement protocol and the Python-based digital signal processing tools, these elements lead to the experimental results analyzed in this section.

The corneoretinal potential generated by the retinal pigment epithelium and other ocular cells activity induces local charge variations on the skin near the eyes. This electrical activity is detected by the non-contact electrodes and subsequently amplified and filtered by the PCB. At the output of the main board, the conditioned signal is sent to the oscilloscope, which records the voltage over time and stores the data in CSV format. These data files are then processed using the Python code developed in this work, allowing the signal to be plotted and analyzed using several functions.

As illustrated in Figure 1.6, eye rotation relative to the electrode placement produces a surface potential on the skin. For a simple eye movement, the theoretical EOG signal exhibits a rising phase corresponding to the movement toward one direction, followed by a short plateau (typically less than one second) while the eye position is maintained, and finally a return toward 0 V when the eyes move back to their initial position. The polarity of the signal depends on the direction of eye movement. This theoretical plateau in the EOG potential is transmitted to the nearby skin and detected by the electrodes.

However, instead of observing this plateau, a different behavior is measured in our experiments, as also shown in the supplementary results. The high-pass filters integrated in the recording electrode front-end remove the DC component associated with sustained eye positions. As a consequence, the measured output signal for a simple eye movement differs from the theoretical case. The output consists of a positive or negative spike corresponding to the initial eye movement, followed by a near-zero voltage when the eye remains in the same position and finally an opposite-polarity spike when the eyes return to their initial position. The sign of the spikes depends on the direction of movement.

3.2.1 Output signal characteristics

Figure 3.1 shows a representative output signal obtained during one measurement run. The signal corresponds to the differential voltage recorded over time by the non-contact electrodes placed inside the headband. Each measurement run lasts approximately 40 seconds and follows the protocol defined in Section 3.1.1. The example presented here was selected among ten runs, as it is representative of the typical signal of interest affected by 50 Hz power-line interference at the system output. The measurements in configuration A were performed using non-contact recording and reference electrodes placed inside the headband, with the reference electrode directly connected to the system ground (bypassing the driven right leg circuit) and all variable resistors set to their mid-range values.

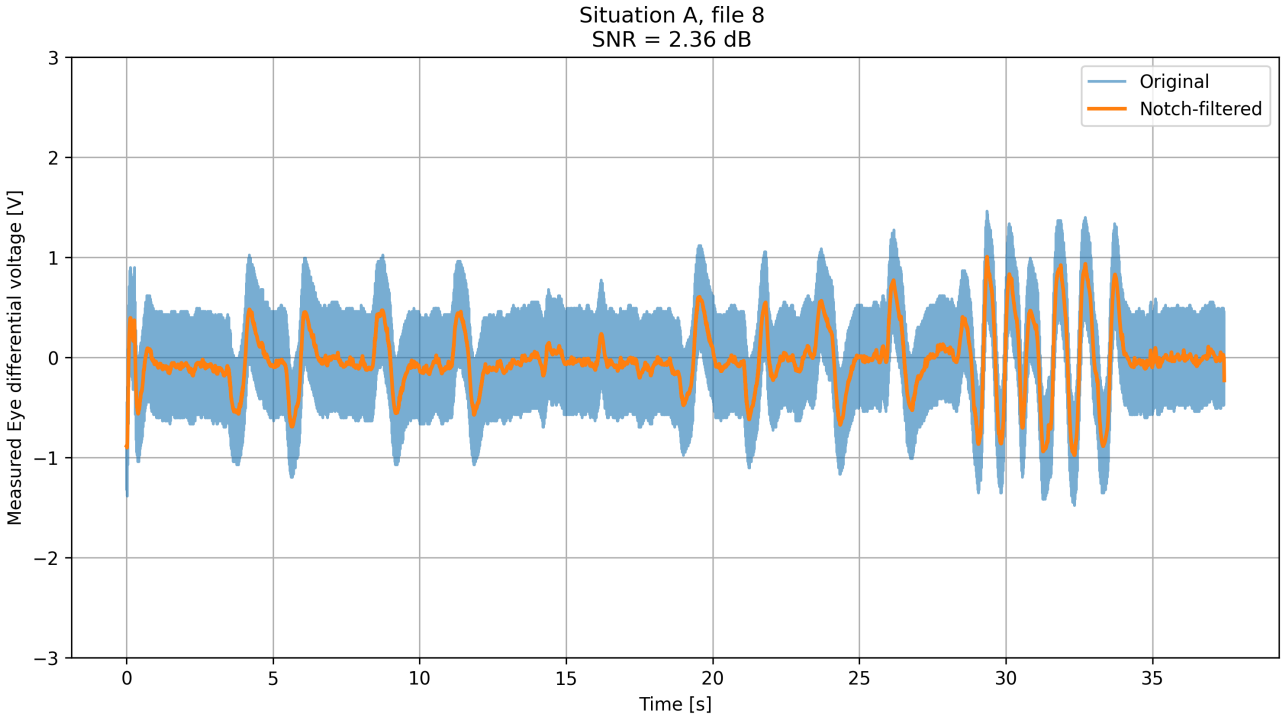

Figure 3.1: Typical 40 seconds run of the non-contact acquisition system output representing the eye movement

Two superimposed curves are visible in the figure. The blue trace represents the raw transient signal directly output by the acquisition system. The orange trace corresponds to the same signal after applying the digital filter function implemented in Python, which strongly attenuates the 50 Hz power-line component and its harmonics while preserving the low-frequency EOG signal of interest.

Despite the analog signal processing on the PCB, the impact of power-line interference at the system output remains significant. The 50 Hz noise can reach amplitudes of up to 1 V, compared to an overall signal amplitude of approximately 3 V. These results show that the non-contact acquisition system de-

veloped in this thesis is capable of recording the EOG signal, but that it remains sensitive to power-line interference. The analog filters and amplification stages were designed to improve the signal-to-noise ratio, although the current implementation does not fully eliminate this disturbance. Possible improvements to enhance signal quality are discussed later in this section.

By analyzing Figure 3.1 phase by phase, different types of eye movements can be associated with specific patterns in the recorded electrooculogram:

- The first and last phases, corresponding to approximately 5 seconds with no eye movement (here around 4 seconds), show a baseline voltage centered around zero. This baseline is clearly affected by 50 Hz interference, which is present throughout the entire run and reduces the computed signal-to-noise ratio.
- During the second and third phases (from 4 to 8 seconds and from 8 to 12 seconds), two eye rotations to the left and then to the right are performed. In the EOG signal, these movements appear as two successive spikes: first a negative spike followed by a positive one (or vice versa depending on direction). As discussed earlier, the DC plateau that would theoretically be present between these spikes is removed by the high-pass filtering stage.
- In the fourth phase (between 12 and 18 seconds), the eyes remain centered while blinking is performed. These blinks are only weakly visible in the raw signal, appearing as small and short spikes around 14 and 16 seconds. In the digitally filtered signal, these spikes become more visible due to the reduction of power-line interference.
- Between 18 and 27 seconds, the same left and right eye movements are repeated with the eyes closed. Comparing these phases with those performed with open eyes shows no significant difference in the EOG signal, confirming that EOG measurements are independent of external light conditions.
- The second to last phase represent random eye movement. In this case, the eyes move in various directions, similar to physiological eye activity during REM sleep. This phase produces larger and more irregular fluctuations in the EOG signal, clearly distinguishing it from the other phases.

Altogether, despite the presence of significant noise and power-line interference, the output signals show that the non-contact acquisition system is able to capture essential EOG information. Different eye movements can be identified in the recorded signal, including left and right eye movements, blinking and random eye movements phase. The latter is a distinguishable pattern and could be used for sleep monitoring in the detection of REM sleep. The example presented here corresponds to a good run among a larger measurement series, in which the level of 50 Hz interference varied depending on environmental conditions, electrode placement and system performances. Even if the noise component in the output remain non-negligible, the main signal processing board with the designed analog amplifiers and filters already remove an important part of the 50 Hz interference. Before processing the signal at the INA's input, the signal is largely dominated by 50 Hz and no EOG signal could be isolated from it contrary to here.

In some runs, the noise amplitude was lower and the EOG features were more clearly visible, while in others the signal was more affected by interference or even reached saturation in some case. Specific cases are presented in the next section. The application of a digital notch filter in the Python processing code, which removes the 50 Hz component and its harmonics, significantly improves the signal quality and makes the observation of low-frequency EOG activity much easier.

Even though the results presented here are limited due to time constraint, it constitutes a proof of concept that the system is capable of detecting and distinguishing different types of eye activity. Further improvements are required to reduce noise and enhance signal quality at the hardware level and obtain a clean EOG signal.

Frequency spectrum

To better understand the frequency content of the recorded signal, a Fast Fourier Transform (FFT) is applied. The FFT converts a signal from the time domain into the frequency domain. While the time-domain signal shows how the voltage evolves over time, the frequency-domain representation reveals which frequencies are present in the signal and how strong they are. This is particularly useful for biopotential signals as EOG, where useful information is at low frequencies, while noise and interference often appear at specific known frequencies like 50 Hz.

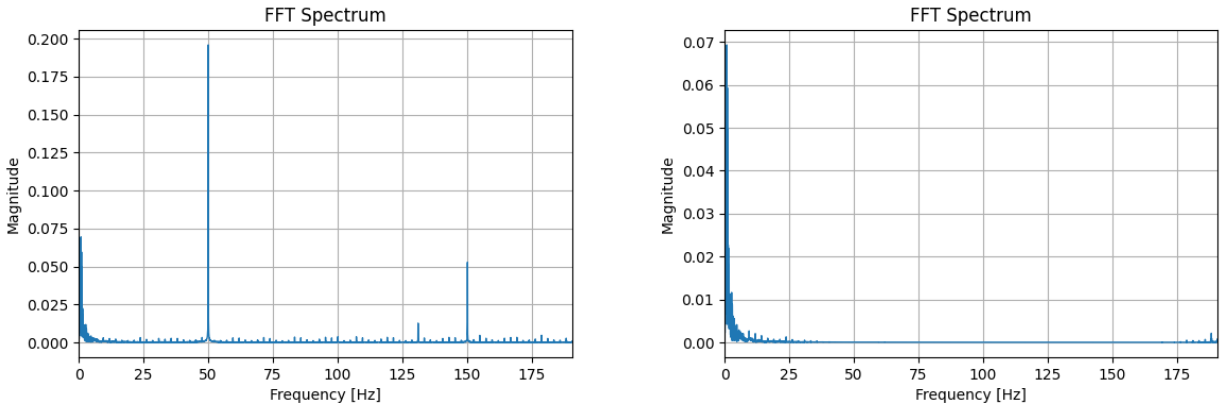

(a) FFT of the original output signal

(b) FFT of the notch-filtered signal

Figure 3.2: Fast Fourier Transform spectrum of the recorded signal

In our case, the FFT in Figure 3.2a clearly highlights the presence of strong power-line interference at 50 Hz and its harmonics with dominant peaks at higher frequencies. By comparing the FFT before and after digital filtering, the digital notch filter effectively remove the main source of interference as shown in Figure 3.2b. Since the quality factor of the notch filter is quite low, the bandwidth affected by it is large, thus filtering also all nearby unwanted high frequencies.This frequency-domain analysis complements the time-domain analysis and justifies the use of filtering strategies to improve the quality of the measured EOG signal.

Signal to noise ratio across all runs

As already mentioned, multiple measurement runs were recorded using the same acquisition configuration (fully non-contact recording electrodes, passive grounded reference electrode and variable resistors set to mid-range values). To quantitatively assess the performance of each run, the signal-to-noise ratio (SNR) is used as a performance metric.

The signal-to-noise ratio expresses how strong the useful physiological signal is compared to the unwanted noise present in the measurement. In the context of EOG acquisition, the useful signal corresponds to voltage variations caused by eye movements, while the noise includes power-line interference, thermal noise, motion artifacts and other environmental disturbances. A higher SNR indicates that eye-movement-related activity is more clearly distinguishable from noise, which directly reflects the quality and reliability of the measurement. Therefore, SNR is a relevant indicator of the overall performance of the non-contact EOG acquisition system.

In this work, the SNR is computed using an empirical method based on the ratio of root mean square (RMS) voltages measured during two different section of the signal. One corresponds to periods of low or no eye activity (baseline), containing mainly noise, while the other corresponds to periods of strong eye

activity, where the EOG signal is dominant eg in random eye movement. The SNR is then calculated as the ratio between these two RMS values and expressed in decibels (dB) using the previously introduced formula. Although this approach is not based on a standardized definition, it provides a consistent and practical way to compare the quality of different measurement runs under the same conditions.

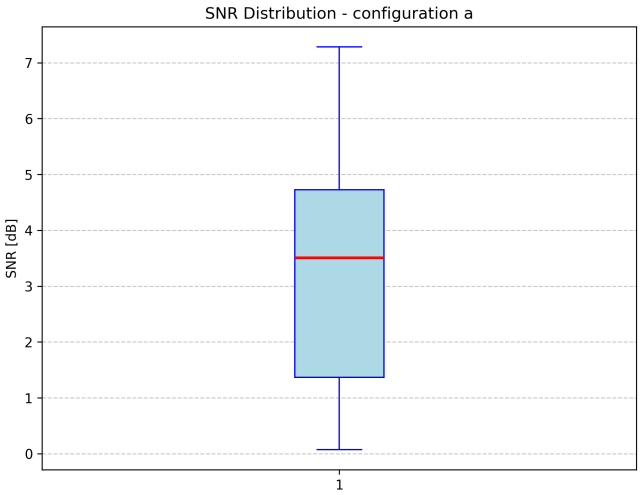

Figure 3.3: Boxplot with all runs in configuration A

This SNR computation is applied to all runs within a measurement series and the resulting values are represented using a box plot, as shown in Figure 3.3. The box plot provides a compact visualization of the variability in system performance across runs. The central line inside the box is the median SNR value of 3.6 dB, indicating the typical performance of the system. The box itself spans the interquartile range, which contains the middle 50% of the measurements and reflects the consistency of the acquisition. The whiskers indicate the minimum and maximum SNR values observed. A wide box or long whiskers reveal significant variability between runs, which can be attributed to changes in electrode positioning, motion artifacts, or environmental noise. Overall, this representation highlights both the average performance and the robustness of the non-contact EOG system under repeated measurements.

3.2.2 Discussion on non-contact electrodes measurement methods

Over all the measurements performed for this results chapter, most runs produced output signals with a structure similar to the reference case shown in Figure 3.1. This shows that the non-contact EOG acquisition system is able to monitor eye movements with a relatively consistent signal shape. Even though the signal remains noisy, the main features associated with eye activity can be identified in most recordings. This overall signal quality is also reflected by the signal-to-noise ratio (SNR) values computed for each run.

However, further testing revealed that the output signal quality is strongly influenced by several experimental and environmental factors reviewed in this section. The general structure of the EOG signal is preserved but the different runs show varying levels of noise. In some cases, the signal is strongly affected by power-line 50 Hz interference, while in others have parasitic low-frequency components or even saturation of the amplification stages can be observed. We identified 4 factors that influence the output results as it would impact the skin-electrode connection or introduce some noise.

One important factor already identified is the influence of power-line interference. Measurements performed with room lighting switched on show a stronger 50 Hz component in the output signal, leading

to a lower SNR. Shown in Figure 3.4, the measured EOG has a twice as important 50 Hz component (2 V amplitude instead of 1 V) in its original version compared to our reference case previously presented. We can directly observe the influence of the electric environment in the measurements which keeps the slightly distinguishable signal of interest, the signal to noise ratio computed in this case lies around 1 dB. By using the digital notch filter to remove the 50 Hz, a clear EOG can be recovered. This confirms that non-contact electrodes are highly sensitive to electric field coupling from the environment and that lighting conditions or any plugged in device can significantly affect signal quality.

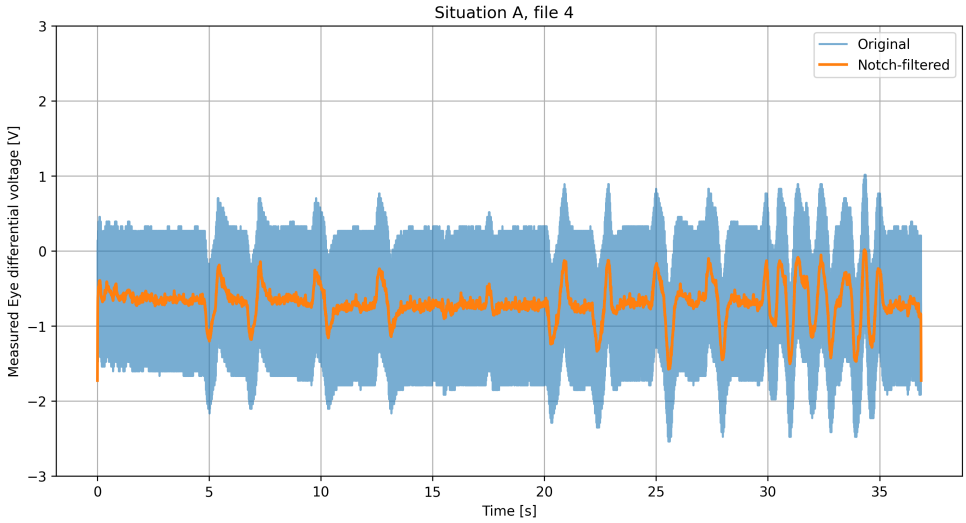

Figure 3.4: EOG measurements with important 50 Hz component associated with power-line interference

Another factor affecting the measurements is skin moisture. Increased moisture due to sweat accumulation in the headband improves the capacitive coupling between the electrode and the skin as wet fabric have a higher permittivity factor, which results in a better quality EOG signal and a higher SNR. Also with wet fabric and due to the conductivity of water, a direct resistive connection between the skin, wet fabric and electrode plate can replace the capacitive coupling and decrease the ultra high input impedance imposed by the initial non-contact electrode interface.

We tested this by adding a drop of water onto the fabric separating the reference electrode and skin while keeping the recording electrode in a non-contact configuration. This makes the direct connection between the body surface and system ground much more efficient thus making the body common-mode voltage connected the reference pin of all amplifiers. The instrumental amplifier outputs a much cleaner output signal with this configuration.

Figure 3.5 illustrates the output of such recording setup where 50 Hz interference component is heavily decreased as the original and notch-filtered signal match very well. Even though the noise component is decreased, the EOG signal characteristic are less recognizable where the voltage spikes from eye movement are much deeper and even reaching saturation in some cases. The signal to noise ratio of this case is about 7dB based on the computation formula. The resulting decrease in 50 Hz amplitude shows that the reference electrode position and body coupling is one of the most important factor to focus on in a future work since the only difference is the small drop making the reference approximately wet. Additionally, it implies that sweat in long term measurement would improve the signal to noise ratio the quality of the measurement but also bring irregularities.

Similarly, mechanical factors such as the pressure applied by the head band or the proximity of the electrodes to the skin play an important role. Applying more pressure generally improves contact stability and reduces air gaps, leading to a clearer signal and improved SNR. This increase the coupling capaci-

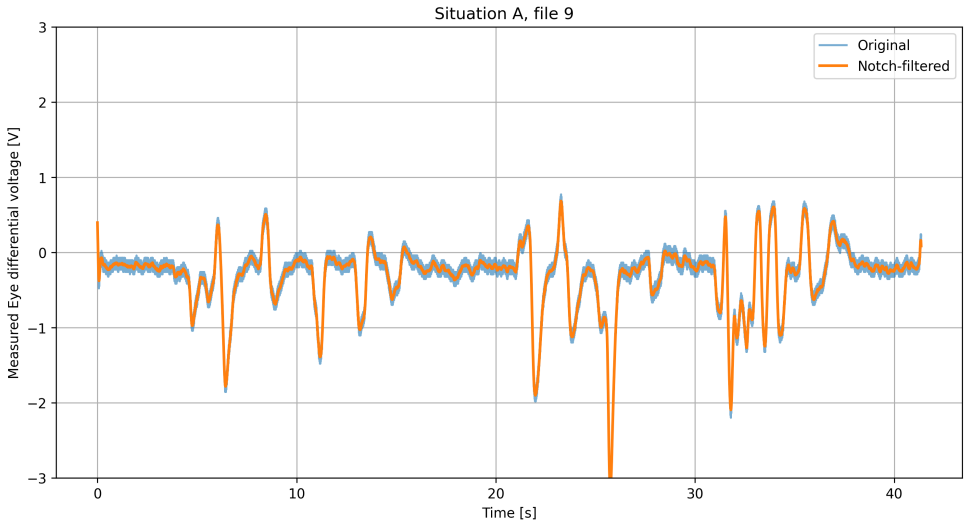

Figure 3.5: EOG measurement with reduced 50 Hz and high amplitude spiking associated with wet reference electrode connection

tance between the skin and the electrodes by reducing the distance in the capacitance formula $C = \frac{\epsilon_r \epsilon_0 A}{d}$. By observing the formula, ϵ_r, the relative permittivity of the dielectric and A, the non contact electrode capacitive area can be increased to improve the coupling. For example, wet cotton is 7 times higher in relative permittivity compared to dry cotton and the reference electrode could be much bigger than the one used in this implementation. Additionally, loose positioning of the electrodes increases sensitivity to noise and motion artifacts due to relative movement between the skin and the electrode.

Finally, in some measurement configurations, cardiac activity (ECG) is visible in the recorded signal and impacts the EOG quality. Since ECG components are not removed by the 50 Hz notch filter, they appear as low-frequency interference and can mask or interfere in the interpretation of the eye-movement-related signal. Figure 3.6 shows this ECG noise in the first 5 seconds of the measurement with the small oscillation every seconds. In the example, the coupling of the electrode is high compared to the reference case as the spikes associated with the eye movement have a higher amplitude and the parasitic ECG is detected. This can be due to more pressure applied on the electrode during the measurements.

In conclusion, this chapter presented the results and discussion of the non-contact EOG acquisition system developed in this work. After validating the PCB configuration and defining a repeatable measurement protocol, several measurement runs were recorded and analyzed using a dedicated Python code. The combination of time-domain analysis, frequency-domain analysis (FFT) and signal-to-noise ratio (SNR) computation allowed to evaluate the system performance.

The output signal analysis showed that, despite a significant level of noise, the system is capable of capturing essential EOG information using fully non-contact electrodes. Typical eye movements such as left and right rotations, blinking and random eye movements were identifiable in most recordings. Among the different eye activity phases, random eye movements produced the most distinguishable patterns and could correspond to applications such as REM sleep.

Frequency-domain analysis using the Fast Fourier Transform confirmed that power-line interference at 50 Hz and its harmonics is the dominant noise source in the system. The FFT justified the use of both analog and digital notch filtering strategies. While the analog filters reduced part of the interference, the digital notch filter applied in the Python code significantly improved it by removing residual 50 Hz components.

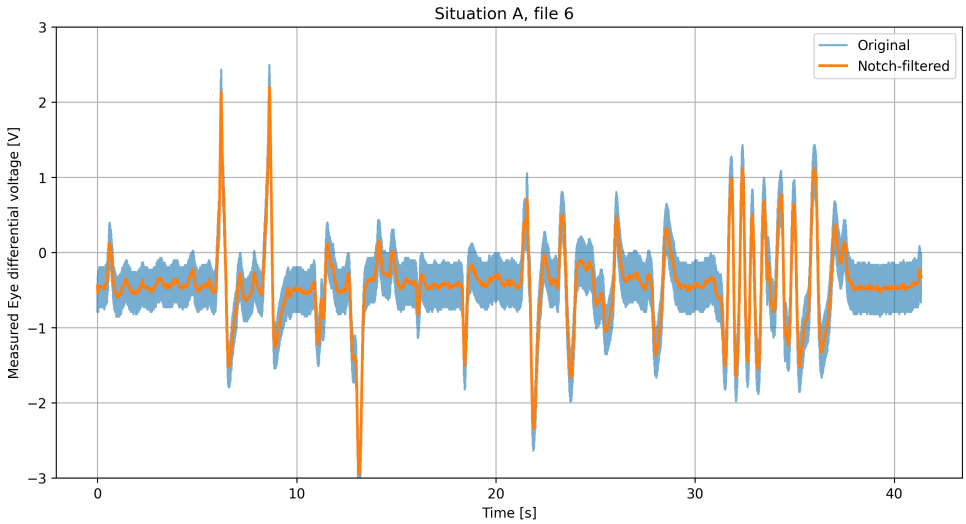

Figure 3.6: EOG measurement affected by ECG artifact associated with high pressure on recording electrodes

The signal-to-noise ratio was used as a quantitative metric to compare measurement runs recorded under identical configurations. The boxplot representation highlighted a median SNR of approximately 3.6 dB with noticeable variability between runs. The analysis showed that environmental conditions (such as lighting and nearby powered devices), skin moisture, electrode pressure and body coupling strongly influence the measurement quality.

Although the system demonstrates proof of concept for non-contact EOG acquisition, hardware-level noise reduction remains a major challenge. Future work should focus on optimizing the reference electrode design, improving shielding and grounding strategies, reducing sensitivity to environmental interference, and refining the analog front-end to limit ECG and low-frequency parasitic signals. Additional measurements on multiple subjects and configurations are also required to assess robustness and reproducibility. Overall, this work shows that non-contact EOG acquisition is realizable but achieving stable, high-quality recordings requires careful design of electrodes, grounding strategy, analog electronics and signal processing.

Chapter 4

Conclusions and perspectives

4.1 Conclusions

This master thesis focused on the design, implementation and evaluation of a non-contact electrooculogram (EOG) acquisition system intended for wearable and comfortable monitoring of eye movements. The motivation of this work originates from the growing need for less invasive and more user-friendly physiological monitoring systems, particularly in the context of sleep disorders such as obstructive sleep apnea. This last sleep disorder represent a major public health issue affecting a large portion of the population and is associated with serious cardiovascular and cognitive consequences.

Current diagnostic methods like polysomnography, provide many clinical information but are expensive, complex and not convenient to organize for the patient. Home sleep apnea tests are less-commonly used diagnosis methods that measures a limited number physiological signal and designed to be used at home. This method lacks a sleep staging related signal thus, measuring the EOG could complement it by detecting REM sleep. These limitations motivate the development of alternative our solution based on wearable devices and simplified signal acquisition techniques.

The electrooculogram is clinically used as physiological signal (together with EEG and EMG) for sleep-stage monitoring. Specific eye movements are associated with different stage of sleep, this is particularly visible for rapid eye movement (REM) sleep. Traditional EOG systems rely on wet electrodes in direct contact with the skin have high precision. But it also reduces comfort and limits long-term or home-based usability due to their gel and irritability. In comparison, non-contact electrodes represent an interesting alternative as they use capacitive coupling through an insulating layer such as fabric. With this layer, the designed electrode is not in direct contact to the skin avoiding irritation and making it easier to wear for the patient. The systems can be easily integrated into a hat, headband or sleeping mask. The differences in electrode types characteristics and electrical equivalent model are highlighted. Compared to wet and dry electrodes, non-contact electrodes offer advantages in terms of comfort and long-term usability but at the cost of ultra high impedance, increased sensitivity to noise, motion artifacts and power-line interference.

Based on this background and on state-of-the-art studies, we designed the complete non-contact EOG acquisition system hardware, from the electrode interface to the analog signal processing stage. The designed capacitive non-contact electrodes uses high-input-impedance buffers to avoid loading the electrode–skin interface and distort the signal. After this, a full analog processing chain was designed and implemented including a instrumental amplifier, filtering stage (low-pass and notch) and two alternative grounding strategies (active driven right leg circuit or passive reference electrode connected to ground). The design choices were guided by bioelectronics course theory, literature references and constraints related to stability and noise.

Before final hardware implementation, the complete system was modeled and analyzed using LTSpice

simulations and validated on breadboard prototype. Several versions of the model were tested, starting from a wet electrode configuration and progressively adapting the system toward a more realistic non-contact electrode model including capacitive coupling through fabric. These simulations and prototype testing allowed validation of the amplification stages, filter bandwidth and general signal behavior before the final PCB implementation. They highlighted the limitations of the non-contact configuration due to weak capacitive coupling with the body and this allowed us to adapt our design by adding feature to the PCB.

The final PCB integrates the complete analog signal conditioning chain, it adds adjustable gains and filters, power management, connectors to the electrodes and different grounding configurations. This represented a major step of the project, as it transformed a theoretical design into a functional hardware platform to be analyzed. Compared to the breadboard version, the PCB offered improved stability, shorter signal paths, better grounding and reduced parasitic effects. The final system integrated the main signal conditioning board, non-contact electrodes and a wearable headband designed to maintain stable electrode positioning on the forehead.

A measurement protocol was then defined to ensure repeatable and comparable recordings. Eye movements were performed following to a predefined sequence, allowing consistencies in identification of signal and noise segments across runs. The recorded signals were acquired using an oscilloscope and processed using a dedicated Python code. This code allows for time-domain plots, digital notch filtering, frequency-domain analysis using FFT and quantitative evaluation through signal-to-noise ratio computation.

The experimental results show that the proposed system is capable to plot and identify essential EOG features using 3 non-contact electrodes. Horizontal eye movements, (blinks,) and random eye movements were identifiable depending on the phase of the measurement protocol, despite the presence of significant 50 Hz noise. Random eye movements detection is important as sleep-related eye movements, such as REM detection, can have similar results. Due to the high-pass filtering in the electrode front-end, eye movement are shown as transient spikes corresponding to eye movement start and end instead of DC level fluctuation.

However, some of the results highlight the limitations of the current implementation. Power-line interference at 50 Hz is identified as the dominant noise source, strongly affecting signal quality and reducing the signal-to-noise ratio. Frequency spectrum analysis confirmed that power-line interference at 50 Hz and its harmonics is the dominant noise source in the system. Although analog filters reduced an important part of this interference, digital post-processing is still necessary to further improve signal quality. The computed signal-to-noise ratio values showed a median SNR of approximately 3.6 dB for the selected configuration with noticeable variability between runs. This variability reflects the strong influence of external and experimental factors on non-contact measurements.

Discussions on the results highlighted several experimental factors were affecting signal quality. Environmental conditions like room lighting and nearby electrical devices had a strong impact on 50 Hz interference. The coupling quality of the reference electrode was identified as one of the most critical parameters. Improved coupling significantly reduced common-mode interference, ways to increase it have been tested with increased moisture, the pressure or electrode surface. This also introduce saturation or ECG artifacts in some case, thus finding the good setting is important to obtain stable results.

Overall, this work demonstrates the feasibility of non-contact EOG acquisition using a custom-designed analog front-end and wearable configuration. We manage to prove the concept that eye movement can be detected in the output EOG without direct skin contact, allowing for the integration in clothing. However, the results show that non-contact EOG is highly sensitive to noise, environmental conditions and mechanical factors. Based on our results, high stability and high-quality recordings are challenging and

requires design of electrodes, main board, grounding strategy, mechanical fixation and signal processing.

In summary, this master thesis combined theoretical analysis, electronic design, hardware implementation and experimental validation to address a challenging biomedical signal acquisition problem. The inspiration for this project arise from the need of simple to use, comfortable and long term sleep monitoring system and diagnose obstructive sleep apnea. While the current system does not yet reach the performance of conventional wet-electrode solutions, it highlights the design choices and limitations that are useful for a future work. It also confirms that non-contact electrode EOG acquisition system is a possible option for future sleep monitoring and wearable health technologies. This work contributes to the development of less intrusive, more user-friendly physiological monitoring systems and serves as an application of non contact electrode system for future advancements in this field.

4.2 Perspective

Non-contact electrodes represent a promising direction for future physiological signal monitoring, particularly in applications requiring long-term comfort and minimal user constraint. Based on recent researches and the results obtained in this work, their use is expected to grow in domains such as sleep monitoring, wearable health devices and human–computer interfaces. Several studies already demonstrate that capacitive electrodes can successfully acquire biopotential signals such as ECG, EEG and EOG with higher signal quality than in this work. Their work showed that physiological signal monitored by non-contact electrode can extract essential health features while being integrated into clothing.

In the context of sleep monitoring, non-contact EOG systems are particularly relevant. Sleep disorders such as obstructive sleep apnea (OSA) require overnight monitoring, ideally in a home environment. Non-contact electrodes embedded in wearable clothing like headbands have advantages over traditional wet electrodes by improving comfort, reducing skin irritation and simplifying device setup for the final user. This could facilitate repeated or long-term recordings for the patient compared to conventional polysomnography systems, it would allow for a wider spread of OSA diagnosis.

However, the experimental results of this thesis show that non-contact electrodes are highly sensitive to environmental noise, motion artifacts and power-line interference. Future developments should focus on decreasing the noise component, increasing coupling capacitance and optimizing reference electrode placement. The improvement of driven capacitive grounding techniques and the selection of active electronic component with less noise could improve signal quality.

Another perspective is the integration of non-contact electrodes into fully wireless systems. Compared to our implementation, the system should not be connected with a shield cable to a oscilloscope and computer. By adding a low-power microcontroller, with analog-to-digital converter and wireless communication modules, the system would become portable and battery powered. Such systems could continuously record physiological signal during sleep and transmit data for analysis.

Overall, non-contact EOG acquisition system is technically challenging, with further development and research, it can play an important role in future wearable and unobtrusive health-monitoring systems. This work contributes as a proof of concept focused on the EOG and highlights design choices and challenges for further improvement.

Appendix A

Use of artificial intelligence disclaimer

For transparency purposes and academic integrity, this master thesis occasionally used artificial intelligence tool as ChatGPT by OpenAI. The artificial intelligence was strictly limited to be used as writing and debugging code assistant. All ideas, design, testing, analyses and interpretation came from my work and is based on everything I have written.

On the writing part, ChatGPT was only used to verify spelling and syntactic mistakes and paraphrase. All the AI writing output based on already written text or draft, have always been verified and modified to align it with my reflection and cited reference. I want to point that it was not used to write any sections from nothing. This is how we treated the artificial intelligence as a writing tool.

For the code, it was used only for the proposition of functions that could simplify the code such as the notch filter and FFT, after the AI proposition the corresponding documentation have been verified to use it as intended. Additionally, it has been used to identify code errors and debugging. Again all decisions in the final code was selected and verified by me.

Appendix B

LTSpice analog chain

This appendix focuses on the LTSpice software model of the analog signal conditioning chain. The main goal is to illustrate how each stage of the circuit affects the signal from the input to the output. This simulation complements the input–output analysis presented in the main report by allowing observation of intermediate signals inside the circuit. The analysis is performed by measuring the simulated circuit shown in Figure B.1 at several internal nodes, labeled from (A) to (G).

All the main elements of the acquisition chain are represented in this model, starting from power-line coupling and the signal of interest, through the skin–electrode impedance model for non-contact electrodes, the recording electrodes, the reference electrode with driven right leg, the instrumentation amplifier, the different filtering stages, and finally the second-stage amplifier before the output. The intermediate signals at each stage are shown in the following figures using multiple plots.

Figure B.2 presents the simulated signals at the first three measurement points. At point A, the signal is measured at the skin–electrode impedance model, just before it is sensed by the non-contact electrode. At this stage, the signal is heavily affected by 50 Hz power-line interference. The amplitude of this interference is higher than what would be expected in a real measurement, but this modeling choice allows a clear visualization of the impact of power-line noise throughout the signal processing chain.

At point B, the signal is measured before the instrumentation amplifier. Compared to point A, the signal appears inverted and the DC offset has been removed by the high-pass filtering effect of the front-end. However, the amplitude of the 50 Hz interference remains unrealistically high for the same modeling reasons.

At point C, the signal is observed after the instrumentation amplifier. At this stage, the EOG signal is amplified and the common-mode rejection ratio (CMRR) of the INA128 removes a significant part of the 50 Hz interference before amplification. Nevertheless, the EOG signal is still not clearly distinguishable from the remaining power-line noise, similarly to what was observed experimentally during breadboard testing (see Figure 2.15).

The following figure B.3 shows the signal after each filter, by applying the first Figure B.3 shows the signal evolution after each filtering stage. After the first low-pass filter, some components of the signal of interest are preserved, but the 50 Hz interference is still present. As the signal passes through the successive filtering stages from points D to F, the amplitude of the 50 Hz component is progressively reduced. After these filters, the remaining signal mainly corresponds to the EOG, although its amplitude is still very small. This confirms that the filtering stages effectively attenuate power-line interference while preserving the useful low-frequency signal.

Finally, the signal is amplified by the second-stage amplifier, as illustrated at point G in Figure B.4. At this stage, the EOG signal reaches an amplitude of several volts and corresponds to the final output of the acquisition system, ready to be recorded or further processed.

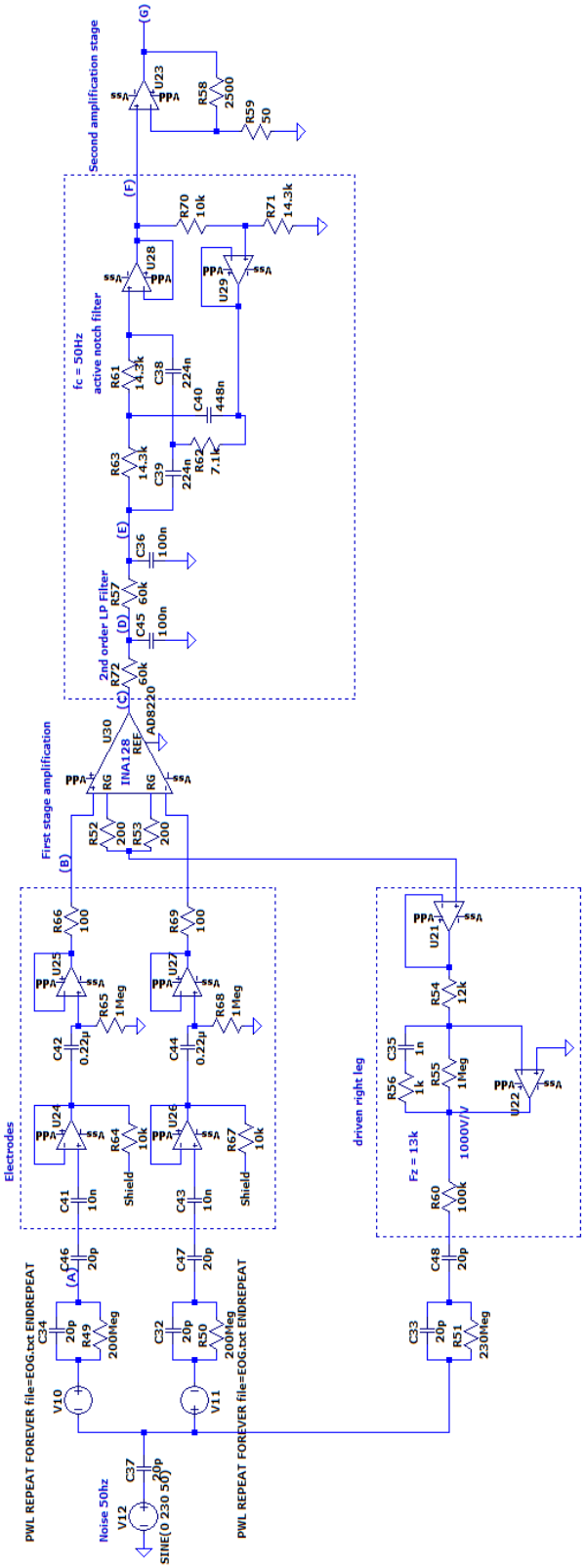

Figure B.1: LTSpice simulation of the analog signal processing chain with 7 points of measurements

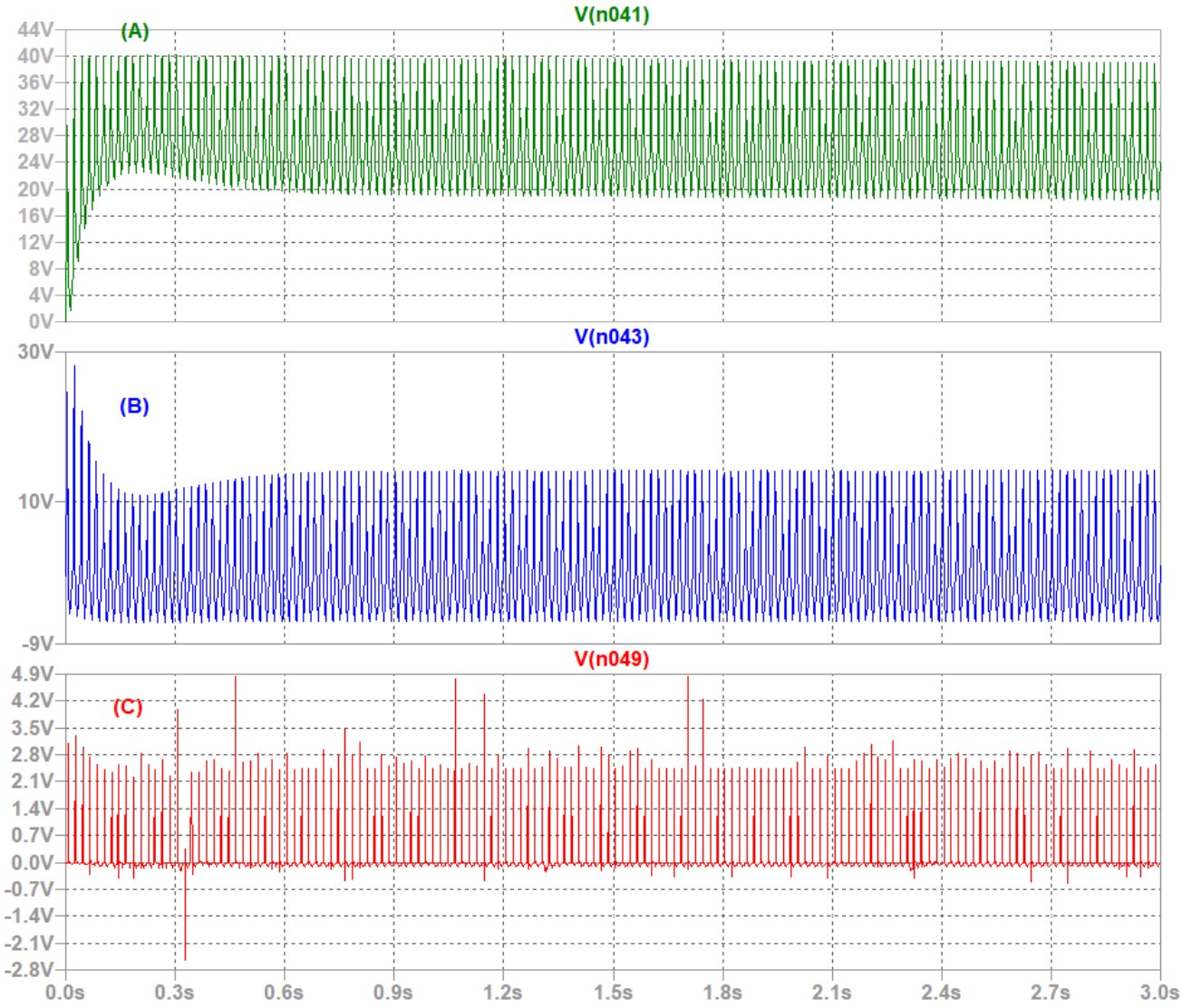

Figure B.2: Intermediate signal plot of the LTSpice simulation : position (A), (B) and(C)

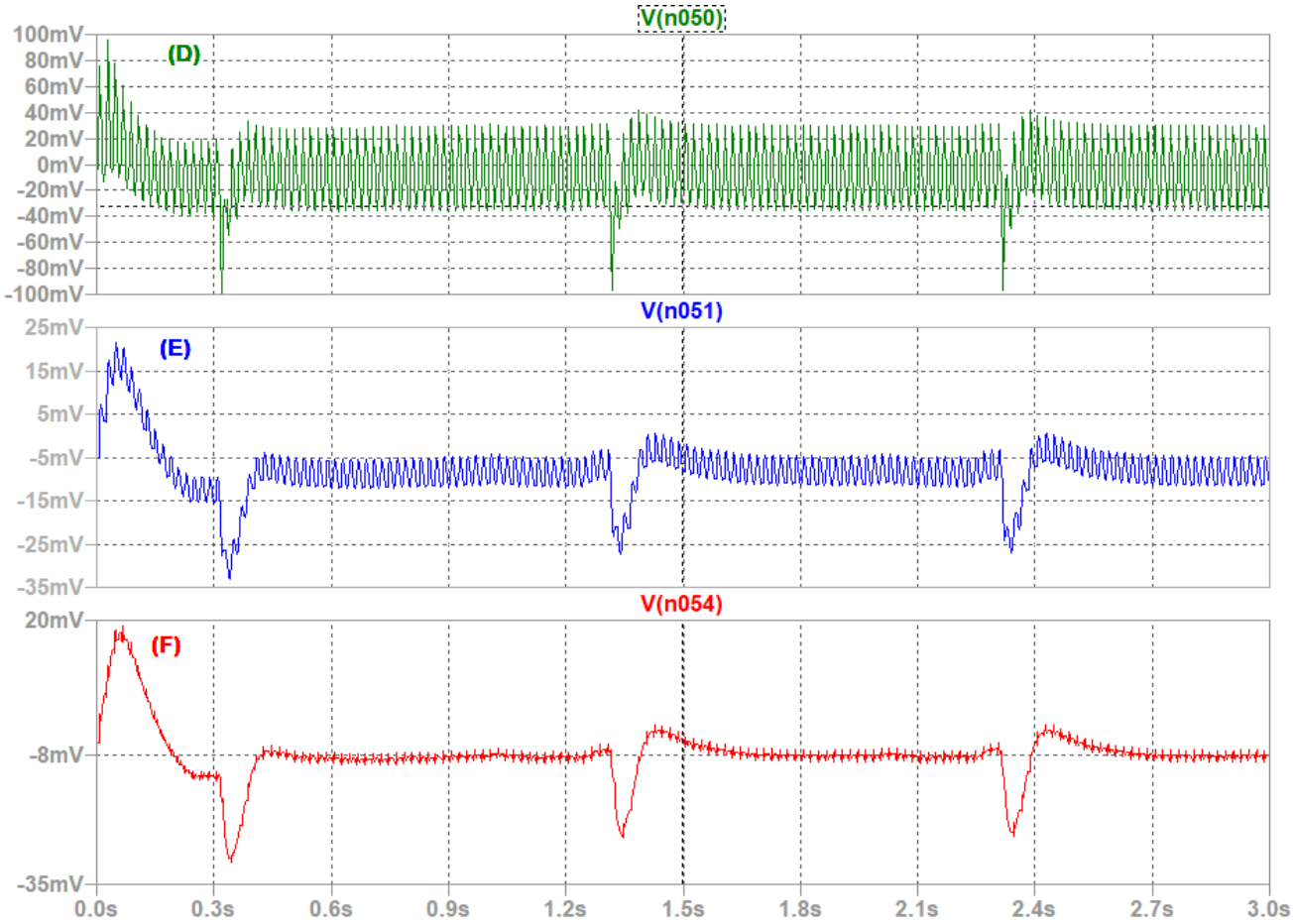

Figure B.3: Intermediate signal plot of the LTSpice simulation : position (D), (E) and (F)

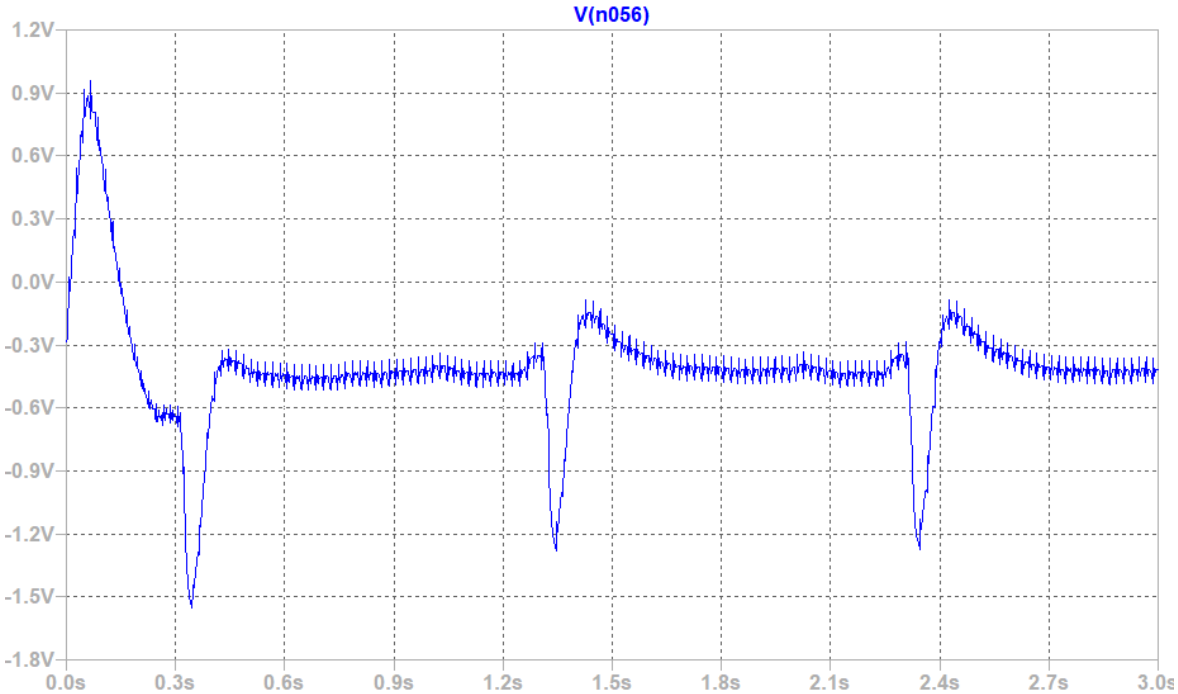

Figure B.4: Output signal plot of the LTSpice simulation

Appendix C

PCB KiCad design

This appendix shows the KiCad design files used to fabricate the printed circuit boards (PCBs) of both the non-contact electrodes and the main signal processing board. These files include the complete schematic designs and PCB layouts that were developed for this master thesis.

The KiCad schematics describe the non contact electrodes with impedance buffers and high pass filter; and the main signal processing board including the power supply unit, instrumentation amplifier, filtering stages, grounding configurations and output stage. The PCB layout files provide information about component placement, routing strategies, ground planes and how each element is connected to acquire the signal.

These KiCad files were used to generate the Gerber files required for PCB fabrication. The resulting boards were manufactured, assembled and experimentally validated as described in the last chapter of this report. This appendix is provided to ensure design transparency, reproducibility and to facilitate future improvements or redesigns of the system.

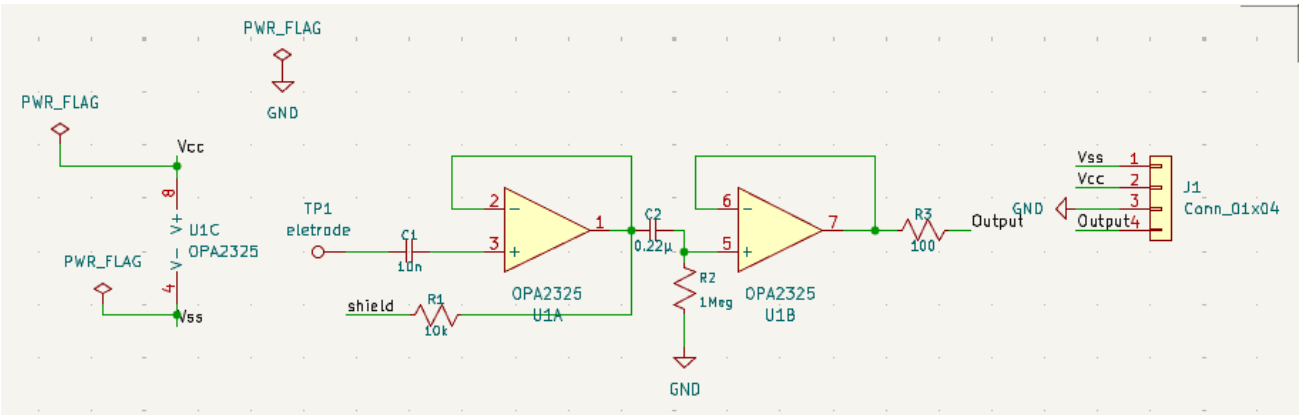

Figure C.1: Non contact electrode circuit schematics for PCB

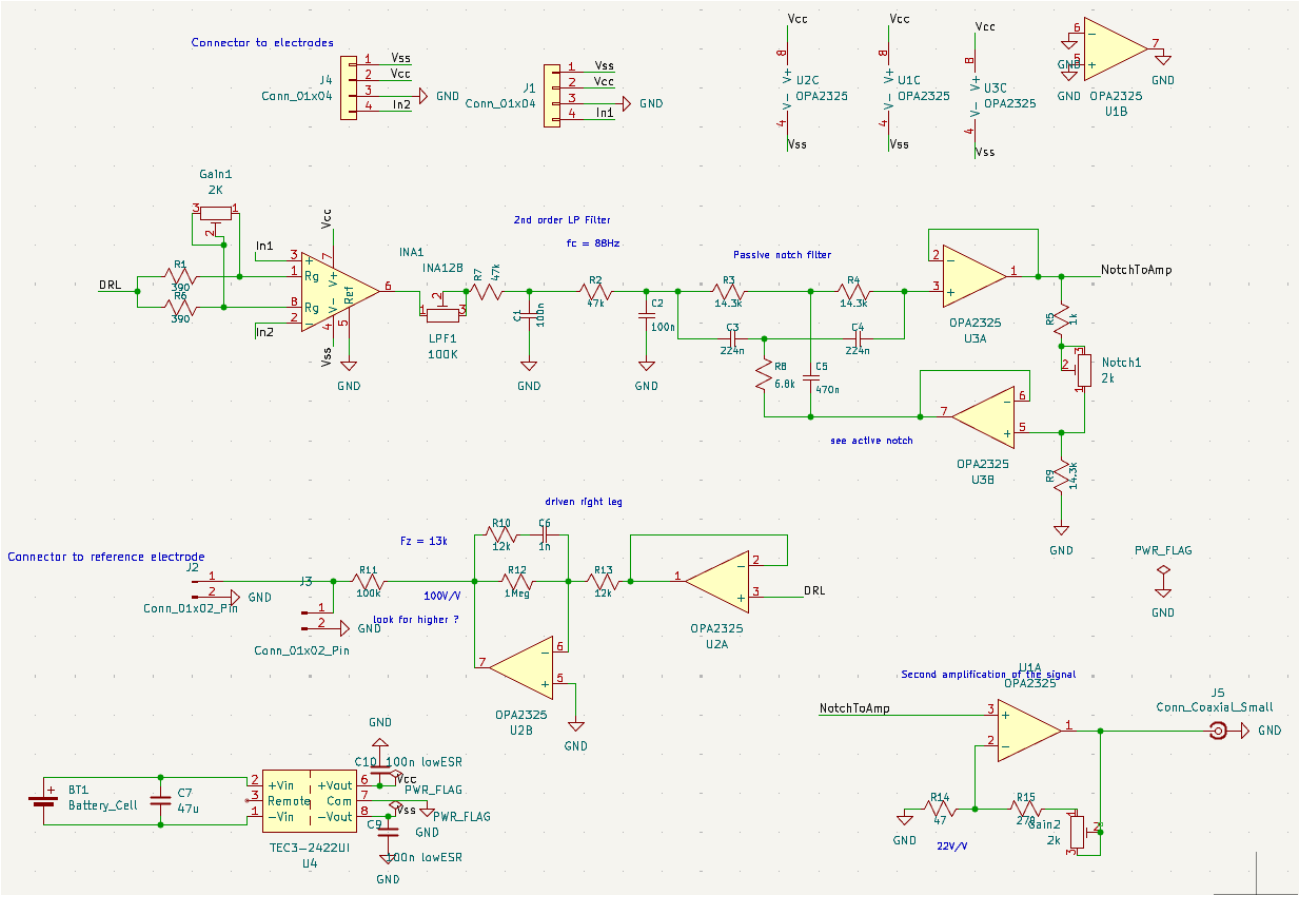

Figure C.2: Main board circuit schematics for PCB

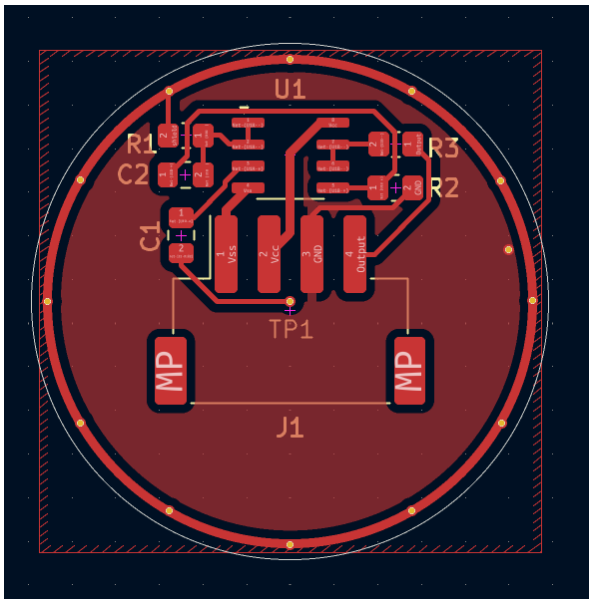

(a) Top view of the electrode

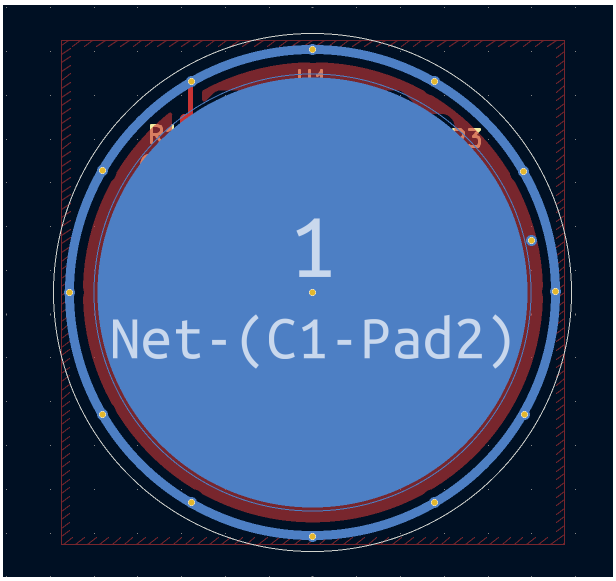

(b) Bottom view of the electrode

Figure C.3: Non-contact electrode PCB implementation: top and bottom views

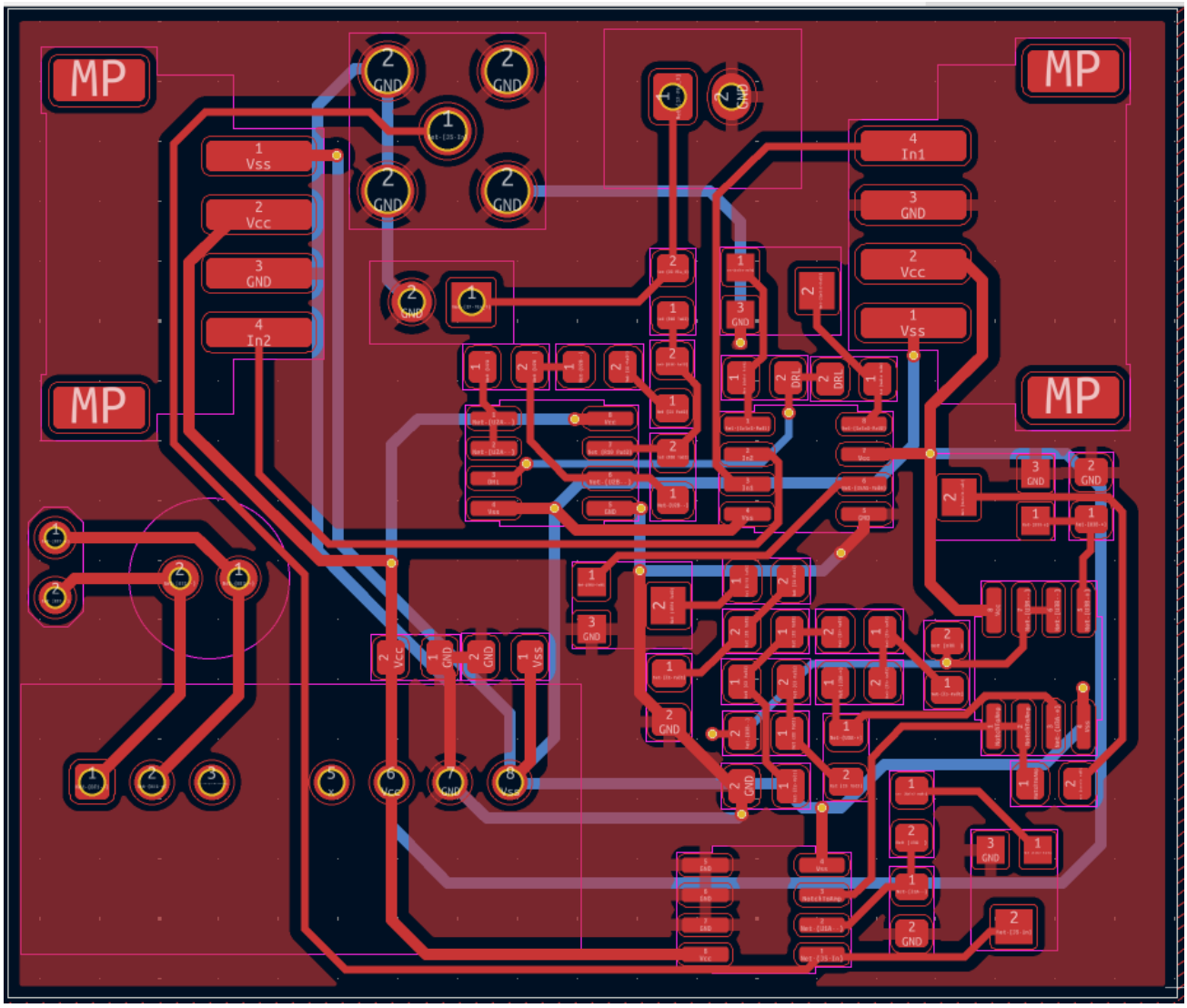

Figure C.4: Main board PCB implementation, top view

Appendix D

Python code for measurements

This appendix show the raw code used for the measurements of our design, an analysis is provided in section 3.1.3.

D.1 Main

First part shows the main code used to plot figures and extract feature from the data

```
    import os
import pandas as pd
import matplotlib.pyplot as plt
import numpy as np
from functions import fft_spectrum, notch_mains_harmonics,plot_segment,
                      compute_snr, plot_snr_boxplot, epoch_snr

# Choose case folder (a to f)
case = "a"
base_dir = os.path.join(case)
data_dir = os.path.join(base_dir, "data")
plot_dir = os.path.join(base_dir, "plots")

os.makedirs(plot_dir, exist_ok=True)

snr_values2= []

# Loop through all CSV files in the folder
for i in range(0,11):
    file_path = os.path.join(data_dir, f"Recording{i}.csv")
        # Check if file exists
    if not os.path.isfile(file_path):
        print(f"File {file_path} not found, skipping...")
        continue
    df = pd.read_csv(file_path, sep=";", decimal=",",skiprows=1)

    # Sampling period from C2 (row 1, col 2)
    sampling_period = 0.00262144  # from the metadata
    signal = df.iloc[:, 4].values  # column E
    time = np.arange(0, len(signal) * sampling_period, sampling_period)
```

```
    # Apply optional function
    # Notch filter and harmonics function
    clean = notch_mains_harmonics(signal, 1/sampling_period, base=50.0, max_harm=3, Q=1)

    #signal to noise ratio function
    snr_db2 = epoch_snr(time, signal, epochs={'signal':(20,35), 'noise':(1,5)})
    print(f"{i}) SNR: {snr_db2:.2f} dB")
    snr_values2.append(snr_db2)

    #Fast Fourier Transform function
    freq, spectrum = fft_spectrum(sampling_period, signal)
    # require additional code to be plotted

    # Plot
    plt.figure(figsize=(12, 6), dpi=300)
    plt.plot(time, signal, label="Original", alpha=0.6)
    plt.plot(time, clean, label="Notch-filtered", linewidth=2)
    plt.xlabel("Time [s]")
    plt.ylabel("Measured Eye differential voltage [V]")
    plt.title(f"Situation {case.upper()}, dB file {i} \nSNR = {snr_db2:.2f} ")
    plt.legend()
    plt.grid(True)
    plt.ylim(-3, 3)

    # Save plot
    plt.savefig(os.path.join(plot_dir, f"{case}_{i}.png"), format="png",dpi=300)
    plt.close()

plot_snr_boxplot(snr_values2, case_name="Case a",
                    save_path=os.path.join("a", "plots", "snr_boxplot.png"))
```

D.2 Functions

Second part shows the functions used in the main code

```
import numpy as np
import matplotlib.pyplot as plt
from scipy.signal import iirnotch, filtfilt


def notch_mains_harmonics(signal, fs, base=50.0, max_harm=3, Q=30.0):
    """

    Cascade notch filters at base*1, base*2, ... base*max_harm.
    Apply a 50 Hz notch filter (zero-phase) to remove mains interference.

    Parameters:
    - max-harm to get the higher harmonics
    - signal: 1D array of original noisy signal sample
    - fs: sampling frequency in Hz
    - f0: notch center frequency (default 50 Hz)
    - Q: quality factor; larger Q = narrower notch (typical 20-50)

    Returns:
    50Hz (and harmonics) -filtered signal

    """
    x = signal.copy()
    for k in range(1, max_harm + 1):
        f0 = base * k
        if f0 < fs / 2:  # only if within Nyquist
            b, a = iirnotch(w0=f0, Q=Q, fs=fs)
            x = filtfilt(b, a, x)
    return x


def compute_snr(signal, clean):
    """
    Compute Signal-to-Noise Ratio (SNR) in dB using original and cleaned signals.

    Parameters:
    - signal: 1D array of original noisy signal sample
    - clean: 1D array of 50Hz-filtered signal

    Returns:
    - snr_db: float SNR in decibels
    """
    noise = signal - clean
    rms_signal = np.sqrt(np.mean(clean**2))
    rms_noise = np.sqrt(np.mean(noise**2)) if np.any(noise) else np.finfo(float).eps

    snr_linear = rms_signal / rms_noise
```

```
    snr_db = 20 * np.log10(snr_linear)
    return snr_db

def epoch_snr(time, signal, epochs):
    """
    Compute the SNR using two time intervals: one for the signal and one for the noise.

    Parameters :
    - time : 1D array containing the time values of the signal
    - signal: 1D array of original noisy signal sample

    epochs : Dictionary with 'signal' and 'noise' keys,
    each containing (start, end) times in seconds.
    (eg epochs={'signal':(20,35), 'noise':(1,5)})

    Returns :
    - snr_db: float SNR in decibels

    """

    mask_signal = (time >= epochs['signal'][0]) & (time <= epochs['signal'][1])
    mask_noise  = (time >= epochs['noise'][0]) & (time <= epochs['noise'][1])

    rms_signal = np.sqrt(np.mean(signal[mask_signal]**2))
    rms_noise  = np.sqrt(np.mean(signal[mask_noise]**2))

    snr_db = 20 * np.log10(rms_signal / rms_noise)
    return snr_db

def fft_spectrum(sampling_period, signal):

    """
    Compute the single-sided FFT spectrum of a signal
    using a known sampling period.

    Parameters
    -sampling period in seconds (e.g., 0.00262144).
    - signal: 1D array of original noisy signal sample

    Returns
    -------
    freqs : array
        Positive FFT frequencies.
    spectrum : array
        Magnitude of the FFT (normalized).
    """
    N = len(signal)
    fft_vals = np.fft.fft(signal)
    fft_freqs = np.fft.fftfreq(N, d=sampling_period)
    return fft_freqs[:N//2], np.abs(fft_vals[:N//2]) / N
```

```
def plot_snr_boxplot(snr_values, case_name="Case", save_path=None):
    """
    Create a boxplot (boîte à moustache) of SNR values.

    Parameters:
    - snr_values : list of floats with the SNR values in decibel to plot.
    - case_name : string to label for the plot (e.g., case 'a', 'b', etc.).
    - save_path : string or None
        If provided, saves the plot to this path (PNG format).
        If None, just shows the plot.
    """
    plt.figure(figsize=(8, 6), dpi=300)
    plt.boxplot(snr_values, vert=True, patch_artist=True,
                boxprops=dict(facecolor="lightblue", color="blue"),
                medianprops=dict(color="red", linewidth=2),
                whiskerprops=dict(color="blue"),
                capprops=dict(color="blue"),
                flierprops=dict(markerfacecolor="orange", marker="o", markersize=6))

    plt.ylabel("SNR [dB]")
    plt.title(f"SNR Distribution - configuration {case_name}")
    plt.grid(True, axis="y", linestyle="--", alpha=0.7)

    if save_path:
        plt.savefig(save_path, dpi=300, bbox_inches="tight")
        plt.close()
    else:
        plt.show()
```

Bibliography

[1] Brooke A Krbec, Xiang Zhang, Inbar Chityat, Alexandria Brady-Mine, Evan Linton, Daniel Copeland, Brian W Anthony, Elazer R Edelman et Jonathan M Davis : Emerging innovations in neonatal monitoring: a comprehensive review of progress and potential for non-contact technologies. *Frontiers in Pediatrics*, 12:1442753, 2024.

[2] Yu M Chi et Gert Cauwenberghs : Wireless non-contact eeg/ecg electrodes for body sensor networks. *In 2010 International Conference on Body Sensor Networks*, pages 297–301. IEEE, 2010.

[3] Xin Wang, Shuting Liu, Mingxing Zhu, Yuchao He, Zhilong Wei, Yingying Wang, Yangjie Xu, Hongguang Pan, Weimin Huang, Shixiong Chen *et al.* : Flexible non-contact electrodes for wearable biosensors system on electrocardiogram monitoring in motion. *Frontiers in Neuroscience*, 16:900146, 2022.

[4] VLDSN Button et E Costa : Electrodes for biopotential recording and tissue stimulation. *Principles of Measurement and Transduction of Biomedical Variables; Academic Press: Oxford, UK*, pages 25–76, 2015.

[5] Adam V. et Al. Benjafield : Estimation of the global prevalence and burden of obstructive sleep apnoea: a literature-based analysis. *The Lancet Respiratory Medicine*, 7(8):687–698, 2019.

[6] Jussi Virkkala, Joel Hasan, Alpo Värri, Sari-Leena Himanen et Kiti Muller : Automatic sleep stage classification using two-channel electro-oculography. *Journal of neuroscience methods*, 166(1):109–115, 2007.

[7] Md Mosheyur Rahman, Mohammed Imamul Hassan Bhuiyan et Ahnaf Rashik Hassan : Sleep stage classification using single-channel eog. *Computers in biology and medicine*, 102:211–220, 2018.

[8] Jessica Vensel Rundo et Ralph Downey III : Polysomnography. *Handbook of clinical neurology*, 160:381–392, 2019.

[9] Lawrence Y Deng, Chun-Liang Hsu, Tzu-Ching Lin, Jui-Sen Tuan et Shih-Ming Chang : Eog-based human–computer interface system development. *Expert Systems with Applications*, 37(4):3337–3343, 2010.

[10] Mayo Clinic Staff : Polysomnography (sleep study). Online; Mayo Clinic Health Library, janvier 2025. Accessed: 2025-09-03.

[11] Kevin K Motamedi, Andrew C McClary et Ronald G Amedee : Obstructive sleep apnea: a growing problem. *Ochsner Journal*, 9(3):149–153, 2009.

[12] Melissa Knauert, Sreelatha Naik, M Boyd Gillespie et Meir Kryger : Clinical consequences and economic costs of untreated obstructive sleep apnea syndrome. *World journal of otorhinolaryngology-head and neck surgery*, 1(01):17–27, 2015.

[13] Colleen M. Story : The effects of sleep apnea on the body, 2025. Accessed: 2025-10-17.

[14] Yu M Chi, Patrick Ng, Eric Kang, Joseph Kang, Jennifer Fang et Gert Cauwenberghs : Wireless non-contact cardiac and neural monitoring. *In Wireless Health 2010*, pages 15–23. 2010.

[15] Yu Mike Chi, Tzyy-Ping Jung et Gert Cauwenberghs : Dry-contact and noncontact biopotential electrodes: Methodological review. *IEEE reviews in biomedical engineering*, 3:106–119, 2010.

[16] Qing Liu, Liangtao Yang, Zhilin Zhang, Hui Yang, Yi Zhang et Jinglong Wu : The feature, performance, and prospect of advanced electrodes for electroencephalogram. *Biosensors*, 13(1):101, 2023.

[17] Alhassan Haruna Umar, Mohd Afzan Othman, Fauzan Khairi Che Harun et Yusmeeraz Yusof : Dielectrics for non-contact ecg bioelectrodes: A review. *IEEE Sensors Journal*, 21(17):18353–18367, 2021.

[18] Jaakko Malmivuo et Robert Plonsey : The electric signals originating in the eye. *In Bioelectromagnetism*, chapitre 28. MIT Press, 1994. Accessed: 2025-09-03.

[19] Belgian Health System INAMI/RIZIV : Polysomnography key figures. Web page, HealthyBelgium (For a Healthy Belgium), 2023. Accessed on 2025-09-04; see section "Key figures".

[20] Seithikurippu R Pandi-Perumal, D Warren Spence et Ahmed S BaHammam : Polysomnography: an overview. *Primary care sleep medicine: A practical guide*, pages 29–42, 2014.

[21] Tom PulmCritSleep : Orientation to polysomnography. YouTube video, 2025. Accessed: 2025-09-02, Figure copied from.

[22] Mukesh Kapoor et Glen Greenough : Home sleep tests for obstructive sleep apnea (osa). *Journal of the American Board of Family Medicine*, 28(4):504–509, 2015.

[23] Sleepscope : Home-based sleep study. Web page, Sleepscope Services. Accessed: 2025-12-03.

[24] O Kellner, H Bastuji et P Adeleine : Actimetry in sleep medicine. *Sleep & Breathing*, 2(1):33–39, 1997.

[25] Brett Duce, Jasmina Milosavljevic et Craig Hukins : The 2012 aasm respiratory event criteria increase the incidence of hypopneas in an adult sleep center population. *Journal of clinical sleep medicine*, 11(12):1425–1431, 2015.

[26] Jean-Michel Redouté : Course notes for [bioelectronics]. University of Liège, 2023. Lecture material.

[27] John G Webster : *Medical instrumentation: application and design*. John Wiley & Sons, 2009.

[28] Yusuke Mukai : *Dielectric properties of cotton fabrics and their applications*. North Carolina State University, 2019.

[29] John R Heckenlively et Geoffrey B Arden : *Principles and practice of clinical electrophysiology of vision*. MIT press, 2006.

[30] Won-Du Chang : Electrooculograms for human–computer interaction: A review. *Sensors*, 19(12): 2690, 2019.

[31] Cleveland Clinic : Sleep basics – rem nrem, sleep stages, good sleep habits more. Online article. Accessed: 2025-12-03.

[32] Mary Carskadon et William Dement : Normal human sleep: An overview. *Principles and practice of sleep medicine*, 01 2017.

[33] Shibam Debbarma et Sharmistha Bhadra : A lightweight flexible wireless electrooculogram monitoring system with printed gold electrodes. *IEEE Sensors Journal*, 21(18):20931–20942, 2021.

[34] Shibam Debbarma et Sharmistha Bhadra : A flexible wearable electrooculogram system with motion artifacts sensing and reduction. *IEEE Transactions on Biomedical Circuits and Systems*, 16(2):324–335, 2022.

[35] Francesca Romana Parente, Marco Santonico, Alessandro Zompanti, Mario Benassai, Giuseppe Ferri, Arnaldo D'Amico et Giorgio Pennazza : An electronic system for the contactless reading of ecg signals. *Sensors*, 17(11):2474, 2017.

[36] Anthony J Portelli et Slawomir J Nasuto : Design and development of non-contact bio-potential electrodes for pervasive health monitoring applications. *Biosensors*, 7(1):2, 2017.

[37] Wagner Hoffmann, Andrew Lowe, Matt Wilson et Matthew MY Kuo : Investigation of non-contact electrodes for electrocardiogram monitoring. *In 2023 45th Annual International Conference of the IEEE Engineering in Medicine & Biology Society (EMBC)*, pages 1–4. IEEE, 2023.

[38] Irien Sadighiani : Design and implementation of a contactless ecg acquisition system. Master's thesis, Université de Liège, Faculté des Sciences appliquées, 2019. Defense date: 09 Sep 2019; Accessed: 2025-11-26.

[39] Texas Instruments : *LMP7702 — Precision, CMOS Input, RRIO, Wide Supply Range Dual Amplifier*. Texas Instruments, 2015. Accessed: 2025-12-03.

[40] Marian Walter : Course notes for [medical systems]. Helmholtz institut für biomeizinische technik der RWTH AACHEN, 2024. Lecture material.

[41] Texas Instruments : *INA128 — Precision, Low-Power Instrumentation Amplifier*. Texas Instruments, 2015. Accessed: 2025-12-03.

[42] Ruye Wang : Active filters — frequency response of op amp circuits. Online lecture notes, Harvey Mudd College, 2025. Accessed: 2025-12-03.

[43] Fuming Fang et Takahiro Shinozaki : Electrooculography-based continuous eye-writing recognition system for efficient assistive communication systems. *PloS one*, 13(2):e0192684, 2018.